UNIVERSITÀ
DI SIENA
1240

Department of Information Engineering and Mathematics

PhD in Information Engineering and Science - XXXIV cycle

MODELLING AND CONTROLLING SOFT INTERACTIONS

Sara Marullo

Supervisor: Prof. Domenico Prattichizzo
Co-supervisor: Prof. Monica Malvezzi

PhD Thesis
March 2022

Abstract

Compliance is a key factor during physical interactions between agents and objects, allowing delicate and robust manipulation. Such a compliance can reside in human and robotic hands, as well as in objects present in the environment. This Thesis arose from the quest for mechanical conditions fostering object manipulation, and shaped as an investigation on techniques to model and control the compliance in soft interactions. Human and robotic hands are considered, functional and biomechanical models are discussed, devised and validated. To deal with unpredictable configurations assumed by intrinsically and passively-compliant underactuated robotic hands, a solution based on magnetic actuation is proposed. The exploitation of small magnetic elements allows also to simplify the robotic end-effector design by relying on local interactions to manipulate extremely deformable objects like garments. Moreover, mechanical forces exchanged during physical interactions are used to devise a control strategy for human-robot cooperative grasping, relying on a novel contact model exploiting linear elastic patches to ensure the contact permanence. The Research work contained in this Thesis shows that developing techniques for implementing robotic soft interactions is feasible and can significantly broaden the spectrum of robotic applications in real-world scenarios. An extensive experimental validation of the theoretic work supports the discussion.

Table of contents

Introduction

Soft interactions are the *fil rouge* running through this Thesis.
During such interactions, humans and robots will exchange forces among them and with the environment, posing several Research challenges. This work wants to be a contribution to the development of modelling and control tools for effective autonomous and human-robot cooperative task execution.

In this work, the term *softness* will refer to different types of compliance: soft actuation, soft materials and soft environment.

Robot-environment, human-robot, human-human and robot-robot interactions will be investigated, with particular focus on grasping tasks. As it will be evident in the following, the actual core of soft interactions lies in the way in which the human hand structured the way we interact with the world. Human hands, indeed, are soft and compliant, meaning that the materials they are made of easily deform under interaction with the environment, both at the skin and articular levels, servoing the hand configuration to the object shape and to the task to be accomplished. This adaptability of the hand allows interactions that are delicate and robust at the same time. However, whenever the softness is present in hands or in objects, several challenges appear, due to the difficult predictability of the way in which the soft structure deforms during interactions. Basically, this is the reason why the world of robotic

grasping started a recasting in the last 15 years. Although great steps have been made, grasping modelling and actuation strategies for soft interactions are still far from being assessed. In general, modelling deformations is an extremely complex task, requiring object-specific and material-specific assumptions. Moreover, such assumptions are usually affected by several simplifications, leading to unavoidable mismatches between what happens in the real-world and what happens in the simplified representation. In addition, when more realistic representations are implemented, they allow to reduce the aformentioned mismatches at the cost of higher computational burden. Hence, such solutions are usually not suitable for real-time robotic applications. In this Thesis we will not focus on modelling deformations, but we mainly discuss how to model key components to control soft interactions occurring with soft hands or soft objects present in the environment.

Soft hands have usually *soft actuation*, which is inspired by the human neurophysiology. To say it with an engineering metaphor, there is a sort of software compliance in the human hands, residing in the way in which the brain coordinates the motion of the fingers. The hand articulations, indeed, are not controlled joint-by-joint, but through actuation patterns (called synergies) controlling multiple joints through coordinated strategies. Moreover, as soon as some parts of the hand contact an object, joints are controlled by the brain so to maximize the grasp robustness according to the task to be performed. This implies that during a successful interaction, the hand adapts to the object shape, while satisfying acquired, implicit constraints related to the task execution. Inspired by the human hand, the research line on Soft Manipulation developed the fist underactuated, compliant robotic hands. As it will be discussed in *Part A* of this Thesis, in such hands, the exploitation

of passive elements and proper transmission systems allows to control the motion of all the joints by realizing coordinated actuation patterns that kinematically constrain the underactuated joints motion. Moreover, the transmission system is designed so to allow the hand to adapt to the object shape after the contact has been established. We will refer to this behaviour with the expression *soft actuation*.

A further step towards the softness exploitation consists in developing robotic hands made of *soft materials*, i.e. highly deformable, elastomeric compounds. Such hands are intrinsically soft and underactuated, meaning that they are intrinsically capable of adapting to the object shape, realizing delicate and enveloping interactions, similarly to what the human hand does.

Robotic hands with soft actuation and hands made of *soft materials* pose to the robotic community the challenges of developing *i)* suitable tools for modelling the underactuated behaviour and *ii)* proper strategies for the control of such devices. In this framework, a minimalistic and functional approach to model and control such hands will be presented in Chapter 1: The Closure Signature of two hands representative of the aformentioned types of softness will be devised for different types of grasps, and an extensive experimental evaluation will be provided. Problems related to the difficult control of intrinsically soft hands will be analyzed more in detail in Chapter 2, where we will investigate the possibility of providing such hands with magnetic actuation to cope with uncertainties in control, and to provide additional Degrees of Actuation.

The neurophysiological actuation of the human hand, joined with the high modularity of its morphological structure (about 27 little bones and 15 articulations, 20 Degrees of Freedom), provides the human hand with high dexterity, allowing to successfully accomplish tasks

requiring fine manipulation. One paradigmatic example of such tasks is the garment folding and unfolding, where the intrinsic deformability of the object allows the object to potentially deform in infinite different ways. This extreme, intrinsic deformability makes the autonomous manipulation of such items really hard, opening several challenges related to the strategies needed to establish and maintain the desired grasps. In this respect, Chapter 3 will consider a robotic end-effector that has to interact with a garment present in the environment, and we will framework this study case in the context of *soft environment*. We will propose to exploit Mag-Gripper, a novel robotic hand that is simple in its design, but exploits the magnetic attraction to perform precise and repeatable task execution.

As mentioned before, humans are *soft*, and one of the consequences is that during physical interactions our muscoloskeletal behaviour can be modelled by means of spring-damper systems. In Chapter 4, we will consider soft interactions between humans and robots mediated by a large object, and we will devise a robot control strategy relying on the Extended Patch contact model, which is specifically designed for extended, elastic contacts.

In closing, in Chapter 5 we will apply the theory of grasping for devising a biomechanical model of a posture of the human hand suitable for writing on touchscreen devices. In such a posture, called FingerPen, the hand grasps the hand itself, in a soft interaction that merges the writing tool and the gesture in a single operating organ.

The material of this Thesis is organized in two parts: *Part A* will focus on soft interactions for autonomous robotic manipulation (Chaps. 1, 2, 3), while *Part B* will focus on human-robot and human-human soft interactions (Chaps. 4, 5). At the end, conclusions are drawn.

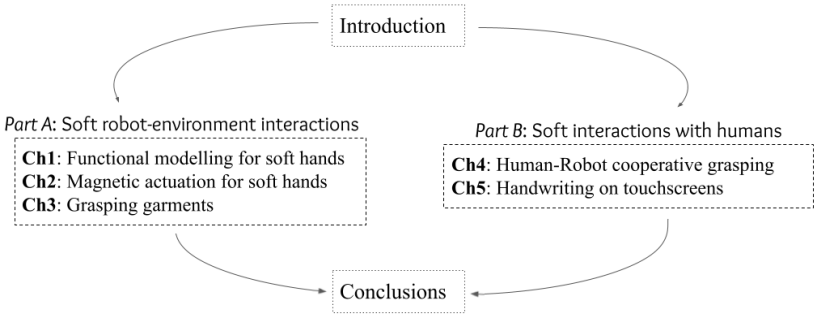

Main Contributions

The main contributions of this Thesis are here listed for the sake of conciseness:

- Extensive validation of the Closure Signature, a functional model for soft hands, suitable to represent the behaviour of such devices during closing motions. Tendon-driven and pneumatic hands have been used, and different types of grasps were investigated. The work has been published in M. Pozzi, S. Marullo, G. Salvietti, J. Bimbo, M. Malvezzi and D. Prattichizzo. "Hand closure model for planning top grasps with soft robotic hands", in *The International Journal of Robotics Research*, 2020.

- Proposal of magnetic actuation for soft hands: to counteract difficulties in the control of soft hands, magnetic funnels generated by magnetic elements embedded in strategic locations of such devices can be exploited. Physics laws for modelling electromagnets and permanent magnets were applied to uncertainty compensation, affordance exploitation, augmentation of the De-

grees of Actuation and non-contact manipulation. The content of this work has been submitted for publication in S. Marullo, G.Salvietti, D. Prattichizzo, "On the use of magnets to robustify motion control of soft hands", for *Soft Robotics*, 2021.

- Novel approach to garment manipulation: to achieve repeatable manipulation of garments while dealing with their extreme deformability, magnetic attraction between gripper and garment can be exploited, by embedding ornamental soft ferromagnetic plates in key locations of the garment, leading to fast task accomplishment. The work is published in S. Marullo, S. Bartoccini, G. Salvietti, M. Z. Iqbal and D. Prattichizzo. "The Mag-Gripper: A Soft-Rigid Gripper Augmented With an Electromagnet to Precisely Handle Clothes", in *IEEE Robotics and Automation Letters*, Oct. 2020.

- Novel contact model and robot control strategy for human-robot cooperation focused on transportation of large objects. To have contact permanence, linear elastic compliance is required at the area of interaction between object and robot, leading to a linear distribution of the contact pressure. Proper pressure and force constraints allow to retrieve robot velocities. Work published in

  S. Marullo, M. Pozzi, D. Prattichizzo and M. Malvezzi, "Cooperative Human-Robot Grasping With Extended Contact Patches", in *IEEE Robotics and Automation Letters*, Apr. 2020.

- Novel posture of the hand for writing on touchscreens without using pens: a biomechanical model of a hand posture merging tool and gesture is presented and compared with the most common way to write on a touchscreen, i.e. with the index finger only. An

extensive user-study accompanies and validates the theoretical discussion. Work published in S. Marullo, M. Pozzi, M. Malvezzi and D. Prattichizzo, "Analysis of postures for handwriting on touch screens without using tools", in *Scientific Reports*, Jan. 2022.

Part A

Soft Robot-Environment Interactions

Soft Robot-Environment Interactions

This part of the Thesis focuses on soft interactions for autonomous robotic manipulation tasks.

Autonomous manipulation in unstructured environments is an open challenge in robotics [1], requiring the development of advanced algorithms for grasp planning and control (software) and cutting-edge robotic hands and grippers (hardware). Modularity and synergistic approaches between software and hardware solutions are strategic means, allowing to decentralize and distribute the *intelligence* of the system among the different components.

Providing robots with the capability of interacting in a dynamic environment that requires fine perception and high dexterity is paramount, since robots are expected to autonomously perform some tasks or subtasks, either in industrial either in service settings. Moreover, as robots get closer to humans, their ability to safely interact with unstructured environments is much more relevant than their force or velocity performance, and the adoption of *soft* end-effectors becomes crucial [2]. Compliant and underactuated robotic hands have been studied since the late 1970's [3, 4]. More recently, advancements in the field of *soft robotics* boosted the creation of the first completely soft manipulators and grippers [5]. Nowadays, there is a growing need of mathematical tools and shared standards to tackle the challenge of soft manipulation, by devising methods that are general enough to be applicable to different robotic setups.

Moreover, adapting robots to perform tasks requiring complex dexterity (e.g., the manipulation of deformable objects) poses several challenges. Deformable objects, indeed, cannot be grasped according to classic grasp planning methods [6], and the manipulation strategy strongly depends on the object global and local configuration.

In this Thesis, we will discuss the case of garments, extremely deformable objects whose configuration during manipulation is significantly affected by the grasping points and the handling arm trajectory. Relatively small changes in the grasping points can cause a significant change of the garment configuration, potentially leading to a task failure. Garments are the quintessence of deformable objects. However, what in garment makes the autonous manipulation difficult (i.e., the compliant deformability) can be a game changer when embedded in robotic end-effectors. Exploiting mechanical compliance in a robotic end-effector, indeed, allows the end-effector to adapt to the object shape, and is particularly useful to face the typical issues related to sensitivity to uncertainties in sensing and control that strongly affects classical grasp planning methods [7, 2]. Such a mechanical compliance can be achieved in active or passive manners. Active compliance is related to fully actuated (or hyper-actuated) usually rigid hands (such as the Allegro [8] and Awiwi [9] hands), and can be achieved by controlling separately each joint. The control of these hands can be fast and very accurate, but mechanical and computational complexity are very high, reflecting on high manufacture price and chance of hardware failure. Much more robust hands can be achieved by exploiting passive compliance. In these hands, fingers, palm and also joints can be made of elastomeric and flexible materials. Spatial volume and mechanical

complexity are reduced, and the choice of proper materials allows to lower the impact forces, realizing a safe robot-environment interaction.

In soft-rigid hands, links are not made of soft materials, and compliance resides in the actuation system. In such hands, indeed, some passive elements (e.g., springs) are used together with a transmission system (e.g., gears, pulleys, tendons) to distribute the actuation torque also to the underactuated joints [4], making these joints passively driven with kinematically constrained motion. Moreover, the mechanical structure of these devices is such that the transmission system allows the motion of some joints to continue after the contact has occurred [2], so to allow the hand to adapt to the object shape. An example of such hands is given by the Pisa/IIT SoftHand [10], a compliant, underactuated, anthropomorphic robotic hand. Such a hand is a tendon-driven actuated device with one motor and 19 degrees of freedom, designed to reproduce the first human hand synergy [11]. In the structure of this hand, rolling contact articulations substitute almost completely the standard revolute joints, and just one tendon routes all joints by using passive anti-derailments pulleys.

It is clear now that embedding passive compliance in the mechanical structure of robotic hands allows such hands to be adaptable, versatile, and robust. Delicate manipulation and robust grasps [4] can be achieved through an enhanced hand/object adherence, compensating also for uncertainties on the desired grasping points [2]. Hence, part of the grasping system "intelligence" can be embodied in the hardware design, instead of being exclusively allocated in the planning and control algorithms. Despite remarkable advantages in using soft hands, indeterminate kinematics and a priori unpredictable deformations lead classic strategies for hand modelling and control [12] to be no longer

suitable. Adapting classical techniques to grasp planning with soft hands is not the most efficient way, since classic grasp planning methods prescribe the exact position of fingers for ensuring force closure, but do not encapsulate information on how the hand actually behaves while performing a given motion. Classic methods need to be extended, or even overcome, so to exploit the intrinsic features of soft hands [13].

The Closure Signature that will be presented in Chapter 1 follows this philosophy: It is a functional model that can be retrieved for different robotic hands and, by modelling closure motions, it is able to describe *how* the chosen device *actually* works. In the planning phase, the CS-alignment gives a way to increase grasp success, and exploits the hand compliance to gain adaptability to the object shape, safe interaction with the environment, and robustness to uncertainties coming from sensor inaccuracies. The Closure Signature can be computed for soft-rigid hands as well as for intrinsically soft hands (i.e., made of highly compliant material). An example of intrinsically soft hand is the RBO Hand 2, made of 7 pneumatic actuators, 5 for the fingers and 2 for the palm [14]. Actuators are made of silicon, sustained by a 3D printed structure, and surrounded by passive wires constraining their motion.

In Chapter 1, the Closure Signature of the Pisa/IIT SoftHand and of the RBO Hand2 will be computed for different types of grasps.

As previously said, one driving force for soft hands inception was the simultaneous need of enhancing grasp robustness and stability, and the need of reducing hand complexity and encumbrance. However, the intrinsic underactuation of these hands yield a not precise motion control. Hence, to overcome the dexterity limitations [15, 16] due to underactuation and software/hardware motion coupling [17], current research on soft manipulation is turning again to complexity both in

design and control (as the RBO Hand 3, evolution of the RBO Hand 2, exemplifies [18]). Classic approaches to DoAs augmentation, indeed, rely on the replication of the same actuation system, e.g. increasing the number of inflatable chambers in pneumatic structures [18]. In this Thesis, instead, in Chapter 2 we propose to equip soft hands with magnetic elements, acting as additional degrees of actuation (DoAs). Interestingly, magnetic actuation for manipulation can be achieved by exploiting magnetic elements that can be easily embedded in existing hands and designs. Moreover, magnetic DoAs provide an actuation on specific locations of the hand. Hence, they can act synergistically with the more global effect provided by tendons and/or pneumatic actuators, arousing a complementarity enriching the device's capabilities.

One of the main reasons behind the exploitation of magnetic actuation resides in the possibility of performing manipulation tasks by interacting with the environment in specific points. The need of grasping in specific locations is deeply felt when performing autonomous garment manipulation. In this respect, in Chapter 3 we propose Mag-Gripper, a novel type of jaw gripper augmented with an electromagnet. Small ferromagnetic parts embedded in the garment as ornamental or brand elements are involved in the attractive gripper-fabric approach. Although our long-term vision involves the manufacture of garments that can be easily manipulated by robots, Mag-Gripper features an immediate field of application in the robotic community: It is meant to be a support tool for the research in Machine Learning-based garment manipulation, where high repeatability in grasp location is required for data collection.

1 Functional modelling for soft hands

This Chapter is focused on grasp planning with soft hands. The Closure Signature functional model of a robotic hand will be discussed from a theoretical point of view, and then computed for the compliant Pisa/IIT SoftHand [10] and for the intrinsically soft RBO Hand 2 [14].

To investigate the CS capability of properly modelling different types of grasps, the Closure Signature of such hands will be computed for power, lateral and pinch grasps. Then, a modular approach to grasp planning will be proposed: on one side, being object-centric, on the other side, being hand-centric. The Closure Signature is the connecting element allowing the synergy of the two modules. The CS, indeed, maps a given hand closing motion to the direction along which the largest deformation occurs during that motion. This direction is akin to the grasping direction of a parallel-jaw gripper. Based on these considerations, we will show that top-grasps can be successfully planned by aligning the hand CS to a suitable direction on the object, retrieved using a grasp planner for parallel-jaw grippers. In particular, we integrated the CS-alignment (see Fig. 1.1) with a state-of-the-art grasp planner for parallel-jaw grippers relying on deep learning [19].

In this Chapter, hence, we propose the Closure Signature functional model as a viable strategy to actuate and control the behaviour of a soft

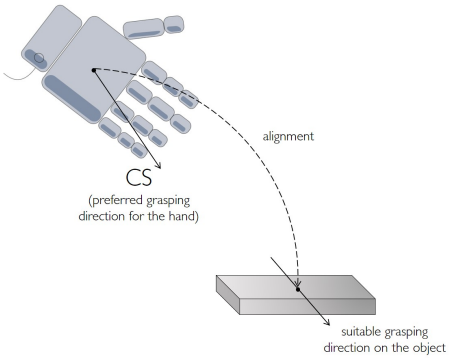

Fig. 1.1 Block scheme of the CS-alignment proposed in this Chapter. Given a certain robotic hand and a possible closing motion, the Closure Signature indicates a "preferred grasping direction" for that closure, that can be thought as the grasping direction of a parallel-jaw gripper and can be aligned with a suitable direction on the object.

robotic hand, rather then focusing on the difficult-to-retrieve deformations of the hand when interacting with objects and environments[1].

1.1 The Closure Signature: a hand functional model

The *Closure Signature* (CS) of a hand is a functional model aimed at capturing the hand function, rather than its kinematic or morphological structure. The CS is specific for a given hand and a given closing motion performed by the hand, meaning that the same hand can have different CSs depending on the considered closing motion. Being aimed at providing insights on the hand capabilities, the CS represents how the

[1] This Chapter contains an extract of the work published in [20].

hand closes in free space, i.e., without considering specific interactions with objects or surfaces.

In principle, the CS could be applied to any robotic hand performing any closing motion. However, it is mainly conceived for soft hands. Rigid hands, indeed, can be modeled as kinematic chains using well known kinematics and dynamics principles. Soft hands, instead, are difficult to model with a unique formalism, as they have very different designs and actuation systems. The CS was introduced to fill this gap. The following sections extend the theoretical and experimental work firstly introduced in [21], and show the generalizability of the CS to different robotic hands and different grasp types.

Computation of the Closure Signature (CS)

The computation of the Closure Signature requires to identify and track a set of reference points located on the hand. The CS of the hand performing a given closure motion is then defined as the direction along which the set of reference points is most deformed during that motion, and is characterized by an application point $\mathbf{o}_h$ and a unit vector $\mathbf{v}_{CS}$.

Reference points can be placed in different locations, however they must be representative of the analyzed closing motion. Trivially, if during a hand closure the palm is still, reference points should be placed in the fingers rather than in the palm. As long as reference points are chosen with the rationale of favouring the parts of the hand that move more during the selected motion, the transformation has low sensitivity to the reference points location [22].

For a given robotic hand, let us consider n_{ref} reference points. At the end of the tracking procedure, we have a path with n_s samples for

each reference point

$$r_j(k) \in \mathbb{R}^3, \quad j = 1, \ldots, n_{ref}, \quad k = 1, \ldots, n_s.$$

Let us indicate with $\mathbf{r}_{j,in} = \mathbf{r}_j(1)$ and $\mathbf{r}_{j,fin} = \mathbf{r}_j(n_s)$ the coordinates of a generic reference point j in its initial and final configuration, respectively. We assume that the variation of the reference points can be represented as a linear transformation $\mathbf{T}$, i.e., for each point $\mathbf{r}_j \in \mathbb{R}^3, j = 1, \ldots, n_{ref}$, we can write

$$\hat{\mathbf{r}}_{j,fin} = \mathbf{T}\hat{\mathbf{r}}_{j,in}, \tag{1.1}$$

where the symbol $\hat{}$ indicates the homogeneous representation of the vector.

The 4×4 matrix

$$\mathbf{T} = \begin{bmatrix} t_1 & t_2 & t_3 & t_4 \\ t_5 & t_6 & t_7 & t_8 \\ t_9 & t_{10} & t_{11} & t_{12} \\ 0 & 0 & 0 & 1 \end{bmatrix} = \begin{bmatrix} & \mathbf{A} & & \mathbf{b} \\ 0 & 0 & 0 & 1 \end{bmatrix} \tag{1.2}$$

is a homogeneous matrix, where $\mathbf{A}$ is a 3×3 matrix representing the linear map and $\mathbf{b}$ is a three-dimensional vector representing the translation [23].

Let us define the vectors containing the initial and final positions of all reference points, $\mathbf{r}_{in} = [\mathbf{r}_{1,in}^T, \cdots, \mathbf{r}_{n_{ref},in}^T]^T$ and $\mathbf{r}_{fin} = [\mathbf{r}_{1,fin}^T, \cdots, \mathbf{r}_{n_{ref},fin}^T]^T$

respectively. According to Eq. (1.1), we can write

$$\hat{\hat{\mathbf{r}}}_{fin} = \begin{bmatrix} \mathbf{T} & \mathbf{0} & \dots & \mathbf{0} \\ \mathbf{0} & \mathbf{T} & \dots & \mathbf{0} \\ \vdots & \vdots & \ddots & \vdots \\ \mathbf{0} & \dots & \mathbf{0} & \mathbf{T} \end{bmatrix} \hat{\hat{\mathbf{r}}}_{in},$$

where the symbol $\hat{}$ indicates that the vectors contain the homogeneous representations of all the single vectors they include.

To find matrix $\mathbf{T}$ we can solve the linear system

$$\mathbf{r}_{fin} = \mathbf{M}\mathbf{t}, \tag{1.3}$$

where matrix $\mathbf{M} \in \mathbb{R}^{3n_{ref} \times 12}$ is defined as

$$\mathbf{M} = \begin{bmatrix} \mathbf{M}_1 \\ \dots \\ \mathbf{M}_{n_{ref}} \end{bmatrix}, \quad \mathbf{M}_j = \begin{bmatrix} \hat{\mathbf{r}}_{j,in}^T & \mathbf{0}_{1,4} & \mathbf{0}_{1,4} \\ \mathbf{0}_{1,4} & \hat{\mathbf{r}}_{j,in}^T & \mathbf{0}_{1,4} \\ \mathbf{0}_{1,4} & \mathbf{0}_{1,4} & \hat{\mathbf{r}}_{j,in}^T \end{bmatrix} \in \mathbb{R}^{3\times 12}$$

and vector $\mathbf{t} \in \mathbb{R}^{12}$ contains the components of $\mathbf{T}$ (see Eq. (1.2)), $\mathbf{t} = \begin{bmatrix} t_1, \cdots, t_{12} \end{bmatrix}^T$. The resulting $\mathbf{T}$ matrix represents the average transformation between the initial and final reference points positions.

The solution of the system depends on the properties of matrix $\mathbf{M}$. Basically, if $rank(M) < 12$, the system admits infinite solutions, and is not possible to identify a unique $\mathbf{T}$ matrix. This case occurs when $n_{ref} < 4$ or when in the initial configuration they lie on the same plane. However, the problem can be reformulated by considering more restrictive conditions on $\mathbf{T}$ (e.g., if a planar transformation is assumed, only 6 elements of $\mathbf{T}$ are independent).

If matrix $\mathbf{M}$ is square and full-rank, the system has a unique solution, and $\mathbf{T}$ satisfies exactly Eq. (1.1) for all the reference points.

If matrix $\mathbf{M}$ is full-rank, but $\mathbf{n}_{ref} > 4$, the system does not admit a solution in general, i.e., it is impossible to find a homogeneous transformation able to represent the displacement of *all* the reference points. In this case the $\mathbf{T}$ matrix elements evaluated by means of $\mathbf{M}$ pseudo-inverse are those minimizing the overall quadratic error $\|\mathbf{Mt} - \mathbf{r}_{fin}\|^2$. $\mathbf{T}$ represents then an average approximation of all the motions of the reference points.

Matrix $\mathbf{T}$ represents a generic linear transformation, that can be further decomposed into a composition of primitive transformations [24], that can be written in a compact way as:

$$\mathbf{T} = \mathbf{T}_{rb}\mathbf{T}_{def}.$$

where $\mathbf{T}_{rb}$ refers to a rigid body motion and $\mathbf{T}_{def}$ to a deformation.

We relate the CS to $\mathbf{T}_{def}$ assuming that the non-rigid part of the motion is strictly related to the grasp tightness. This consideration comes from literature on grasp analysis. [25] demonstrated that, in a grasp such that *internal forces* can be exerted, i.e., the object can be squeezed, the rigid body motions are defined as coordinated hand/object motions in which contact forces are constant, while the non-rigid deformation is related to contact force variations. [26] showed that contact force variations due to hand activation are *internal*, i.e., they are self balanced, and demonstrated that they play a key role in grasp stability. In other words, the rigid body component mainly contributes to the motion of the grasped object, while the non-rigid part is strictly related to the grasp tightness. This distinction characterizes the hand motion itself,

and is not object-dependent. This is why it can be applied to the CS computation, even though the CS is based on the analysis of the free hand motion.

Among the available methods in literature to decompose a generic 4×4 matrix into a product of simpler transformations, we require one that allows the distinction between rigid and non-rigid components. The extraction of the translation part of the rigid body motion from the starting matrix $\mathbf{T}$ is straightforward considering (1.2). The matrix $\mathbf{A}$ in Eq. (1.2) can be written, with the polar decomposition, as the product

$$\mathbf{A} = \mathbf{RU},$$

in which $\mathbf{R} \in SO(3)$ is orthogonal and represents a rigid rotation, and $\mathbf{U}$ is a positive-semidefinite Hermitian matrix that takes into account the non rigid deformation [27]. $\mathbf{U}$ in general contains both anisotropic scaling and shear deformation components, however it is possible to identify three principal directions defining a frame with respect to which the transformation is a pure anisotropic scaling. Such directions can be identified as the eigenvectors of $\mathbf{U}$ matrix, while the corresponding eigenvalues represent scaling factors.

Definition: Closure Signature. Let us indicate with λ_i and $\mathbf{v}_i$ ($i = 1,2,3$) the eigenvalues and the eigenvectors of the matrix $\mathbf{U}$, respectively, and with $\mathbf{o}_h$ the centroid of the reference points trajectories computed as $\mathbf{o}_h = mean(\mathbf{r}_j(k) \in \mathbb{R}^3, k = 1,\ldots,n_s, j = 1,\ldots,n_{ref})$. The closure signature CS is defined as the direction of the eigenvector corresponding to the smallest eigenvalue of $\mathbf{U}$, $\mathbf{v}_{CS} = [v_{cs,x}, v_{cs,y}, v_{cs,z}]^{\mathrm{T}}$, applied in $\mathbf{o}_h$. □

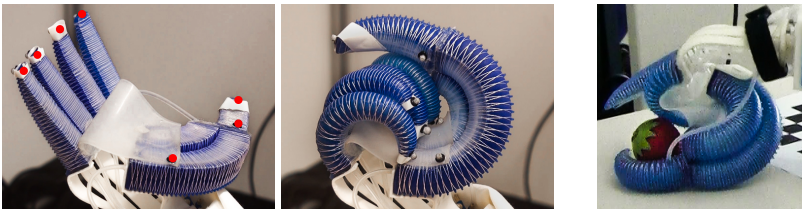

(a) (b)

Fig. 1.2 Power grasps with the RBO Hand 2. (a) "Heavy wrap" closing motion: from fully open (left) to fully closed hand (right). Reference points are indicated with red dots over the open hand. (b) Example of "lateral pinch".

1.1.1 Closure signature for power grasps

The CS of the Pisa/IIT SoftHand complete closing motion (i.e., from completely open to completely closed) was computed in [21]. The top-grasps performed using this information had greater success rate and robustness with respect to a baseline method.

In this Chapter, the generality of the CS computation for power grasps is shown by applying it to the pneumatically actuated RBO Hand 2 [14], that significantly differs from the Pisa/IIT SoftHand.

Concerning the complete closure of all the fingers, we investigated a motion resembling the first hand synergy (see [28]), obtained by actuating all the RBO Hand 2 DoAs. Seven reference points (shown in Fig. 1.2a), 5 located on the fingertips of the hand and 2 on the palm, are chosen and tracked with a motion capture system (Motion Analysis). We will refer to this closure with the expression "heavy wrap" [29].

Moreover, we will investigate another type of power grasp, the "lateral pinch" [30] (see Fig. 1.2b), considering a subset of 4 reference points located in the palm and in the thumb and index fingertips. Fig. 1.3

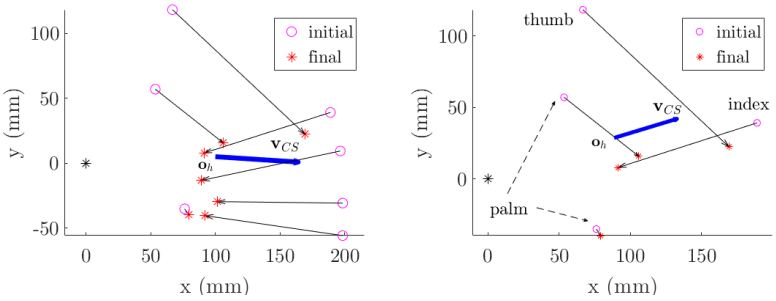

Fig. 1.3 RBO Hand 2: CS computation ($\mathbf{o}_h$, $\mathbf{v}_{CS}$) for two different closing motions. The device is a right hand and is seen from the top. The points are expressed in a reference frame placed on the hand wrist, with x-axis pointing towards the middle finger, y-axis pointing in the direction of the thumb and z-axis exiting from the plane. Magenta circles and red stars indicate initial and final positions of the reference points, respectively. (a) Closure signature of the heavy wrap motion (shown in Fig. 1.2a), when considering 7 reference points: 5 in the fingertips, 2 in the palm. (b) Closure signature of the lateral pinch motion that corresponds to the grasp shown in Fig. 1.2b, when actuating only index, palm and thumb. Reference points are placed in the palm and in the fingertips of the thumb and of the index.

reports initial and final positions of the reference points and the Closure Signature corresponding to these two different motions.

In a reference frame placed on the hand wrist, with x-axis pointing towards the middle finger, y - axis pointing in the direction of the thumb and z- axis exiting from the plane, the CS for the power grasp is $\mathbf{v}_{CS} = [0.9164, -0.0592, -0.3958]$ mm and $\mathbf{o}_h = [100, 5, -30]$ mm. The CS for the lateral pinch is $\mathbf{v}_{CS} = [0.8847, 0.2668, -0.3822]$ and $\mathbf{o}_h = [89, 29, 35]$ mm. As it can be noticed, the CS direction, $\mathbf{v}_{CS}$, slightly varies between the two cases, but this is not the most relevant aspect. What really makes the difference in the closure description - and also in the experiments - is that in the second case the center of the

CS, $\mathbf{o}_h$, falls between the thumb and the index, thus allowing a good alignment with the object to perform a lateral pinch, as in Fig. 1.2b.

1.1.2 Closure Signature for precision grasps

Most of the soft hands known in literature are designed to perform power grasps where fingers completely envelop the object. Using these hands to perform *precision grasps* is often an issue, due to the low number of controllable degrees of freedom (DoFs) and to the lack of accurate on-line proprioceptive measurements necessary to precisely place the fingertips over an object.

To properly describe a precision grasp exploiting the CS approach, we considered appropriate to split the closing motion in two subsequent sub-movements: *i)* from a starting configuration to a pre-shaping configuration, where a *pre-shaping configuration* is intended to be an intermediate configuration of the hand during the closing motion, and *ii)* from the pre-shaping configuration to the completely closed hand configuration. As we showed in [20], tracking the reference point during motion *i)* or during the complete motion *i)+ ii)* leads to a little variation in the CS direction. However, what changes most is the application point $\mathbf{o}_h$. When dealing with precision grasps, we considered more meaningful to track the reference points only in step *ii)*. The rationale is that hand pre-shaping is important to guarantee contacts at the fingertips. Approaching the object with the hand partially closed, in fact, allows to perform a small closure near the object, without executing the whole closure, which might cause undesirable collisions with the object, often reorienting the object and causing a grasp failure.

(c) (d)

Fig. 1.4 Pisa/IIT SoftHand: Partial closure for precision grasps. (c) Example of pinch grasp: Initial configuration (partially closed hand) and final configuration (fully closed hand) of the partial closure motion.

Hence, to provide an example of Closure Signature for precision grasp (Fig. 1.4c), we used the Pisa/IIT SoftHand and considered reference points located only in the thumb (fingertip, proximal phalanx) and the index (fingertip, middle phalanx), whose trajectories were tracked in the Gazebo simulator. The closure motion under consideration starts with the hand partially closed (half of its range of motion), and ends with the hand fully closed (see Fig. 1.4d). Assuming a reference frame placed on the hand wrist with x-axis pointing towards the middle finger, y-axis pointing in the opposite direction with respect to the thumb and z-axis exiting from the plane, $\mathbf{v}_{CS} = [0.74, 0.67, -0.01]$ mm and $\mathbf{o}_h = [98, -36, -31]$ mm, shown in Fig. 1.5.

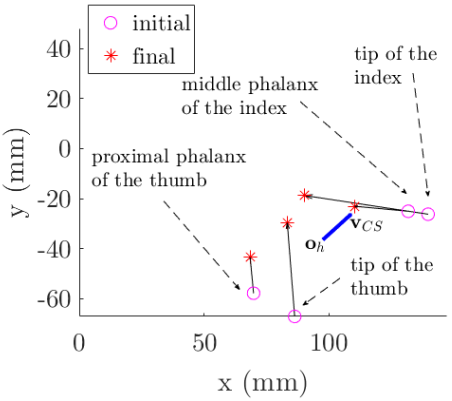

Fig. 1.5 Pisa/IIT SoftHand: CS computation ($\mathbf{o}_h$, $\mathbf{v}_{CS}$) for performing precision grasps. The device is a left hand and is seen from the top. The points are expressed in a reference frame placed on the hand wrist, with x-axis pointing towards the middle finger, y-axis pointing in the opposite direction with respect to the thumb and z-axis exiting from the plane. Magenta circles and red stars indicate initial and final positions of the reference points, respectively. Closure signature for the motion illustrated in Fig. 1.4d, considering reference points placed in the fingertip and proximal phalanx of the thumb and fingertip and middle phalanx of the index.

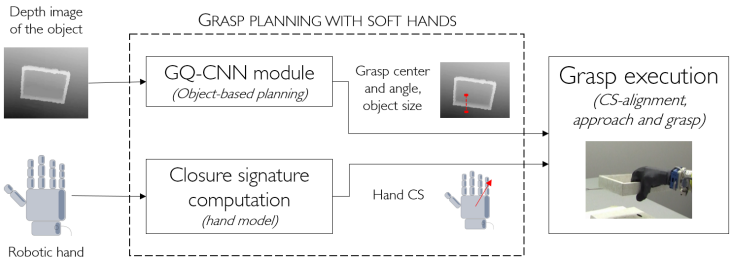

Fig. 1.6 Block diagram of the proposed approach.

1.2 Grasp planner

As previously mentioned, the Closure Signature is ment to be a tool for grasp planning and execution with soft hands. Our grasp planner is composed of two modules, one object-centric and the other one hand-centric. The former is related to grasp planning with the aid of Artificial Intelligence, and we named it *GQ-CNN module*. Given a depth image of the object to be grasped, it exploits all the encapsulated information and provides an on-line estimate of the optimal grasp (center and direction) to be performed. The latter module is related to soft hand modeling, and we termed it *CS module*. Chosen a robotic hand, such a module computes off-line the functional model of a certain closure (i.e., the previously defined Closure Signature), thus providing an estimate of the best way to align the hand to an object for performing top-grasps. As shown in Fig. 1.6, and detailed in the following, the two modules are put together to align the hand to the object. Then, the grasp can be executed.

As we mentioned above, the idea behind this module integration is that the CS allows to approximate a hand closure with a direction, and

this direction can be thought as the closing direction of an equivalent parallel-jaw gripper. In other words, the CS abstraction allows to use a planner that was trained for parallel-jaw grippers without retraining it, even if the end-effector is different.

In the proposed approach, the softness of the hand is not explicitly modeled, but it is the condition that actually allows us to apply such a simplified grasp planning strategy. The passive adaptability typical of soft hands allows to compensate for the adopted simplifications (grasp planner for rigid parallel-jaw gripper, hand modeling as a jaw-gripper), to cope with uncertainties, and to safely interact with the environment. This would not be possible with rigid hands, for which even small uncertainties in the fingers positioning might lead to unwanted and dangerous collisions with the environment [13].

1.2.1 Grasp Quality Convolutional Neural Network (GQ-CNN) module

The Grasp Quality Convolutional Neural Network (GQ-CNN) has been presented by [19]. It is the core component of the so-called *CEM-augmented DexNet 2.0 grasp planner*, which can be used for grasp planning, since it provides an estimation of the most robust grasp under uncertainties in sensing and control. The planner considers a parallel-jaw gripper performing top-grasps of objects resting on a planar surface. Given a depth image of the object to be grasped, a set of grasp candidates is sampled with the rejection sampling algorithm [31], and the robustness of each candidate is evaluated by the neural network. This step is shown in the first image in Fig. 1.7, where the different colors correspond to different robustness values. After this preliminary step,

the most robust grasps, i.e., the "elite grasps", are selected. Then, the cross-entropy method (CEM) iteratively computes a Gaussian Mixture Model of the most robust grasps, and new grasp candidates are sampled from this distribution ("sampled grasps"). This procedure is iterated for a predefined number of times, after which the most robust grasp is selected (see Fig. 1.7). Its center ($\mathbf{o}_{NN}$) and direction ($\mathbf{v}_{NN}$) are returned as outputs of the planner.

The image of the object to be grasped is acquired thanks to an overhead depth camera, and the estimation of the grasp candidate robustness is achieved by feeding the GQ-CNN with the candidate center depth z relative to the camera and the depth image. The grasp robustness is computed by means of the so-called robustness function Q, which, given the grasp u and the point cloud y of the object, returns the probability of the grasp success S:

$$Q(u,y) = \mathbb{E}[S \mid u,y].$$

Uncertainties in sensing are included in the problem formulation [19]. The approximation $Q_\theta(u,y)$ of the function Q was learned by the GQ-CNN, and the evaluation on the grasp candidates allows to apply a grasping policy selecting the grasp that maximizes the success:

$$\pi_\theta(y) = \arg\max_{u \in C} Q_\theta(u,y),$$

where C is a discrete set of grasps respecting some constraints. Learning the robustness function Q instead of the policy π allows enforcing specific task-constraints without the necessity of retraining the neural network. The GQ-CNN has been trained only on the synthetic data

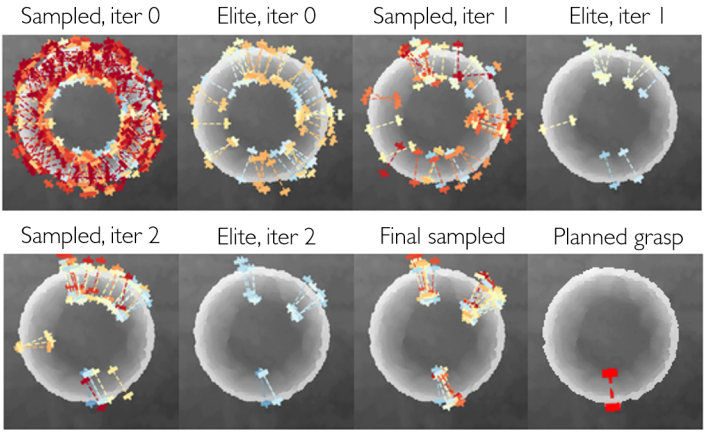

Fig. 1.7 Subsequent steps for finding the most robust grasp.

collected in the so-called Dexterity Network (Dex-Net) 2.0, which is a dataset consisting in 6.7 million data points and associating parallel-jaw grasps with analytic grasp quality measures. Although the neural network was trained only on synthetic data, the CEM-augmented version of the planner achieved a 94% of success rate [19].

In addition to the grasp center $\mathbf{o}_{NN}$ and direction $\mathbf{v}_{NN}$, our object-centered module outputs also the estimated *actual width* of the object along the grasping direction. The expression "actual width" of the object refers to the width of the object that will be actually involved during the grasp execution, and neglects lower parts of the object that cannot be reached by the hand during the top-grasp.

We devised an algorithm that provides such estimate based on the inspection of the data captured by the depth image. First, a mask is applied to the raw depth data in order to store only the data related to the object to be grasped. Let us denote with $\mathscr{V}$ the set of these valid

points. Each element of $\mathscr{V}$ contains the spatial coordinates of the pixel it refers to with respect to a reference system associated to the depth camera. Then, in the set of candidates $\mathscr{C}$, we store only the elements of $\mathscr{V}$ satisfying the condition $|z - z_G| < \varepsilon$ and belonging to the line passing through $\mathbf{o}_{NN} = [x_G, y_G, z_G]$ with angular coefficient related to the estimated grasping direction $\mathbf{v}_{NN}$. ε is the largest projection on the vertical direction of the distance between the fingers and the palm during the closing motion. Among the points stored in $\mathscr{C}$, i.e., all the points lying on the line, we consider only those that are antipodal with respect to the grasp center, and we search for the two that are at the maximum distance. We considered this distance as the estimated size of the object along the grasping direction.

1.2.2 Closure Signature (CS) module

The CS module implemented for the experimental validation of the proposed approach involves the off-line computation of the CS corresponding to:

- the complete closure motion (heavy wrap) of the Pisa/IIT SoftHand (computed in [21]);
- the complete closure motion (heavy wrap) of the RBO Hand 2 (computed in the previous section);
- a partial closure motion of the RBO Hand 2 leading to a lateral pinch (computed in the previous section);
- a partial closure motion of the Pisa/IIT SoftHand leading to a precision grasp (computed in the previous section).

It is worth remarking that, in general, if the considered robotic hand can perform more than one closure motion (e.g., power and precision grasps), a list of closure signatures can be associated to the hand. In this case, the CS module could automatically perform an on-line selection of the most suitable CS to be used for grasp execution. The choice could be based on the object size, computed, for example, as previously explained. To select the best CS, one could either leverage intuitive rules as those that we applied in the experiments here described (e.g., heavy wrap for objects with a size that is comparable with that of the hand, lateral pinch and precision grasp for smaller objects), or rely on an algorithm that compares the object size with a certain *size* associated to the closure signature. A strategy could be the following: among the closure signatures with sizes that are bigger than the object size, the CS whose size is the closest (or second closest) to the object size would be a good candidate for the grasp. Research on establishing this "CS size", however, is still on-going, since it is not trivial to identify a general way of evaluating the size of a closure only based on the motion of the reference points, and taking into account that the hand has to achieve a certain orientation over the object.

1.2.3 Modules integration: grasp planning with soft hands

The Closure Signature provides a simplified way to treat soft hands characterizing a specific closing motion that the hand can achieve through a direction of maximum closure applied at a certain point. The obtained center and direction can be thought as the grasping center and direction of a parallel-jaw gripper. This is the fundamental principle of the proposed integration between the GQ-CNN module and the CS

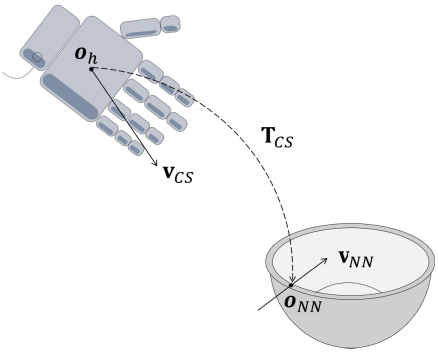

Fig. 1.8 General CS-alignment procedure.

module. We named *Planning with soft hands* the resulting module, which was then integrated with the *Grasp Execution* module, allowing object approaching and grasping (Fig. 1.6).

The GQ-CNN output data and the CS hand model are combined to perform the so-called *CS-alignment*, i.e., the alignment between the hand CS and the grasp angle and center retrieved by the neural network. In general, this can be achieved by computing the transformation $\mathbf{T}_{CS}$ that brings $\mathbf{o}_h$ on $\mathbf{o}_{NN}$ and aligns $\mathbf{v}_{CS}$ with $\mathbf{v}_{NN}$ (see Fig. 1.8).

Let us consider a world reference frame $\{\mathbf{W}\}$ that has the xy-plane parallel to the surface over which the object is lying, and the z-axis exiting from it. Since the GQ-CNN outputs assume that the direction of closure of the gripper lies always on the table, the fist step is to align the CS parallel to the xy-plane.

Let us indicate with α the angle between CS and the $xy-$plane, and with θ the angle between CS projection on $xy-$plane and $\mathbf{v}_{NN}$, these angles are not shown in Fig. 1.8 for the sake of clarity. The

overall transformation $\mathbf{T}_{CS}$ to be imposed to the hand reference frame to perform the *CS*-alignment will result from the combination of a rotation of α with respect to an axis parallel to the plane xy, a rotation of θ with respect to the z-axis, and a translation between $\mathbf{o}_h$ and the center of the grasp $\mathbf{o}_{NN}$.

1.3 Experiments

The experimental validation of the proposed approach consists of three experiments.

- *Experiment 1* evaluates the capabilities of the grasping policy integrating CS-alignment and GQ-CNN module in terms of success rate over a large object dataset. The Pisa/IIT SoftHand is used for performing heavy wrap power grasps.
- *Experiment 2* assesses the applicability of the proposed approach to heavy wraps performed with an intrinsically soft robotic hand, the RBO Hand 2. Results obtained with our grasp planner are compared to a baseline method, called S-alignment.
- *Experiment 3* tests the functioning of the devised grasp planner for performing grasps that are not heavy wraps: lateral pinch and precision grasps.

While the advantages of using the CS when planning heavy wraps with the Pisa/IIT SoftHand, compared to aligning the hand straight with the object, has already been established in [21], Experiment 1 aims to verify the success of its integration with the GQ-CNN module, that relies on a grasp planner for parallel-jaw grippers.

The purpose of Experiment 3 is to show that the CS-alignment also works for grasps that are less commonly implemented with soft hands. Since, to the best of our knowledge, there is no well-established baseline in the literature for such types of grasps performed with soft hands, comparison with other strategies remains an open problem.

1.3.1 Experimental setup

We performed experiments either with a 7 DoF Sawyer collaborative robot arm (Rethink Robotics) or with a LBR iiwa (KUKA AG), having an ATI Gamma 6-axis force-torque sensor (ATI Industrial Automation, Inc.) and either a Pisa/IIT SoftHand [10] or a RBO Hand 2 [14] mounted on its end-effector (Fig. 1.9). The depth image of the object to be grasped was acquired with an Asus Xtion PRO Live camera (ASUSTeK Computer Inc.) positioned in front of the robot, at a distance from the tabletop in the range 55-70 cm, similarly to [19]. We used ROS to implement information exchange between devices [32]. Experiments ran on a notebook having the Intel Core i7-8750H as processor and the Nvidia GeForce GTX 1050 as GPU. On average, the GQ-CNN module returned an output in 0.9 s.

We tested our grasping policies on objects having different weights and shapes. Adversarial surface properties, e.g., reflectivity, smoothness, softness and roundness were considered. Depending on the performed experiment, we used all or a subset of the objects that are shown in Fig. 1.10, and whose properties are listed in Table 1.1.

The cylindrical chips can and the cuboid boxes are objects with prototypical shapes. The funnel and the bowling pin are interesting because they can easily roll and generate unwanted dynamic behaviors

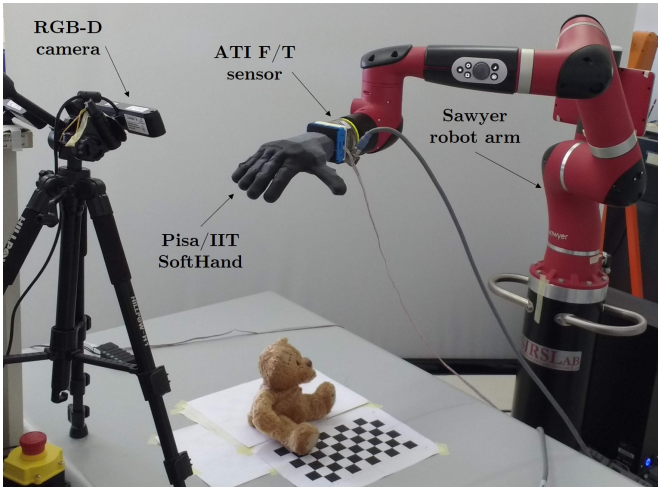

(a) Experimental setup with Pisa/IIT SoftHand

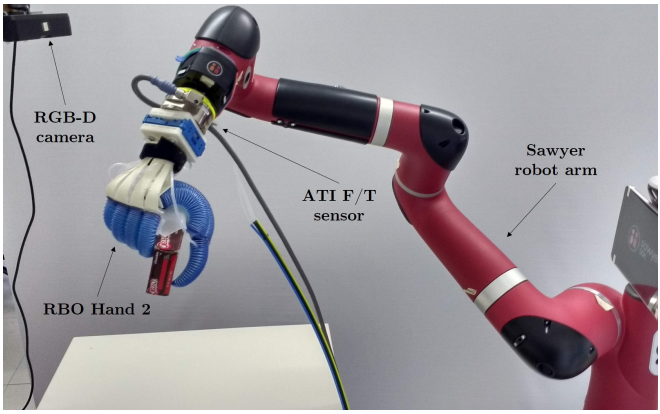

(b) Experimental setup with RBO Hand 2

Fig. 1.9 Experimental setup: the RGB-D camera detects the object on the table and the robotic arm equipped with a force/torque sensor and a soft hand executes the grasp.

Table 1.1 Physical properties of the objects used in the experiments. The chips can, the pudding and sugar boxes, the small cube, the Lego Duplo piece and the strawberry are taken from the YCB Dataset [33]. d and h denote object diameter and height, respectively.

Object	Size (mm)	Weight (g)
chips can	$d = 75,\ h = 250$	205
cuboid box	$200 \times 100 \times 40$	51
sugar box	$175 \times 89 \times 38$	514
pudding box	$110 \times 89 \times 35$	187
funnel	$d = 140,\ h = 140$	45
bowling pin	$h = 170$	17
big funnel	$d = 150,\ h = 70$	96
plastic bowl	$d = 200,\ h = 75$	84
hollow box	$220 \times 165 \times 45$	52
plastic toy	$h = 90$	66
teddy bear	$h = 170$	111
small cube	$h = 25$	8
Lego Duplo piece	$42 \times 30 \times 30$	13
strawberry	55×43.8	18
small vial	$d_{max} = 20, h = 50$	15

Fig. 1.10 Objects set (from back to front, from left to right): hollow box, sugar box, chips can, funnel, teddy bear, cuboid box, big funnel, plastic bowl, pudding box, bowling pin, strawberry, Lego Duplo piece, small cube, plastic toy. (The small cube, the Lego Duplo piece, and the strawberry are standard objects taken from the YCB Dataset [33])

when touched by the hand, due to their roundness, non regular shape, and lightness. The plastic bowl, the hollow box, and the big funnel are objects that should be picked up from their edges. The approach followed in [21], based on building the bounding box of the entire object, would lead to failures in these cases, since the grasp center would end up to be in the hollow part of the object. The plastic toy was chosen as it has a rather irregular surface. The teddy bear was selected because it is made of compliant material, but is not soft and lightweight enough to undergo large deformations modifying its shape and spatial configuration when the hand touches it. The occurrence of such deformations would lead to results possibly unrelated to the planning output.

The first 11 objects were used in Experiment 1, and a subset of them was used in Experiment 2, as they are suitable to be grasped with heavy wraps. The small cube, the Lego Duplo piece, the strawberry, and the small vial are relatively small objects with respect to the used hands and might require delicate handling (strawberry). This is why they were used in Experiment 3, when testing lateral pinch and precision grasps.

1.3.2 Experiment 1: Evaluation of the modules integration

The aim of Experiment 1 was to evaluate the CS exploitation integrated with a grasp planner specifically designed for parallel-jaw grippers. We performed top-grasp experiments with a right Pisa/IIT SoftHand attached to a Sawyer robot arm.

The hand-object alignment was executed at fixed height from the tabletop using the motion planning provided by MoveIt[2]. The robot mo-

[2]https://moveit.ros.org/

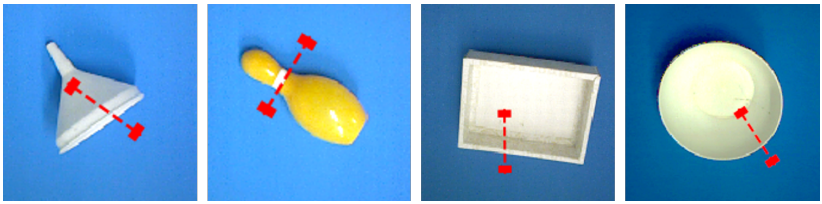

Fig. 1.11 Examples of planned grasps for some of the chosen objects.

tion was then controlled by means of a feedback-driven state machine, and the hand closed when a certain force threshold was exceeded due to the occurred contact between the hand and the object. During experiments, objects were placed in a random pose in the robot workspace. Fig. 1.11 shows examples of planned grasps[3]. A grasp was considered successful when the hand could stably hold the object while the arm was lifting for 6 seconds with a velocity of 3 cm/s. For each object, 10 grasp attempts were performed. The overall success rate is $97/110$ ($\sim 88\%$). Numerical results per object are reported in [20].

1.3.3 Experiment 2: Application of the method to another soft hand

To investigate the generalizability of the proposed grasp planning strategy, we test it with the intrinsically soft RBO Hand 2. The hand Closure Signature for the complete closure was computed as explained in the previous section. Then, we performed top grasps over four different objects, representative of three classes of objects that are present in Table 1.1: those with a prototypical shape (chips can, cuboid box), those

[3]Note that, to better observe dynamical effects during hand-object interactions, the chips can, the funnel and the bowling pin were always lying on the tabletop in horizontal position, as shown in Fig. 1.11.

that easily roll over the table top (bowling pin), and those that have a hollow part (bowl).

To investigate if exploiting the RBO Hand 2 CS-alignment allows better grasping performance, we compared it with the baseline hand alignment used also in [21]. Such baseline has been called S-alignment (i.e., straight alignment) and consists in aligning the hand middle finger parallel to the chosen direction on the object, similarly to [7, 21].

As in Experiment 1, a grasp was considered successful when the hand could stably hold the object while the arm was lifting for 6 seconds with a velocity of 3 cm/s. Moreover, for each object, 10 grasp attempts were performed. The total success rate of the CS-alignment is 90%, and of the S-alignment is 42.5%.

1.3.4 Experiment 3: Other types of grasps

1.3.4.1 Lateral pinch

We implemented another type of power grasp with the RBO Hand, a lateral pinch (see Fig. 1.2b), using the CS computed as in Fig. 1.3. We tested the strategy with two cuboid objects with different sizes (small cube, Lego Duplo piece) and one round object (strawberry). We observed that with the strawberry and the Lego Duplo piece, the grasp was always successful, while it always failed with the small cube. The trends were so clear that we limited to 5 the number of trials per object. The grasp execution was implemented as for the heavy wrap presented above: the hand started closing when a certain force threshold was overcome. It is interesting to notice that in the case of the lateral pinch, such event was determined by the exploitation of environmental constraints: the hand contacted the table, the force

threshold was exceeded and triggered the closing motion, the fingers slid on the table and then performed the grasps.

1.3.4.2 Precision grasp

To show that the CS model can also be exploited for closures leading to precision grasps, we tested the previously computed CS for the index and the thumb of Pisa/IIT SoftHand to plan precision grasps over a small cube and a small vial (see Table 1.1 for their properties). In this case, we chose two very small objects, requiring a precision grasp, one with a squared base, and one with a round base. The hand pre-shaping and the height from the table were selected according to the object size. In particular, the hand started closing at a height such that the fingers almost touched the table. The overall success rate is 0.75 (small cube 7/10, small vial 8/10). In this case, we used a left Pisa/IIT SoftHand attached to a KUKA LBR iiwa robot arm.

1.4 Discussion

1.4.1 Experiment 1: The module integration works well for planning top-grasps with soft hands

The grasping task that we consider is mainly composed of two complementary sub-tasks: object-centric grasp planning (i.e., the problem of identifying which are the best contact point locations satisfying a given criterion) and the grasp execution (which relies on the closing motion of the chosen hand). The two parts have already been validated separately. The GQ-CNN module providing the grasp planning has been compared with other methods in [19].The CS module providing the functional

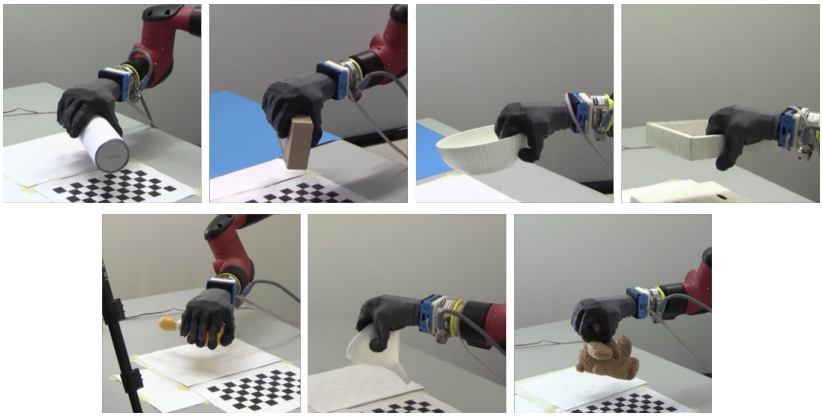

Fig. 1.12 Some of the successful grasps with the Pisa/IIT SoftHand.

hand model involved in the grasp execution has been tested in [21], by comparing the CS-alignment with the so called S-alignment.

In this work, we show that the integration between the two modules not only is feasible, but also allows grasping objects that would have been impossible to grasp with the simple bounding-box based grasp planner used in [21]. Planning how to grasp an object based only on its bounding box may lead to an oversimplificated representation of the object, and cannot be successfully applied to object categories such as, for example, hollow objects, since the hand would end up on the empty part of the object (instead of on an edge).

Failures and successes observed during the experimental trials depend on multiple aspects: the interaction between the hand and the object, the setup features (hand characteristics, robot workspace, etc.), and the planned grasp. Examples of successful and unsuccessful grasps are shown in Figs. 1.12 and 1.13, respectively.

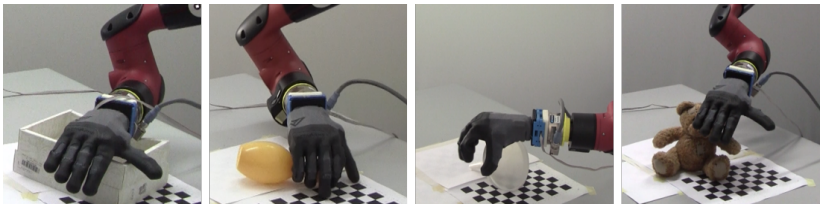

Fig. 1.13 Some of the unsuccessful grasps with the Pisa/IIT SoftHand.

Our approach was always successful for the objects with a prototypical shape. This is something that was expected for two reasons: *i)* for these objects, the neural network typically outputs a grasping point that is very close to the object center of symmetry as seen from the top, and *ii)* results described in [21] show that, with the CS-alignment, regular objects are picked up most of the times. There was only one failure on the sugar box, due to its weight. Also the plastic toy was grasped as if it was a small box, and its irregular surface did not prevent grasps from being successful.

A high success rate was obtained also for objects that can be picked up from edges, i.e., the bowl, the hollow box, and the big funnel. Failures with the hollow box were due to collisions between hand wrist and object (see Fig. 1.13), whereas those with the big funnel were due to the fact that the network output a grasp center on the smaller opening of the funnel and the "actual width" of the object was so large that the hand lied on the object without being capable of trapping it.

When complex objects were considered, our approach still resulted successful most of the times, but additional considerations should be done: *i)* The funnel was correctly grasped when either the fingers or the thumb were placed inside the cave part of the object (see Fig. 1.13). One of the failures was due to the planned grasp, that was significantly

laterally displaced from the center, thus leading to an unwanted object motion when the contact with the hand occurred. The other failure was caused by an accidental collision between the hand and the object, leading to a displacement of the funnel. *ii)* Bowling pin failures occurred when the grasp center was in proximity of the object neck (see Fig. 1.13). In these cases, in fact, the hand entered in contact with the object in a region that was higher than the goal point, and remained stuck there. The force threshold was thus exceeded too soon and the hand closed without being in contact with the right grasp center and without caging the object. *iii)* For the teddy bear, the failure occurred because the planned grasp center was near to the ear, and this led to a lateral head displacement during the grasp execution.

1.4.2 Experiment 2: The Closure Signature computation and use generalizes well to other soft hands

The Pisa/IIT SoftHand and the RBO Hand 2 are different devices with different possible motion capabilities (see *Part A*). This reflects in the CS computation of the whole hand closure with heavy wrap [29]. While the first hand generates a deformation that remains mainly in the *xy*-plane, the second produces a more complex 3D motion, not only due to the thumb and palm actuation, but also related to the specific way in which each finger closes, i.e., by depicting a sort of self-rolling spiral. If compared with the RBO Hand 2, the Pisa/IIT SoftHand has a less spiral-like closing motion, due to the different actuation, resulting in a different desired alignment between the hand and the object.

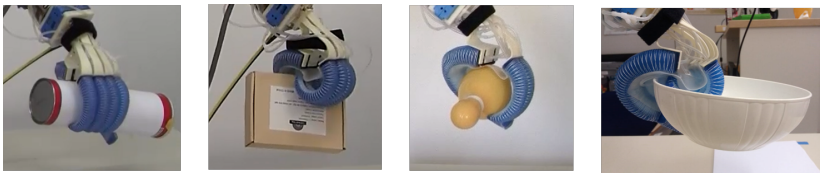

Fig. 1.14 Examples of successful grasps with the RBO Hand 2.

For the Pisa/IIT SoftHand, the angle θ around the axis normal to the table is more relevant. The RBO Hand 2, instead, requires also a rotation about an axis parallel to the plane of the table.

It could happen that for some physical constraints it is not possible to make both rotations, for example, due to possible collisions of the robot arm with the table while aligning the hand. In these cases it could be better to privilege the alignment with the angle θ than the angle α, since θ is on the plane of the grasp. In other terms, aligning the hand with a wrong θ, may increase the possible grasp failures. Aligning the hand with a wrong α, instead, could be better compensated by the intrinsic compliance of the hand.

Examples of successful and unsuccessful grasps with the RBO Hand 2 are shown in Fig. 1.14 and Fig. 1.15, respectively. The CS-alignment for the heavy wrap of the RBO Hand 2 is effective with prototypical objects, apart from a failure with the box which was due to the fingers touching the box and moving it before starting to close. Also the bowl was always grasped successfully. The bowling pin remains a difficult object to grasp (*cf.* results of Experiment 1), mainly due to the fact that sometimes the planned grasp center lies on the neck of the pin, or to object displacements resulting from unwanted collisions with the hand.

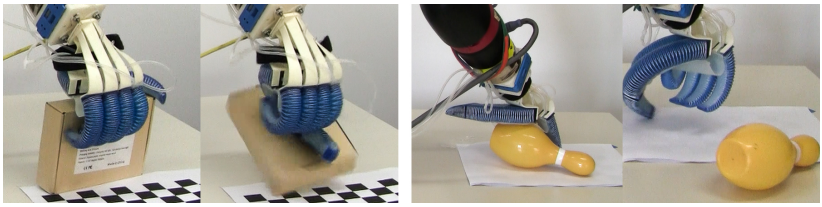

Fig. 1.15 Examples of failures with the RBO Hand 2.

Concerning the baseline method, we observed that *i*) the performed grasps were not robust enough to stably lift the object, and *ii*) regarding the chips can, the failures were due to its weight and to the fact that the palm could not envelop it properly, since the palm lied on the can and the finger rolling motion prevented the thumb opposability exploitation.

1.4.3 Experiment 3: The closure signature can be used to plan different grasps with respect to heavy wraps

Experiment 3 shows that the Closure Signature provides feasible models for lateral pinches and precision grasps.

For the lateral pinch with the RBO Hand 2, there were two main factors influencing the grasp. First, the interaction with the environment allowed the caging of the object and was fundamental in order to get a successful grasp, as shown in Fig. 1.16. Second, the height of the object determined the grasp success, as too small objects were not caged in time between the thumb and the index during the closing motion (see Fig. 1.17). This is due to the fact that the fingers close with a certain velocity and with some delays between each other, so a better tuning of these parameters could lead to higher success rates.

When grasping small objects using a precision grasp, even small uncertainties on the hand and object positions may lead to failures. This is why, particularly when using highly underactuated hands, considering a reduced set of fingers (e.g., thumb and index), and starting from a partially closed initial position is important to achieve a good alignment on the object. Preliminary experiments where we considered reference points in all the fingers led to unsuccessful grasps, as the center of the CS was too close to the middle of the palm and the objects were too small to be caged by the fingers. On the other hand, when considering just two fingers but starting from a completely open position, unwanted collisions with the objects occurred.

Fig. 1.18 shows a successful grasp of a small cube. The hand starts from half of its total closure and then gently grasps the object between the fingertips of the thumb and index. Failures, as the one shown in Fig. 1.19, were mainly due to misalignment between hand and object. In fact, the alignment of the planar components of the center of the CS to the center of the object is prone to uncertainties coming from the vision system and from the camera-to-robot calibration. When performing power grasps, such uncertainties are mitigated thanks to hand compliance and to the fact that the hand starts closing after the palm touches the object. Besides, in precision grasps, also uncertainties on the positioning in the direction normal to the plane are relevant.

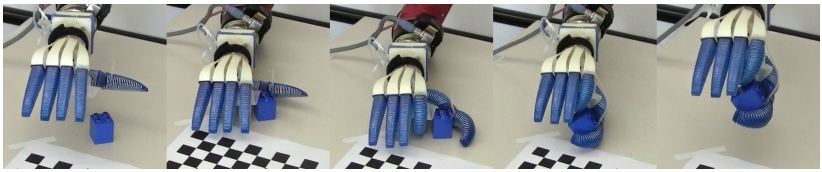

Fig. 1.16 Execution of a lateral pinch over a Lego Duplo piece (frames sequence).

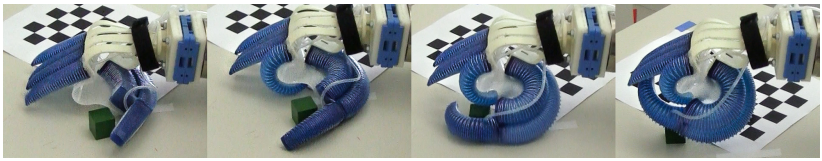

Fig. 1.17 Execution of a lateral pinch over a small cube (frames sequence).

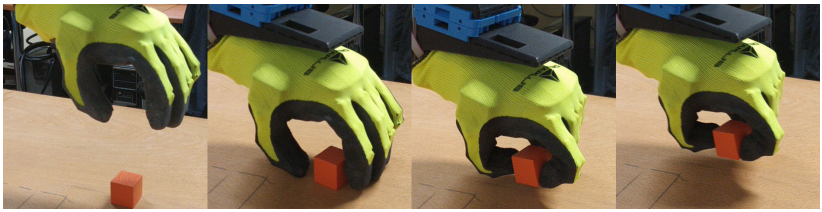

Fig. 1.18 Execution of a precision grasp over a small cube (frames sequence).

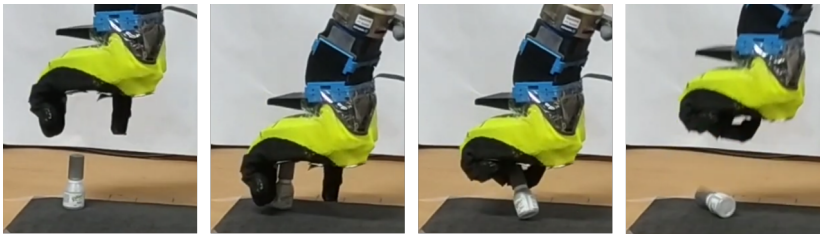

Fig. 1.19 Execution of a precision grasp over a small vial (frames sequence).

1.4.4 General considerations

Besides the discussion of experimental results, we will conduct here a higher level analysis of the proposed grasp planning approach. In particular, we want to characterise our system by means of the four key aspects of systems building suggested in [34], i.e., modularity vs. integration, computation vs. embodiment, planning vs. feedback, generality vs. assumptions.

Modularity vs. integration. Modularity allows breaking down a problem in easier-to-solve sub-problems. Our system is the result of a tight integration of different modules. The *GQ-CNN module* provides an estimation of the center and orientation of the most robust grasp, and the *CS module* provides a simple model of a closing motion of a chosen hand. The resulting integration is the *Grasp planning with soft hands module*. Subsequently, it has been integrated with the *Grasp execution module*, which, in turn, is given by the integration of a trajectory planning achieved with the standard module MoveIt and a force-feedback guided state machine. Our system works on ROS, which allows a great level of module integration. Note that the *CS module* plays a key role in the proposed method, as it allows to decouple the planning on the object, that can be performed with any grasp planner designed for parallel-jaw grippers, from the used end-effector, whose closing motion can be described in terms of closure signature.

Computation vs. embodiment. This aspect describes the relations between software computation and embodiment of some processes in the robot hardware. To characterise our system, we think that it is appropriate to split the entire process in two subsequent stages. The first stage includes the grasp planning and the hand alignment to the desired

grasp, while the second stage includes only the hand closure. The first stage relies only on computation, while the second one relies on the embodiment of the grasping capabilities of the soft hand, whose compliance allows safe interaction with the environment and high adaptability to objects.

Planning vs. feedback. In [34], the difference between these aspects relies on the type of solutions that they obtain: planning allows finding general solutions, while feedback is involved in local solution search. Our approach is closer to planning than to feedback. In fact, after the acquisition of the object depth image, grasp planning and robot end-effector alignment work without explicitly needing feedback from the scene. In Experiments 1 and 2, during the object approach, however, the execution is feedback-driven, since the robot motion stops and the grasp begins when the force exerted on the object exceeds a certain threshold.

Generality vs. assumptions. When building robotic systems, it is crucial to find a trade-off between the generality of the proposed solution and the presence of underlying assumptions [34]. The assumption that mainly affects our system is that the neural network is trained for executing grasps with a parallel-jaw gripper. This assumption is clearly too restrictive in the case of grasping using a multi-fingered soft hand. However, modelling the hand through the closure signature, overcomes this difficulty, showing high generalizability to different robotic hands.

1.5 Final remarks

In this Chapter, a general method for grasping objects from the top with the aid of soft robotic hands has been proposed. The strength of

the approach resides in the Closure Signature (CS), i.e., a model that associates a preferred grasping direction to a closure motion performed by a robotic hand. The CS is general enough to model power and precision grasps and its computation requires only the tracking of some chosen reference points on the hand during the motion that one wants to represent. The information provided by the CS can be used to suitably align the hand with the output of a grasp planner prescribing the best way to grasp a certain object (CS-alignment).

To validate the feasibility of the proposed approach, we tested different Closure Signatures of two different robotic hands in combination with an Artificial Intelligence-based grasp planner. Multiple experimental trials showed that: *i*) the proposed integration generates successful power grasps from the top over a variety of objects (Experiment 1); *ii*) the CS-alignment generalizes well to heavy wraps performed with intrinsically soft hands (Experiment 2); *iii*) the CS model can be used also to perform grasps that are not heavy wraps, like lateral pinch and precision grasp (Experiment 3).

2 Magnetic actuation for soft hands

In the introduction to *Part A* of this Thesis, advantages and disadvantages of soft hands have been discussed. Advantages have been echoed several times: Soft hands allow to perform a manipulation that is delicate with the objects and robust to uncertainties at the same time.

This Chapter proposes a way to overcome some of the limitations of soft hand. As previously mentioned, a precise control of soft hands is difficult to achieve, and the dexterity limitations due to the software/hardware motion coupling resulting from the device underactuation are steering the research on Soft Manipulation towards complex structures, both at hardware and software levels. This way, however, we are failing one of the most relevant motivations for the adoption of soft hands: to reduce devices' encumbrance and complexity. In this respect, in this Chapter we propose to augment the classic actuation systems of soft hands by exploiting magnetic actuation, i.e. magnetic elements capable of improving the soft hands manipulation capabilities.

The interaction that is generated between magnetic elements, indeed, allows to realize a physics-based guidance capable of compensating uncertainties on control due to softness and underactuation, besides the possibility of performing non-contact manipulation of thin and light objects, and an augmentation of the hand DoAs. Hence, in this Chapter

we will exploit physics *modelling* to (partially) *control* some motions that soft hands can perform[1].

In the literature on robotics, magnets have been exploited especially as tools for locomotion and reconfigurability of milli-, micro- and nano-robots, often made of MEs (magnetic elastomers)[35] and meant for biomedical applications [36–39]. Micro-manipulators [40], self-folding degradable [41], helical[42], aquatic-inspired, aerial [43], millipede and flower-like [44] devices are examples of magnetically actuated small-scale robots exploiting external magnetic fields. To model the kinematics of soft continuum robots, heat-assisted shape-morphing [45], continuation method and bifurcation analysis [46] have been investigated. Concerning devices larger than small-scale, magnets were employed to drive catheters [47–49], develop tracking systems [50], provide climbing robots with suitable adhesion force [51], and to allow fast and reconfigurable modular assembly [52, 53]. In robotic grasping, magnets have been exploited to increase the force during adaptive pinch grasps [54], build tactile sensors for contact points location estimation [55], and devise a compliant, variable-stiffness gripper [56]. Recent works focus on food handling [57] and autonomous garment manipulation [58]. To the best of our knowledge, no works are focused on manipulation with soft robotic hands exploiting the magnetic force for hand control and reconfiguration.

[1]The content of this Chapter has been submitted to the *Soft Robotics* journal for publication. The manuscript is entitled "On the use of magnets to robustify motion control of soft hands", by S. Marullo, G. Salvietti, D. Prattichizzo (2021).

2.1 Methodology

We propose to augment the hand capabilities by means of magnetic force exploitation. Such augmentation relies on a behavior that can be modelled by means of contiguous magnetic funnels, and the overall effect of the funnels can be seen as a position control. Such funnels will be described in Section 2.1.2 and details on the modelling of magnetic elements (permanent magnets and electromagnets) will be provided in Section 2.1.1. Then, the interaction of the hand with the environment and with the hand itself will be examined, and relevant physics laws will be applied to position uncertainties compensation (Section 2.2.1), non-contact manipulation (Section 2.2.2) and DoAs augmentation (Section 2.3.1).

2.1.1 Permanent magnets and Electromagnets

Electromagnets or permanent magnets can be used to exploit the magnetic force depending on the envisaged use case. Electromagnets are composed of a conductive coil with a variously shaped, usually ferromagnetic, core. When the coil windings are supplied with electrical current, a magnetic field is generated. Turning off the current, the magnetic field associated with the coil vanishes, whereas the contribution provided by the core lasts. To exploit the magnetic interaction only when needed, avoiding undesired interactions with ferromagnetic objects, this contribution should be as small as possible. Hence, magnetic cores with low remanence are recommended (e.g., soft iron, ferrites, silicon steels). Permanent magnets, instead, after the magnetization process, show a permanent magnetization due to the coupling of atomic

moments, and are capable of generating magnetic fields without external intervention. The constitutive materials can be classified as soft or hard depending on the ease of magnetization/demagnetization (coercivity). Once magnetized, the magnet's capability of re-orienting the magnetic domains according to another external field is called permeability. Neodymium alloys (e.g., NdFeB) are examples of widespread, hard, rare-earth permanent magnets with relatively low permeability. Since this work is focused on robotic manipulation (i.e., on the exploitation of magnetic elements embedded in hands and objects), using electromagnets rather than permanent magnets is preferable, as they allow the magnetic attraction exploitation only when desired. Moreover, DC electromagnets are preferable to AC ones, since the drawbacks (e.g., time-dependent attraction/repulsion, eddy currents, overheating, ...) are less relevant. If needed, a cooling system (e.g., thermally-conductive materials, electrothermal devices, ...) can be used. Furthermore, to limit the encumbrance, the magnetic elements should be small. In the following, we will show how the physics laws can be exploited to robustify the motion control of soft hands and to augment the number of DoAs of such devices.

2.1.2 Physics-based funnels

In the following, the expression *magnetic elements* will denote either permanent magnets or electromagnets. Since we will consider elements with a size suitable for the embedding in a hand, they can be modelled as magnetic point dipoles [59] as a first approximation. Let us consider an unconstrained, initially still magnet C_1 represented as a point dipole with moment $\mathbf{m}_1$ and located in $\mathbf{p}_t$, immersed in the magnetic field $\mathbf{B}$

generated by a second magnet C_2, represented likewise as a dipole with moment $\mathbf{m}_2$ and constrained in the origin of a reference system for simplicity. C_1 will spontaneously move on a trajectory minimizing the potential energy U held by C_1 and due to $\mathbf{B}$ [60], i.e.

$$\mathbf{p}_{t+1} = \underset{\mathbf{p} \in I(\mathbf{p}_t)}{\arg\min} U(\mathbf{p}, \mathbf{p}_t, \mathbf{m}_1, \mathbf{m}_2), \tag{2.1}$$

where $\mathbf{p}_{t+1}$ denotes the position of C_1 at time $t+1$ and belongs to a neighborhood of $\mathbf{p}_t$. As it can be seen in Fig. 2.1, the potential energy generates *funnels*, whose tips correspond to points with low energy. Since the funnels are intrinsically interconnected by physics, they are sequential, providing an hardware-based position control without discontinuity.

In the more general case of moving magnets, the Least Action Principle holds [61], whose non-relativistic expression is

$$\min I = \min \int_{t_1}^{t_2} (T - U)\, dt,$$

where T and U are the kinetic and the potential energy, respectively, and t denotes the time variable. In this case, considerations similar to those above are valid.

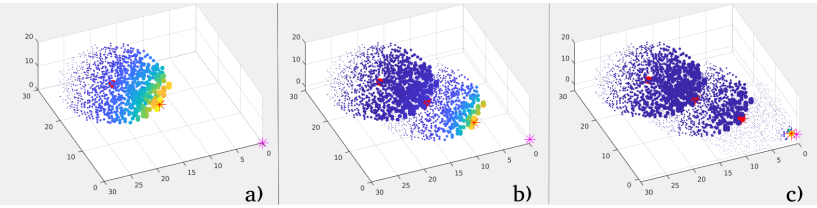

Fig. 2.1 Pictorial representation of the potential energy related to the magnetic elements C_1 (represented with a red circle) and C_2 (whose position is represented by a purple star). The value of the potential energy U in points belonging to a neighbourhood of $\mathbf{p}_t$ (location of C_1) is represented by heatmap-coloured circles, the smaller the potential energy, the larger the dot. The red star indicates the point belonging to the neighbourhood and minimizing the system potential energy. Same reasoning applies to a neighborhood of $\mathbf{p}_{t+1}$ (Fig. 2.1-b), and of $\mathbf{p}_{t+2}$ (fig. 2.1-c), and so on. As it can be seen, the potential energy generates sequential funnels, that are capable of providing physical guidance without discontinuity (i.e. C_1 approaches spontaneously C_2).

2.2 Hand and object/environment interactions

2.2.1 Guidance

The control of soft and underactuated hands frequently suffers from uncertainties due to the manufacturing process, the control strategy modelling and the actuation system [62, 20]. In the robotic trajectory-planning framework, sequential optimization funnels have been identified [63] to compensate for uncertainties on the target pose estimate [64]. In Section 2.1.2, we showed that sequential magnetic funnels can be found. Hence, exploiting such a magnetic system can allow to compensate for a finger misplacement due to the actuation system, finally reaching the desired target. In Section 2.1.2, magnets C_1 and C_2 have been assumed unconstrained and constrained, respectively, for the sake of simplicity. The aim was to show from a conceptual perspective the existence of magnetic funnels acting as hardware controllers exploiting a non-contact force to reach the target location. However, in real-world situations, magnets can be embedded in robotic hands, objects and/or in the environment. Hence, Eq. (2.1) should be considered together with

$$\mathbf{F} - \boldsymbol{\beta}\dot{\mathbf{p}} = \mathbf{M}\ddot{\mathbf{p}}, \tag{2.2}$$

where $\mathbf{F}$ denotes the magnetic force, while $\boldsymbol{\beta}$ and $\mathbf{M}$ are tensors encapsulating the damping and inertia felt by the dipole and due to the embedding in the hand/object structure. Unfortunately, the dynamics of a soft and underactuated hand is so complex (and usually indeterminate) that no closed-form of Eq. (2.2) is possible. Hence, a simulator is

needed to have insights on the actual hand/object motion related to the magnetic force.

In the following, a lumped-parameter model of the pneumatic RBO Hand 2 [65] based on the P10 actuator [66] will be considered. The hand consists of 4 pneumatic actuators; by design, each finger is capable of bending about an axis orthogonal to the finger principal direction.

Regarding magnetic element modelling, values inspired by specs of commercially available devices are adopted hereinafter.

Let us consider now a manipulation sequence prescribing a delicate interaction with an object in specific points. Let us suppose also that an undesired displacement between the desired contact point on the hand and the desired point on the object is present. This undesired displacement can be due to uncertainties affecting the hand nominal working pressure (caused by real-world pressure leakages or uncertainties on the valves' opening time), or they can be due to the difficulties of executing fine control movements for affordance exploitation (as in the case of grasping a mug by means of its handle, see Fig. 2.3). If an estimate of the displacement between the desired point on the hand and the desired point on the object is available, simulation by software allows to properly choose the magnetic elements that are capable of compensating for undesired displacements.

Let us consider the current fingertip location in $\mathbf{p}_f$ (associated to that uncertainty) and the target location on the object in $\mathbf{p}_T$. Let us assume that two small magnetic elements (modelled as point dipoles) are embedded in the hand and located on the object, respectively. To exploit the magnetic force only when desired without disturbances during other manipulation steps, the hand is equipped with an electromagnet in the fingertip, and a permanent magnet is located on the object (hence, no

additional voltage source is needed). Let us suppose that the object is such that the weight force is greater than the magnetic force (or, equivalently, the object position is constrained). According to the charge model for magnets [67], a dipole with moment $\mathbf{m}_1$ generates a magnetic field $\mathbf{B}_1$ which depends on the distance vector $\mathbf{r}$ from the dipole and can be expressed as Eq. (2.3):

$$\mathbf{B}_1(\mathbf{r}) = \frac{\mu_0}{4\pi}\left[\frac{3\mathbf{r}(\mathbf{m}_1\cdot\mathbf{r})}{r^5} - \frac{\mathbf{m}_1}{r^3}\right], \tag{2.3}$$

where μ_0 is the magnetic permeability of free space.

The dipole with magnetic moment $\mathbf{m}_1$ acts on a second dipole with moment $\mathbf{m}_2$ through the wrench $\mathbf{w} = [\mathbf{F}, \boldsymbol{\tau}]'$, where the dipole-dipole interaction force and the toque are given by:

$$\begin{aligned}\mathbf{F} &= -\nabla U = \nabla(\mathbf{m}_2\cdot\mathbf{B}_1) = \\ &= \tfrac{\mu_0}{4\pi}\tfrac{3}{r^5}[(\mathbf{m}_1\cdot\mathbf{m}_2)\mathbf{r} + (\mathbf{m}_1\cdot\mathbf{r})\mathbf{m}_2 + (\mathbf{m}_2\cdot\mathbf{r})\mathbf{m}_1 - \tfrac{5(\mathbf{m}_1\cdot\mathbf{r})(\mathbf{m}_2\cdot\mathbf{r})\mathbf{r}}{r^2}]\end{aligned} \tag{2.4}$$

and

$$\boldsymbol{\tau} = \mathbf{m}_2 \times \mathbf{B}_1, \tag{2.5}$$

where $\mathbf{r}$ is the distance vector between the dipoles, i.e. $\mathbf{r} = \mathbf{p}_2 - \mathbf{p}_1$.

More specifically, let us consider a single-coil electromagnet with a cylindrical, ferromagnetic core. Solenoid and core magnetic moments (denoted with $\mathbf{m}_s$ and $\mathbf{m}_c$) can be treated as dipole moments, generating the overall moment $\mathbf{m}_e = \mathbf{m}_s + \mathbf{m}_c$. A solenoid with windings, supplied with a current i and with cross-sectional area S generates a moment $\mathbf{m}_c = Ni\mathbf{S}$, whose direction is perpendicular to S and oriented according to the right-hand rule.

Concerning the permanent magnet located on the object and the electromagnet core, the magnetic remanence specific of the material allows to estimate the residual magnetization per unit of volume through the constitutive relation:

$$M_r = B_r/\mu_0. \tag{2.6}$$

By exposing the magnet to an external magnetic field, its magnetization increases according to the material M-H hysteresis curve. However, the residual magnetization is sufficient for a conservative estimate, hence we can consider $M = M_r$. Therefore, the magnitude of the permanent magnet magnetic moment is given by $m_2 = MV$, where V is the magnet volume. Analogous reasoning applies to the estimate of the core moment $\mathbf{m}_c$.

To provide an example, let us consider now that the undesired displacement between the target point on the object and the grasping point on the hand is $\mathbf{r} = [25, 10, 4]$ mm. Consistently with what has been argued above, let use equip the finger (actuated with 10 kPa) with an electromagnet located in the 8-th node of the lumped parameter model, and pinpoint the desired point on the object with a permanent magnet. Structure and supply specs of the electromagnet are $i = 0.41$ A, $S = 133$ mm^2, $N = 1200$ and an iron-silicon core ($B_r = 0.49T$) is present. Furthermore, let us suppose that the permanent magnet is a N52 NdFeB (B_r = 1 T), with a cylindrical shape of 10 mm diameter and 5 mm height. Simulation shows (Fig. 2.2) that the system is capable of acting as an attractive controller, compensating the initial gap between finger position and target.

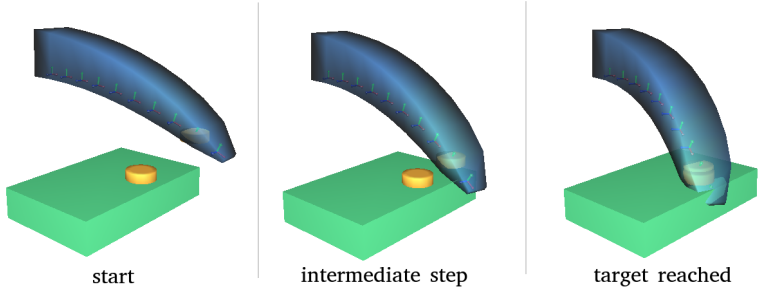

Fig. 2.2 Hand interacting with the object: magnetic guidance for uncertainties compensation.

Fig. 2.3 Hand interacting with the object: magnetic guidance for affordance exploitation.

2.2.2 Non contact manipulation

Thin and flat objects are usually difficult to grasp with robotic end-effectors. Most of the time the problem is addressed with a soft end-effector establishing a so-called sliding grasp [68], a triadic interaction between object, end-effector and environment. However, light objects are prone to fall off the support during the pre-grasping phase, leading

to task failures. In this subsection, we will consider such objects, either embedding ferromagnetic parts by design (like paper clips, coins, ...) or by purpose (e.g., by adding a small plate with ferrite on the handle of a comb). Since we are considering common objects to be grasped by a robot, soft magnetic materials with high permeability will be considered. By equipping the end-effector with an electromagnet (N turns run by current i), the non-contact latching force can be exploited to generate an attractive motion of the object towards the end-effector, as long as the magnetic force is greater than the weight force of the object. To properly channel the magnetic field, a U-shaped magnetic core with high permeability is considered, as in the arrangement shown in Fig. 2.4.

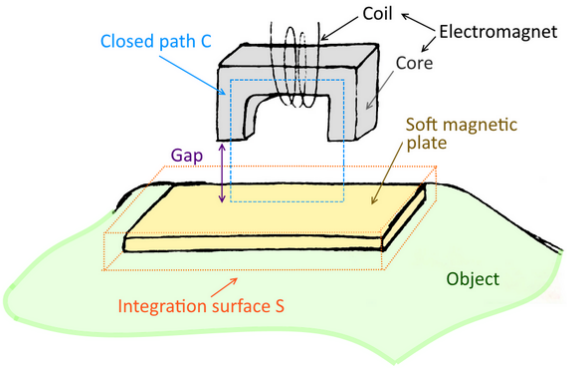

Fig. 2.4 Representation of relevant elements and quantities for magnetic non-contact manipulation. Between the electromagnet (composed of core + coil) and the soft magnetic plate located on the object, there is a gap of length l_g and cross-sectional area A_g. Integration path and surface required for force computation are reported.

From Ampère's circuital law:

$$\oint_C \mathbf{B} \cdot d\mathbf{l} = \mu_0 I_{tot} = \mu_0 N i$$

and magnetic circuit analysis [69], accounting for $\mu_{air} \sim \mu_0$ and $\mu_{core} >> \mu_0$, follows

$$B_g = \frac{\mu_0 N i}{2 l_g},$$

where B_g = field in the gap and l_g = gap length.

The attraction force is computed by exploiting the Maxwell's stress tensor [70]:

$$\mathbf{F} = \frac{1}{2\mu_0} \oint_S B_n^2 \, ds \, \mathbf{n},$$

where B_n is the component of the field orthogonal to the surface S, $\mathbf{n}$ is versor outgoing from S, and S is the surface identified by the orange line in Fig. 2.4. Due to the magnetic core high permeability, the field is channelled orthogonally to S. Hence,

$$\mathbf{F} = \frac{\mu_0 N^2 i^2 A_g}{4 l_g^2} \mathbf{n}$$

generates an attractive motion of the object towards the hand.

To provide an example, let us suppose to equip the hand with an electromagnet located in the 4-th node of the palm lumped parameter model. Electromagnet structure and supply specs are $N = 1200$, $i = 0.41$ A, A_g = 1 cm^2 with the core made of soft ferromagnetic material ($B_r = 0.49$ T). The thin, light object is located on a table distant 8 cm and represented by a parallelepiped with size l_1 = 5 cm, l_2 = 15 cm, l_3 = 0.3 cm, and mass 25 g (similar to a hair comb). A cylindrical N52 NdFeB permanent magnet with 10 mm diameter and 5 mm height is located at half of the length. As shown in Fig. 2.5, the system is able to generate a magnetic attraction capable of exceeding the object's weight force, achieving the desired motion.

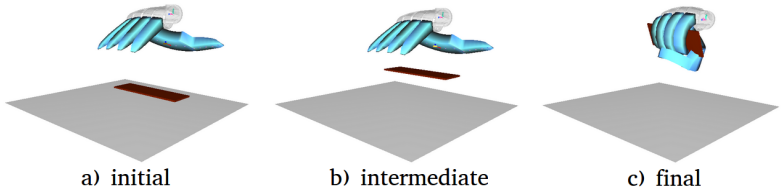

Fig. 2.5 Hand interacting with objects: example of intermediate steps in non-contact manipulation exploiting the magnetic attraction.

2.3 Interaction of the hand with itself

2.3.1 DoAs augmentation

The intrinsic underactuation of soft hands on one side leads to a control simplification, on the other side entails a limitation of the possible manipulation capabilities. Therefore, to provide soft hands with more dexterous movements, current research on design is frequently steering towards novel complications, resulting in classical drawbacks (weight, encumbrance, ...) joined to specific control issues due to underactuation and modelling issues related to soft material deformation [18]. Here we propose to exploit magnetic elements as actuators to augment the spectrum of movements that the hand can perform. As an example, let us consider the RBO Hand 2. By design, fingers adduction/abduction cannot be performed, unless a different actuation is attained. Let us consider index and middle fingers, modelled via lumped parameters as above, equipped with magnetic elements in the fingertips. To exploit magnetic wrenches only when desired, let us consider electromagnets. For the sake of simplicity, two cylindrical electromagnets with single coil, C_i and C_m, are located in r_i and r_m, respectively. The dipole

moment of such elements can be figured out as shown in Section 2.2.1. To fulfil the adduction motion, the dipoles have to be arranged so that the sequence of poles is N-S-N-S. C_i and C_m are subjected to the magnetic wrenches $\mathbf{w}_i$ and $\mathbf{w}_m$, respectively:

$$\mathbf{w}_i = [\mathbf{F}_i, \boldsymbol{\tau}_i]', \tag{2.7}$$

$$\mathbf{w}_m = [-\mathbf{F}_i, \boldsymbol{\tau}_m]', \tag{2.8}$$

where $\mathbf{F}_i$ is the magnetic force in Eq. (2.4) with $\mathbf{r} = \mathbf{r}_i$ - $\mathbf{r}_m$, while $\boldsymbol{\tau}_i = \mathbf{m}_i \times \mathbf{B}_m$ and $\boldsymbol{\tau}_m = \mathbf{m}_m \times \mathbf{B}_i$. $\mathbf{B}_m$ is the magnetic field experienced by C_i and induced by C_m, whereas $\mathbf{B}_i$ is the magnetic field experienced by C_m and generated by C_i.

To achieve abduction of fingers, instead, the dipoles can be arranged so to generate repulsion between magnetic elements, e.g. N-S-S-N. Eq. (2.7) and Eq. (2.7) still hold.

To provide an example of DoAs augmentation by magnetic actuation, let us equip middle and index fingers with cylindrical electromagnets (S = 133 mm^2, N = 1200, i = 0.41 A, with iron-silicon core with B_r = 0.49 T), located in the 8-th node of the fingers lumped-parameter model. As shown in Fig. 2.6, the system is able to generate the adductive motion (initial gap of 2.8 cm).

By inverting the verse of the current flow in one electromagnet (i.e., by inverting the verse of its magnetization), the same system exploits the magnetic repulsion to realize abduction of fingers, as shown in Fig. 2.7, generating a distance between fingertips of 4.3 cm.

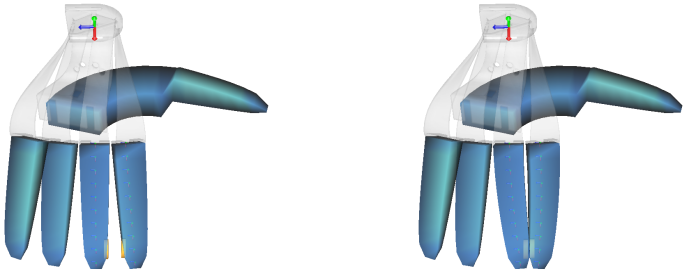

a) initial configuration b) adduction

Fig. 2.6 Hand interacting with itself: Adductive motion between fingers allowed by small electromagnets located in the fingertips.

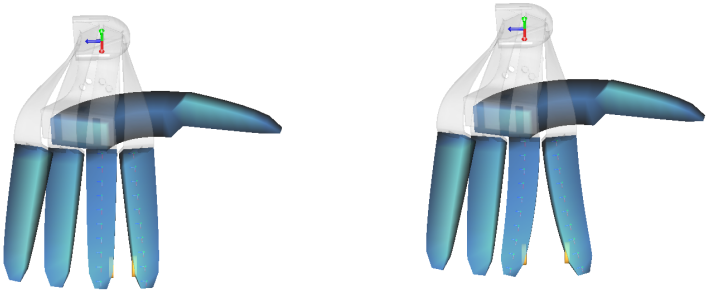

a) initial configuration b) abduction

Fig. 2.7 Hand interacting with itself: Abductive motion between fingers allowed by small electromagnets located in the fingertips.

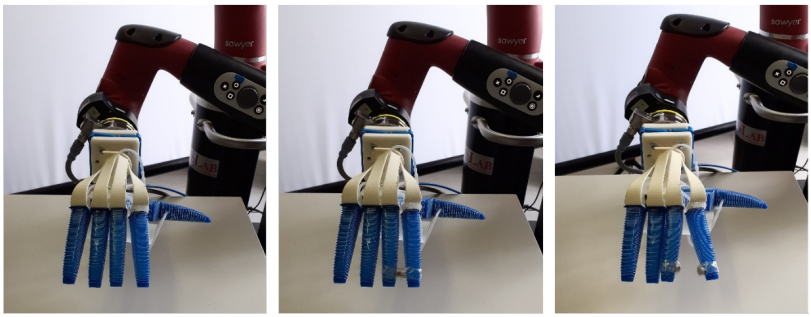

a) Hand without magnets b) Adduction by magnets c) Abduction by magnets

Fig. 2.8 Hand interacting with itself: Adductive (b) and abductive (c) motion between fingers allowed by small electromagnets located in the fingertips.

2.4 Discussion

Magnetic field modelling is challenging, and the dipole approximation for magnetic elements (first term in the field multipole expansion) holds for small sized devices as long as they are not too close. However, since the aim of this work is to provide tools for the design of soft hands embedding magnetic elements, what is relevant is to choose proper values for the parameters describing these elements in such a way that they are able to trigger the desired motion. Then, the magnetic guidance will be in charge of realizing the desired contact. If a more accurate field modelling is required, some results are available for specific configurations [71, 72], or simulation software on magnetism can be used (e.g. COMSOL, QuickField, ...).

Concerning the choice of permanent magnets, parallelepiped or cylindrical shapes are almost equivalent if embedded in soft-rigid hands, while cylindrical and thin-shaped elements are more suitable to pneu-

matic hands, embeddable in external elastic rings if needed (e.g., if the hand cannot be supplied with current).

Concerning ferromagnetic materials available with different grades (like NdFeB), the trade-off between grade and size must be chosen according to the needs, keeping in mind that thin magnets (about 1 mm) are prone to realize a weak magnetic interaction. It is not uncommon that relatively small variations of size have a greater impact than a small change of grade.

Concerning applications, magnetic guidance can be a game changer when the interaction between object and hand must occur in specific locations, but uncertainties on the actual configurations are present. Moreover, in multi-contact interactions, magnetic elements could be embedded also in locations different from the ones in charge of establishing the main interaction, achieving an overall grasp stabilization, which is a common issue to deal with when grasping with soft-rigid hands (e.g., tendon-driven devices with rigid links covered by soft materials [10, 73]).

Concerning the hand DoAs augmentation, it has potentially relevant applications either for hand shaping in pre-manipulation steps, either for enhancing in-hand manipulation capabilities. However, a remark should be done concerning abduction. If magnets are not strong enough to counteract material inertia and damping, no motion occurs. On the other side, if the magnets are not in a symmetric configuration with respect to the hand structure and if the hand is not stiff enough, after an initial finger separation, a novel hand configuration occurs, potentially ending up in an undesired fingers adduction. To prevent this situation, proper use-case-based non-backdrivable mechanisms can be designed.

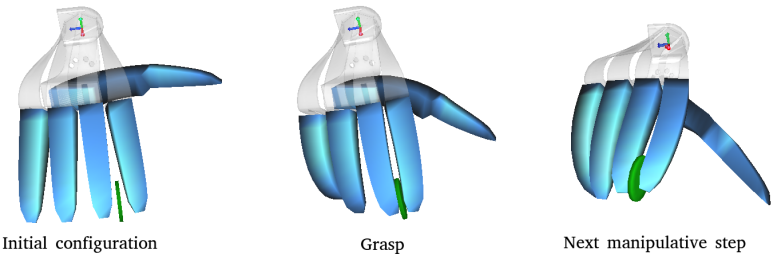

Fig. 2.9 Interaction of the hand with itself: A hand equipped with electromagnets in the fingertips manipulates a thin object.

Another application of the hand interacting with itself can be devised in the interaction with thin objects that can be trapped between the fingers and then moved away, as in Fig. 2.9.

In this case, if the object is made of a non-ferromagnetic material such that the relative permeability $\mu_r \sim 1$ (as in the vast majority of daily objects), then the magnetic flux passes through the object as if the latter would not be present. What is relevant is the object thickness in the region of interaction with the hand: It must not be large enough to make irrelevant the magnetic attraction between fingers. If the object is a permanent magnet, instead, a proper modelling of the object is needed. Moreover, paramagnetic and diamagnetic materials do not provide significant effects at room temperature. If a material with high permeability is employed, furthermore, two closed magnetic circuits can be modelled, one for each finger (similarly to Section 2.2.2), resulting in a double attraction finger-object.

2.5 Final remarks

In this Chapter, we proposed to exploit magnetic elements as additional DoAs to robustify the motion control and augment the manipulation capabilities of soft and underactuated robotic hands. Permanent magnets and electromagnets have been modelled by means of magnetic dipoles and physics laws were discussed in the light of guidance and DoAs augmentation. The interaction of the hand with itself and with the environment has been investigated to apply magnetic funnels to uncertainties compensation, non-contact manipulation of thin and light objects, grasp stabilization and augmentation of the hand's DoAs. Tools for the design of novel soft hands have been provided.

3 Grasping garments

This Chapter deals with robot-environment interactions involving the manipulation of highly deformable objects. We will focus on the manipulation of garments, whose deformability is such that the success of the task execution strongly depends on the global and local configuration assumed by the garment.

In the light of developing techniques suitable for industrial and domestic settings, devising hardware tools for fast and effective task accomplishment is paramount. To counteract the strong dependency of the garment configuration on the grasping points, and on the amount of fabric that is grasped by the end-effector, we propose to exploit the magnetic attraction between garment and end-effector to realize the desired contact. Ornamental or brand elements (such as buttons or small plates) embedding soft ferromagnetic materials (e.g., composites of ferrite, see Chapter 2) could be properly located on the garment to this purpose. As a suitable end-effector, we propose Mag-Gripper, an augmented jaw gripper embedding an electromagnet. This design choice, indeed, allows to achieve repeatable extended point-like grasps, resulting in repeatable garment configuration.

In this Chapter, therefore, we turn down modelling the deformability of the fabrics, and devise an hardware solution that exploits small

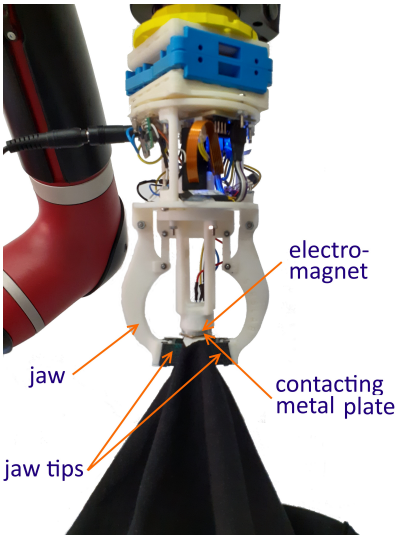

Fig. 3.1 Mag-Gripper: a novel gripper to manipulate clothes

elements to add some *structure* in a difficult-to-manage environment. In this way, the hardware solution fosters the control of the soft interaction aimed at garment manipulation[1].

3.1 Related works

Previous Work on Autonomous Cloth Manipulation

In the last decade, research on autonomous cloth manipulation received great boost. Garment manipulation can be decomposed in two sub-tasks: unfolding and folding. The former is aimed at bringing the cloth from a

[1]The content of this Chapter has been published in [58]. Reprinted with kind permission from IEEE.

random configuration to a known one (usually corresponding to have the garment lying flat on a table), while the latter aims to actually accomplish the desired manipulation starting from that known configuration. Regarding the unfolding task, the most popular approach consists in re-grasping the object until the target configuration is reached. In [74], a geometric approach is proposed, consisting in identifying two grasping points on the garment outline capable of generating an half-folded cloth configuration, to which shape analysis techniques are applied to estimate the novel re-grasping points. In [75], a 2D perception and a Markov Hidden Model are used. In [76], 3D perception is used to compute a mesh of the object, and a Support Vector Machine is employed to implement a greedy policy for the next grasping point estimation. In [77], a data-driven approach joint with Random and Hough forests is used for garment recognition and to estimate the grasping points in a probabilistic planning framework taking into account uncertainties related to the estimation process. In [78], a simulation environment is used to compare the synthetic data in it with a reconstructed mesh of the physical garment to grasp, and mapping the re-grasping points on the synthetic mesh to the physical garment. The main difficulties encountered in the above cited works are: *i)* the time required to accomplish the task; *ii)* the uncertainties on the estimate of the final grasping point; *iii)* the risk of loosing the object during multiple re-grasping. In a more recent work [79], a hierarchical structure of Convolutional Neural Networks is used to recognize the garment category and grasp it directly in two points, avoiding multiple grasps and decreasing the required completion time.

Regarding the folding task, early works proposed geometric approaches [80] relying on the gravity-based folding: in [81], the cloth

is assumed to be representable as a simple polygon, and the task is accomplished by moving a portion of the garment over another one, having a segment termed *g-fold* as separation line, accounting also for the fabric flexibility [82]. More recent works arise from the synergy between Machine Learning and Robotics, relying on Deep Learning, Learning from Demonstration (LfD) and Reinforcement Learning. In those works, the robot is taught to learn the folding task by means of a set of demonstrations provided by a human operator. In [83], a deep convolutional autoencoder joint with a deep time delay neural network is used to process data acquired via teleoperation. In [84], a LfD with Deep P-Network is used to learn a T-shirt folding. In [85], Dynamic Motion Primitives are exploited with LfD and RL. When a given cloth manipulation task has to be learnt by means of human demonstrations, the multiple demonstrations have to start all with the same initial garment configuration [85]. To this aim, grasping the cloth always in the same points is fundamental, since clothes are extremely deformable objects and relatively small changes in the grasping points can cause significant errors in the initial configuration.

Previous Work on Grippers for Cloth Manipulation

In [86], a taxonomy of the grippers used in works on garment manipulation is presented. As highlighted in the paper, usually those grippers are not specifically thought for interacting with clothes, which are extremely deformable objects. Indeed, the most commonly used tools are the parallel-jaw grippers. Multi-fingered hands (such as those used for instance in [87]) allow to exploit the abduction motion and also a more dexterous manipulation (e.g., to identify the boundary of clothes

[88]). Few hands are designed to establish specific interactions with clothes: in [89], force sensors are placed on the tips to perform garment classification according to the material roughness. In [90], an underactuated three-fingered hand capable of generating human-like grasping movements exploiting environmental constraints [91] is presented. However, when these tools are used to manipulate clothes, the grasping task is mainly performed by sliding on the table surface and enclosing a portion of the garment between the jaws. This approach: *i)* restricts the cloth manipulation to occur on a tabletop; *ii)* requires that an enough portion of the fabric is constrained between the tips to avoid undesired slippage. However, *i)* cloth manipulation can be performed also in the air [76, 85], and this is important also in the light of the growing need of tools for assistive robotics; *ii)* grasping by sliding the fabric on the table surface introduces unpredictable variations in the configuration taken by the garment after the grasp has occurred. This is due to the fact that the portion of the fabric actually constrained by the tips is the consequence of the interaction between the garment, the robot and the environment, and the related changes are difficult to face for vision-based Machine Learning techniques.

To the best of our knowledge, no grippers exploiting the magnetic force have been so far exploited for clothing manipulation. Moreover, the difference with generic, commercially available grippers exploiting the presence of a magnet [92] is that we want to exploit the magnetic force only to establish the contact between the gripper and the garment. After the extended point-like grasp has occurred, the magnetic force is no more needed: the electromagnet is deactivated to avoid overheating and a secure grasp maintenance is achieved by exploiting the gripper jaws.

3.2 The Mag-Gripper

Mag-Gripper has been designed to be lightweight, modular and with a limited encumbrance. The prototype has been designed via CAD and realized with additive manufacturing techniques, which allowed small production cost and short production time. The gripper is similar to a jaw gripper (see Fig. 3.1), but the novelty we propose consists in having realized an *augmented* jaw gripper: In its central part, there is an electromagnet mounted on the top of a linear actuator. By activating the electromagnet, a magnetic field is generated, which causes a magnetic force attracting the metal part attached to the cloth. Due to the attractive motion of the metal part, a collision between the end-effector and the cloth occurs, and is detected by a small resistive force sensor (FSR) located near the electromagnet. The contact is deemed to be occurred when the force measured by the sensor exceeds a given threshold, triggering the closing motion of the jaws. The proposed gripper exploits the advantages of both the electromagnet and the jaws: the former allows grasping in the desired point, while the latter allow a secure grasp maintenance during manipulation. In other words, from the dual perspective, the uncertainty brought by the soft fingertips of the jaws is tamed by the action of the electromagnet.

3.2.1 Components

The Mag-Gripper is an augmented jaw gripper, a sketch of which is shown in Fig. 3.2a. In the gripper central part, between the jaws, there is a linear actuator (PQ12-30-12-P by Actuonix), at the top of which an electromagnet (KS0320 by Keyestudio) is mounted. Thanks to a set of

pin joints and connecting links, the motion of the actuator allows both to approach the electromagnet to the cloth, and to open/close the jaws. Thus, the proposed gripper has one degree of actuation, which allows the gripper to be lightweight (181 g, including all the electronics) and with limited encumbrance, taking into account the considerations in [86]. The closed structure width is 9 cm. The maximum opening size of the jaws is 13 cm. When the jaws are at the maximum opening distance allowed by design, the most prominent part is the electromagnet and the distance between the electromagnet and the base is 15.3 cm. When the jaws are completely closed, the most prominent part is given by the jaw tips, and the distance between the tips and the base (bottom plate in Fig. 3.2a) is 15.5 cm. The circular base has 5 cm diameter, and the links connecting the two circular surfaces enclosing the electronics are 5 cm long. To have a robust structure, the gripper base, the jaws and the locations assigned to the actuator and the electromagnet are 3D-printed in ABS. Conversely, the jaw-tips are hollow and realized in TPU, to ensure a more compliant interaction with the cloth. The tips are designed with grooves (see Fig. 3.2b) to increase the friction during the contact with the objects, thus reducing undesired slippage.

The gripper microcontroller is an Arduino Pro Mini with an ATmega328P (running at 16MHz, 5V input voltage). Gripper control is achieved via position control, by exploiting the actuator feedback position and the polarity inversion through the L293B motor-drive. The electromagnet is activated or deactivated through a logic input (H/L), which is a function of the actuator position and sensor measurements (see also Sec. II-B). The gripper receives commands through a Bluetooth connection (RN42 module by Microchip) and its working voltage is 12 V.

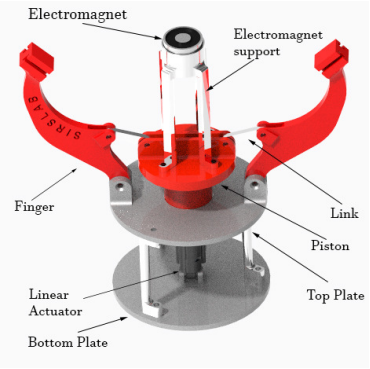

(a) Mag-Gripper CAD

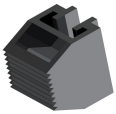

(b) Jaw-tips

Fig. 3.2 Sketches of Mag-Gripper: (a) isometric view, (b) zoom on the jaw tips. Notice the grooves and the hollow structure, designed to provide friction to limit undesired slippage of the fabric.

3.2.2 Working principle

In Mag-Gripper, the electromagnet plays a fundamental role during the approach to the object, while the jaws allow a secure grasp maintenance. As soon as the central cart moves, two orthogonal motions are generated: the first one, along the actuator direction of elongation, corresponds to the direction along which the electromagnet approach the garment, the second one lies on planes orthogonal to that direction, and corresponds to the motion of the jaws.

To avoid undesired collisions between the jaws and the garment during the approaching phase, as well as collisions between the jaws and the electromagnet, three working configurations have been defined: pre-grasping, grasping and release. The working configuration can be seen as a function named *conf* of three independent variables: *ae*, which

stands for activation of the electromagnet, *sr*, i.e., sensor reading, and *at* i.e., translation of the actuator,

$$conf(ae, sr, at) = \begin{cases} pre - grasping \\ grasping \\ release \end{cases}$$

As mentioned in Sec. 3.2.1, during the *pre-grasping* phase, the distance between the jaws is the maximum allowed and the electromagnet is the most prominent part of the gripper. This allows the electromagnet to approach the fabric without collisions between the cloth and the jaws. This configuration is reached as soon as the electromagnet is activated, the force sensor starts sending the measured values and the motion of the linear actuator has not yet started. After the gripper has entered in the pre-grasping phase, the actuator starts translating to approach the object. The contact is considered to occur when the force sensor measures the exceedance of a given threshold. This allows the gripper to enter in the *grasping* configuration: the jaws close and the electromagnet is deactivated (no more needed). The motion of the linear actuator is prevented through a position control until the release command is sent, and the gripper enters in the *release* configuration: the electromagnet is still deactivated, the sensor readings are discarded and the linear actuator is commanded to move so to allow an opening distance between the jaws equal to one half of the maximum allowed (see Fig. 3.3). Notice that the jaws closing motion relies on the force sensor measurements. This is why, in principle, Mag-Gripper can work also without the electromagnet (see also Sec. 3.3.3).

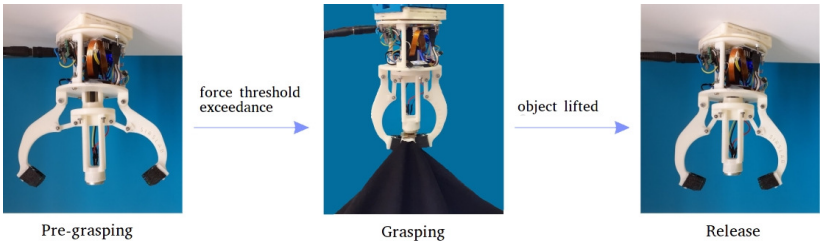

Fig. 3.3 Mag-Gripper working configurations. During the pre-grasping, the electromagnet slot is the most prominent part of the structure, to allow the attractive motion of the ferromagnetic plate without undesired collisions between the jaws and the cloth.

3.2.3 Finite Element Modelling and Analysis

Finite Element Analysis (FEA) and Dynamic Analysis of the gripper have been carried out using COMSOL Multiphysics Software. Boundary load of 18 N (Linear Actuator maximum force) was applied in the y-axis direction. The gripper was cut half to simplify the geometry and a symmetric constraint was applied to compute the solution. Tehtrahedran elements were used for meshing. A mesh convergence test was also carried out on the basis of maximum element size, which suggested that when element size is between 0.00180 m to 0.00375 m the results are almost similar. Hence, maximum element size of 0.00218 m was selected. The result of FEA is depicted in Fig. 3.4. The maximum stress experienced is 5.29 MPa and it is exerted on the link between finger and piston, showing it as the most vulnerable part. For the case of dynamic analysis, a constant force of 18 N was applied and the corresponding velocity and acceleration plots of the jaw tip are shown in Fig. 3.5.

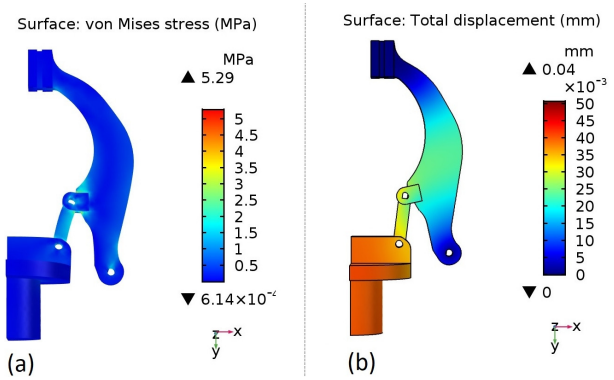

Fig. 3.4 FEA: (a) Stress Von Mises, (b) Maximum Displacement.

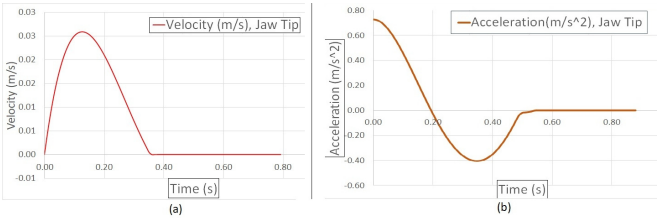

Fig. 3.5 Dynamic analysis: (a) Velocity and (b) Acceleration plot of the jaw tip when the actuator maximum force is applied.

3.3 Experiments

Mag-Gripper is meant to be a tool for autonomous manipulation of clothes, by exploiting the presence of small ferromagnetic parts properly located on the garment. To avoid undesired interactions with the environment, soft ferromagnetic materials can be exploited (see Chapter 2). Grasping the object in the desired points is the first condition to be met to achieve the desired manipulation.

Experiments with a Sawyer collaborative robotic arm (by Rethink Robotics) were performed to test the actual capabilities of the proposed gripper. To this aim, we investigated: *i)* how the performance are related to the size of the ferromagnetic plate and the cloth weight; *ii)* which is the role played by the electromagnet on the configuration taken by the cloth after the grasp has occurred; and *iii)* how to compensate possible uncertainties on the estimate of the grasping points.

For the sake of simplicity, we assumed the desired location of the grasping point to be fixed on the garment (i.e., on a shoulder), and a fiducial marker located in that position had been used to retrieve an estimate of the desired pose with respect to the robot base. The cloth was located on a tabletop and an overhead camera (ASUS Xtion) was used during the marker detection phase.

The trajectory planning was implemented in the *MoveIt* framework, and was decomposed in three steps: *i)* go 4 cm over the estimated location; *ii)* go down until the contact between the gripper and the ferromagnetic part has been detected; and *iii)* lift the garment for 20 cm. Communication between the devices (robot, gripper, PC) ran via ROS (Robot Operating System).

In the following, five different sets of experiments are described. For the sake of simplicity, the gripper orientation at the target location was fixed so to have a non-occluded view of the scene from our desk. However, it can be chosen arbitrarily.

Unless otherwise stated, the garment to grasp was the T-shirt included in the YCB dataset [93], and a squared ferromagnetic plate with side 1.8 cm was involved in the grasping task.

3.3.1 Dependency on the plate dimensions

By means of this set of experiments, we investigated two aspects related to the ferromagnetic plate size: *i)* how the number of successful grasps changes by varying the plate dimensions, and *ii)* the repeatability of the grasp execution. Regarding the former issue, we termed *successful* a detected contact occurred in correspondence of the ferromagnetic plate and maintained without appreciable changes during the lifting phase. Regarding the second investigated aspect, we meant to have a measure of repeatability by estimating the area of the garment contacted by the electromagnet when multiple grasp attempts were performed with the same target. To have this measure, we covered the gripper extremity with a thin rubber layer and put a thin layer of tempera colours on it. During the contact with the plate, the color laid down on the plate, leaving a mark of the executed trial. After 10 grasp attempts, we estimated the radius of a circumference containing all the color marks on the plate by measuring the distance between the two furthest points with a caliper. After each trial, the rubber was cleaned to avoid a dry color layer, which would have reduced the magnetic force. The usage of the thin wet tempera color layer did not reduced appreciably the attraction. Three different squared plates were used, with side of 1.0 cm, 1.8 cm and 2.5 cm, respectively. Results are reported in Table 3.1. Notice that in the bimanual clothing manipulation presented in [75], a grasp configuration is termed successful if both the left and the right grasps occurred within 5 cm from the estimated most likely grasps.

Table 3.1 Grasps repeatability estimate: Number of successful grasps on the YCB T-shirt and radius of the estimated contacting area between end-effector and plate when the grasping attempts are repeated 10 times. Results are related to the plate size.

Square side	Success	radius [mm]
1.0 cm	8/10	15.1
1.8 cm	9/10	21.2
2.5 cm	9/10	24.5

3.3.2 Dependency on the cloth weight

To have insights on how the performance of Mag-Gripper are influenced by the cloth weight, 4 different garments were used to be autonomously grasped 5 times: the YCB T-shirt, a mid-season pullover, an old bib and a terry guest towel. Objects weight and thickness are reported in Table 3.2. Besides the number of successful attempts, we report also the mean distance that was required between the electromagnet and the garment to allow the magnetic force to cause the desired attractive motion of the cloth towards the electromagnet.

3.3.3 Dependency on the electromagnet

By means of this kind of experiments, we investigated which is the role played by the electromagnet on the configuration taken by the fabric when the grasp has already occurred. To this aim, we compared the area involved in the grasp with and without the exploitation of the electromagnet. In other words, we performed 10 attempts equipping the garment with the ferromagnetic plate (E experiments) and then more 10 attempts after having removed it (WE experiments). All the trials

Table 3.2 Objects used to have an insight on how the Mag-Gripper performance are related to the objects weight and thickness. Number of successful grasp attempts and required distance between the electromagnet and the plate are reported. The ferromagnetic plate with side 1.8 cm was exploited.

Object	Weight	Thickness	Successes	Distance
T-shirt	125 g	0.4 mm	5/5	6 mm
Pullover	266 g	0.7 mm	5/5	5 mm
Bib	43 g	1.3 mm	5/5	3 mm
Towel	148 g	2.5 mm	4/5	2 mm

had the same target grasping point. In both the sets of experiments, the gripper closing motion started when the contact between the gripper and the cloth had been detected by the force sensor.

Moreover, in both the set of experiments, a thin layer of tempera colors was laid down on the jaw-tips to mark the areas involved in the grasp execution. In Fig. 3.6, the green marks correspond to the areas contacted without exploiting the presence of the electromagnet, while the blue marks are the areas of interaction when the grasp execution relies on the force of attraction between gripper and cloth. In the first case, the distance between the corresponding centres of the marks is about 10 cm (avg), while in the second case the same distance is about 5 cm (avg). When the ferromagnetic part is lifted by the electromagnet, the portion of the fabric involved in the grasp is smaller than the one involved without the electromagnet exploitation. This reduces the possibility of wrinkling the fabric, increasing the grasp precision and repeatability.

Fig. 3.6 Estimate of the fabric portion involved in the grasp, with and without the electromagnet exploitation (blue and green marks, respectively). A smaller portion produces less wrinkles, increasing the grasp precision.

3.3.4 Target uncertainties compensation

When dealing with grasp planning, it is common to have to cope with pose errors due to the camera-robot calibration process, or to simplifying assumptions affecting the grasp planners, or to undesired uncalibration of the robot arm. To investigate the Mag-Gripper capabilities, we introduced by purpose an error of 1 cm on the x and y coordinates of the estimated grasping point, and 10 grasping attempts were performed.

During 7 grasp trials, the electromagnet was still capable of attracting the cloth. However, in 3 of these experiments, the force sensor did not detect the occurred contact, since it happened in a lateral location not involving the sensor (the sensor radius was about 3 mm).

3.3.5 Common small objects with ferromagnetic parts

This set of experiments was aimed at testing the Mag-Gripper capability in grasping small objects different from clothes that usually would

require the exploitation of environmental constraints for a successful grasp execution [91]. Two small boxes, a comb, hair barrettes and paper clips have been used. The squared plate with side 1 cm (used also in Section 3.3.1) was located on the top of the boxes and on the comb handle. The other objects were already equipped with ferromagnetic parts. The heavier object (box) had a mass of 25 g. The size of the objects spanned between 0.1 cm x 4.5 cm (paper clip) and 4.5 cm x 6.5 cm (box). An overall of 12 grasp attempts have been performed, achieving a success rate of 100%.

3.4 Discussion

3.4.1 On the dependency on the plate dimensions

This set of experiments was aimed at investigating the role played by the ferromagnetic plate size in the grasp execution.

In all the failures, the contact between plate and electromagnet actually occurred but was not detected by the force sensor, since it occurred in a location not involving the sensor. Hence, the garment lifting phase was not triggered and the robot remained stuck.

In respect to the estimate of the actual contacting area between end-effector and plate, as it can be foreseen, the larger is the plate, the larger is area that can be contacted. That area could be represented as a circle enclosing the plate, since the contact between the plate and the electromagnet can occur everywhere on the plate, as long as there is a superposition of the two surfaces. The variability observed during experiments in the location of the area of interaction was due to different aspects: the manual collocation of the marker on the plate, errors related

to the camera calibration, but also to uncertainties on the control of the collaborative robotic arm due to its spring-based joints.

Interestingly, one successful grasp related to the plate with side 1 cm allows a further consideration. During that attempt, the contact between end-effector and plate occurred. However, suddenly the plate fell down before the electromagnet deactivation. Nonetheless, the magnetic force was capable of re-establishing the contact in time and the gripper successfully lifted the T-shirt. This suggests that by properly managing the electromagnet deactivation time, Mag-Gripper could be used to cope with the possibility of loosing the contact with the object, ending up in a successful grasp.

3.4.2 On the dependency on the cloth weight

Experiments aimed at having insights on how much the Mag-Gripper performance rely on the cloth weight revealed that the thickness of the garment is more relevant than the overall object weight. As it can be noticed by looking at the fourth column of Table 3.2, the thicker the garment is, the smaller the distance required to attract the ferromagnetic part. This is due to the fact that changing the thickness results in varying the local mass the electromagnet has to attract. If the local mass increases, the electromagnet needs to be closer to the plate to cause the attractive motion of the ferromagnetic part. This result suggests that the most suitable electromagnet should be chosen either to grasp specific clothes or in a conservative manner, by considering a predefined set of garments and ensuring to be capable of grasping the thickest one. However, this gives us the possibility to remark that the choice should be context-related: in some cases, an unnecessary strong magnetic field

can introduce some disturbances in other devices that are present in the robot workspace. Moreover, we want to stress the importance of having an attractive motion between the gripper and the cloth without the need of getting in contact with the environment to grasp the garment. This capability, indeed, allows an intrinsically safer robot-environment interaction, besides the possibility of performing aerial grasps [94].

3.4.3 On the dependency on the electromagnet

Regarding this set of experiments, as it can be seen in Fig. 3.6, when the grasp execution relies on the presence of the electromagnet (E experiments), the distance between the jaws during the grasp is smaller than in the case where the electromagnet is not exploited (WE experiments). This is due to the fact that the closing motion of the gripper starts as soon as the contact between the end-effector and the cloth is detected. However, in the WE experiments, the gripper needs to reach the table before detecting the contact. As a consequence, when the jaws start closing, the distance between the jaws is close to the maximum allowed (13 cm by design). On the other hand, in the E experiments, the magnetic force attracts the plate before the gripper reaches the table, and when the collision of the plate with the force sensor generates the signal of detected contact, the fabric has already assumed a conic-like shape. This is the reason why the distance between the jaws is smaller in the E experiments than in the WE experiments.

Moreover, a qualitative consideration should be done. As it can be seen in Fig. 3.7, when WE experiments are performed, the part of the cloth located between the jaws is significantly crinkled. This is due to the fact that the grasp is executed by sliding the jaws on the table: The

(a) WE experiments (b) E experiments

Fig. 3.7 Grasps performed with and without electromagnet exploitation (left and right, respectively). The electromagnet exploitation allows a conic-like grasp without unnecessary wrinkles, resulting in a more repeatable cloth configuration.

contact points between cloth and jaws do not change and the minimum distance between these points (i.e., the distance without considering the wrinkles) becomes gradually smaller and smaller, while constraining a non-necessary portion of the fabric to remain trapped between the jaws.

Hence, if the aim is grasping the garment in a desired location, making the fabric assume a configuration easy to manage with vision-based Machine Learning techniques, the exploitation of the electromagnet seems to be a good way to approach the problem. Indeed, the conic-like shape taken by the cloth allows to achieve a sort of pinch grasp [30], which results in a less disturbing configuration of the points located near the actual grasping point. This sort of extended point-like grasp allows a more predictable configuration of the garment, which is an highly deformable object with potentially infinite ways of deforming.

3.4.4 On the target uncertainties compensation

The artificial introduction of uncertainties in the estimate of the grasping point pose was aimed at investigating to what extent the exploitation of the magnetic force can allow grasping the object in the target location, thus achieving a compensation of position estimation errors. Disturbances of 1 cm acting simultaneously along the x and y coordinates resulted in noisy targets located about 1.4 cm far from the desired points. The fact that in 7 grasps over 10 the electromagnet attracted the plate is encouraging, yet not exciting. However, the presence of the electromagnet suggests the possibility of performing a sort of *partially-blind grasp*. A *blind grasp* is meant to be a strategy to be applied when uncertainties on the estimation of the grasping points are present (e.g. when the vision system is not particularly reliable, or uncertainties originate from non-ideal dynamics of the robot arm). According to this strategy, the robot is first commanded to reach the estimated grasping point and, if the contact between the object and the gripper is not detected, the robot starts following a predefined pattern (e.g., inside a square of known side, similar to the one shown in Fig. 3.8). The basic idea is to span a small area around the estimated grasping point to let the magnetic force overcome position uncertainties and establish the desired contact.

The envisaged pattern corresponds to a planar motion occurring at a given height with respect to the ferromagnetic plate, hence it can allow to successfully compensate uncertainties on the xy plane. However, the success of the blind grasp is highly dependent on the distance required to the electromagnet for attracting the garment. That distance, in turn, depends on the fabric thickness. To get a more generalized planning strategy, further investigations are needed. Notice also that if the plate

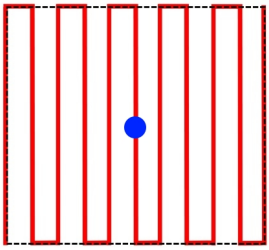

Fig. 3.8 Example of possible motion pattern (in red) for a *blind grasp*: a small area (delimited with the dashed line) is spanned around the estimated grasping point (blue dot) to face position estimation errors.

dimensions are not sufficiently small and the attraction occurs near the borders, the grasp might be unstable.

In principle, the blind grasp could be taken to extremes to perform a *totally-blind grasp*, when the vision system is not present at all and a minimal *a priori* knowledge of the environment is given (i.e., size and pose of the table where the cloth is located).

3.4.5 On common small objects with ferromagnetic parts

This set of experiments was aimed at having insights on the Mag-Gripper capabilities of grasping objects different from clothes. Indeed, we proposed Mag-Gripper as a tool for service robots suitable in home settings or in assistive robotics. In this framework, it could be useful to have a robot capable of grasping small objects of common usage. In particular, we considered objects (i.e., comb, hair barrettes and paper clips) difficult to grasp either with a parallel-jaw gripper either with a more complex robotic hands, and usually requiring environment exploitation [91]. The challenging nature of these objects relies on the fact that they are flat and thin. During experiments, the electromagnet was capable of generating a visually appreciable attractive motion, that allowed the grasps without the end-effector needed to reach the tabletop.

A physics-based model of such a magnetic latching has been provided in Chapter 2 of this Thesis. As a note, we want to point out that the ferromagnetic part located on the object could be small and lightweight, depending on the object: in a hair barrette involved in the experiments, the magnetic element consisted in a spring 5 mm long.

3.4.6 Additional considerations

As previously mentioned, Mag-Gripper features an immediate application in the robotic community: It is meant to be a support tool for the research in Machine Learning-based garment manipulation, where high repeatability in grasp location is required during data collection. However, our long-term vision involves a synergistic cooperation with researchers in Machine Learning and garment manufactures to develop production lines for autonomous cloth manipulation. In this light, we filed a patent application that concern methods exploiting magnetic coupling for autonomous garment manipulation (PCT/IB2021/057293).

Different grippers can be devised, exploiting also tendon-driven fingers and embedded environmental constraints (e.g, like in the Scoop hand [95]). The proper choice will rely on the desired kind of manipulation. Additionally, magnetic elements can be exploited as support points in different, intermediate tasks occurring during the manufacturing process (like cutting, sewing, ironing, and the like). Moreover, the magnetic elements located on the garment can be fixed (like buttons or labels, ornamental or brand elements) or removable (i.e. they can be attached to the fabric during the manufacturing process and removed before packaging the garment).

3.5 Final remarks

This Chapter concerned the autonomous manipulation of highly deformable objects present in the environment, with focus on garments.

In this context, we presented Mag-Gripper, a novel augmented jaw gripper specifically designed for autonomous cloth manipulation. To grasp the garment where desired, we proposed to exploit an attractive force between the desired location on the fabric and the robotic end-effector. To this aim, Mag-Gripper is equipped with an electromagnet. Such an electromagnet establishes an extended point-like contact with the cloth, while the jaws allow a secure grasp maintenance during manipulation. Clearly, clothes have to be equipped with small magnetic parts (properly located ornamental or brand elements, like buttons).

Experiments performed with a collaborative robotic arm showed that the exploitation of the magnetic force allows to perform a repeatable grasp execution and to compensate uncertainties on the estimated location of the target grasping point. Moreover, the extended point-like contact caused by the electromagnet allows grasp without unnecessary wrinkles, achieving clothing configurations more suitable to vision-based Machine Learning techniques for autonomous manipulation.

Part B

Soft Interactions with Humans

Soft interactions with humans

This part of the Thesis deals with soft interactions involving humans. As previously mentioned, humans can be considered to be *soft* agents. This sentence can appear unusual, since thoughts quickly run to our bones, playing remarkable roles when accomplishing different tasks. The hard, osseous skeleton, indeed, is the structural core that allows humans to get the upright posture, which differentiates humans from invertebrates, quadrupeds and apes. Several scholars agree that the upright posture is one of the features that most profoundly affected the physical and cultural evolution of humans [96, 97]. However, the anatomical evolution that led to the upright posture went hand in hand with the brain specialization induced by the progressive specialization of the hand [98], that became capable of dexterous and in-hand manipulative movements. Interestingly, chimpanzees tend to walk upright when they have valuable food in their hands [99].

Although the osseous structure has a fundamental role in the human anatomy, hard bones would allow a negligible impact on the world around us without the synergistic interplay of bones, muscles and skin. Muscles, indeed, envelop the bones and are connected to tendons, realizing a network of fibres capable of transducing in motion the electrical signals coming from the brain. The skin envelops the human body, and

is rich of mechanoreceptors, which are specialized neurons transducing mechanical deformation of the skin into electrical signals. Such signals encapsulate information on the tactile and kinaesthetic interaction with the environment.

Muscles and skin are tissues made of soft materials, whose features are revealed during interactions with the environment. In such interactions, hands are the main means used by humans. As mentioned in the introduction of *Part A* of this Thesis, the compliance of the human hand is located both at the joints and at the skin levels. This allows to perform delicate and robust grasps, as well as to retrieve relevant information on the manipulated object, through the way in which the skin deforms generating pressure distributions related to the object texture and weight.

The compliance of the tissues allowed the development of analytical models focused on humans. Muscles, indeed, can be modelled as spring-damper systems, and functional muscles-tendons units can be represented as series of elastic elements [100]. Also during voluntary movements, the coordinated motion of agonist and antagonist muscles belonging to the same limb can be modelled as a linear spring-damper system. During such movements, moreover, if a small disturbance acts on the limb, the muscular visco-elastic behaviour allows humans to carry on with the desired trajectory, with little deviations [101].

Concerning the human arm, the analysis of experimental stiffness ellipsoids retrieved by perturbing the position of the hand [102] revealed that the principal axis is along the forearm. This means that this is the direction along which the human is more able to reject disturbances, and it is due to the fact that, if needed, muscular contractions of both upper arm and forearm can be performed. The minimum stiffness is along

the direction perpendicular to the direction of maximum stiffness, and corresponds to contracting only the forearm, with negligible contraction of the upper arm. Furthermore, experiments revealed that when humans have to accomplish a task, they spontaneously arrange arms and hands to minimize the impact of possible perturbations [103].

During activities, humans learn feedforward internal models of their body, as well as task-related models of the body parts involved in the task execution. These models map the sequence of the muscular activations into effects produced on the environment, and are adaptive, meaning that humans are able to generalize the learnt patterns for facing previously unseen situations [104]. When interacting physically with objects, variations of the learnt patterns are related to experiencing different force fields, which require to apply different torques at the human joints for a successful task accomplishment [104]. Tactile and kinaesthetic feedbacks, encapsulating information on the actual interaction, are the main actors of motor learning [105]. Interestingly, such models are encoded and stored, leading to the so-called motor memory: the acquired internal models do not disappear when the training stops [106].

In Chapter 4, we will consider a human-robot cooperative task involving the transportation of a large object. The envisaged task is human-centered, meaning that the human will be in charge of deciding the trajectory to be performed, and the robot will have to cooperate.

The forces exerted by the human will implicitly reflect all that has been previously said on the way in which the soft human agent interacts with the environment. Such forces are the core of the robot control scheme, and a compliant surface at the end-effector is exploited. Such a compliance allowed to develop pressure constraints leading to robot velocity commands for a successful task execution. Nonetheless,

accomplishing Human-Robot cooperative tasks is not something that people are used to perform, so we consider the aspect of motor learning by accounting for training and test phases during the experiments.

In Chapter 5, we will consider a hand-focused human-human soft interaction. More specifically, a biomechanical model of a hand posture for writing on touch screen devices will be devised. In such a posture, the hand will interact with itself, realizing a *FingerPen* that will merge gesture and tool into a single operative organ. Bones will constitute the mechanical structure composed of rigid links, while the skin compliance and the arrangements of the fingers will determine the contact models involved in the proposed work. Moreover, velocity ellipsoids, dual of the force ellipsoids, will characterize the workspace. Being a novel hand posture, also in this case we explicitly accounted for a users' training phase, during which visual and kinaesthetic feedbacks allowed the acquisition of task-related motor skills.

4 Human-Robot cooperative grasping

This Chapter focuses on a soft interaction occurring during a human-robot cooperative manipulation task. In the envisaged task, the two co-agents transport a large object, and the robot is not tightly grasping the object, but is contacting it with a compliant extended patch with known geometry (Fig. 4.1). In this framework, a proper contact model named the *Extended Patch model* will be proposed: geometric properties and compliance of the patch will be used to derive pressure constraints, that will be considered in addition to Coulomb and normal friction limits. Then, based on the Extended Patch contact model, a novel control scheme for cooperative human-robot grasping will be introduced. In such a control scheme, the violation of the constraints generates velocity commands that have to be provided to the robot with the aim of maintaining the contact with the object. More specifically, friction constraints are related to robot translational velocities, while the novel pressure constraints are used to derive suitable angular velocities.

The proposed approach provides the robot with some exteroceptive capabilities related to the status of the contact, similarly to the information provided to the human by mechanoreceptors[1].

[1]The content of this Chapter has been published in [107]. Reprinted with kind permission from IEEE.

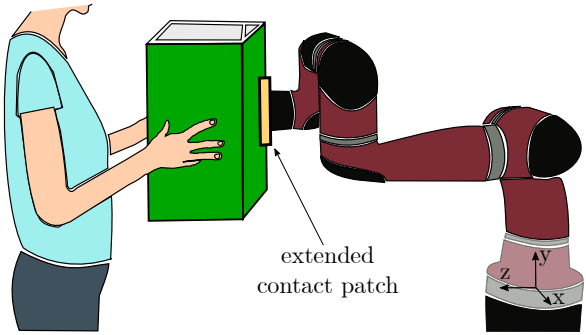

Fig. 4.1 Cooperative grasp between a human and a robot. The human guides the cooperative manipulation task and the robot keeps the grasp stable, avoiding sliding and rolling. The robot end-effector is equipped with a force sensor and a contacting plate ensuring an extended contact patch.

4.1 Related works

Cooperative manipulation between humans and robots is one of the most relevant examples of physical human-robot interaction (pHRI) [108]. Different scenarios have been tackled, from lifting of heavy objects [109], to transport of long or flexible objects [110]. The interaction is usually based either on impedance [111] or admittance [112] control schemes, where the controller parameters are often tuned exploiting observations of human-human interaction. Research works on human-robot cooperative manipulation focus on obtaining smooth human movements [113] and optimal load sharing [114] for a seamless and natural collaboration. Most of the times it is assumed that the robot is either tightly grasping the object with its gripper(s) [114], or that the object is attached to the robot through a universal joint [112]. So far, in the field of cooperative human-robot grasping, less focus has been put on deriving a

model of the robot contacts taking into account the actual properties of the contacting surface. Also in the field of cooperative robot-robot manipulation, the common assumption is to consider the grasped object as firmly attached to each manipulator's end-effector (tightly grasped object) [115], and there are only a few works that explicitly model the contact points. In [116], for example, rotational/prismatic joints are used to model the rolling/sliding of the contacts. Most of the literature on grasp analysis is based on models in which both the hand and the object are represented as rigid bodies, and contacts are identified in single points [117, 118]. These assumptions are at the basis of the main grasp quality measures [119, 120], and are also adopted in other applications, including the analysis of cooperative robot-robot and human-robot manipulation. Gupta *et al.* , for example, starting from the work conducted by Erdmann [121], assumed single point frictional contacts to plan carrying tasks with robots equipped with flat palms [122]. Contact models considering the resistance to torques about the contact normal direction (soft finger contact model [118]) have been exploited, instead, to simulate human grasp capabilities [123], and to detect rotational slip with force and tactile sensors [124].

Extended contact patches have been explicitly modelled in many works on non-prehensile manipulation (e.g., planar pushing [125], planar sliding [126]), and, more recently, the concepts of *limit surface* [126] and *motion cone* [125] were used for planning prehensile in-hand manipulation actions through planar pushes [127]. Also the diffusion of soft robotic hands and their introduction in unstructured contexts [128], lead to an upgrade of the contact model, in order to consider contact patches with a finite and non-negligible area and local material deformation [129].

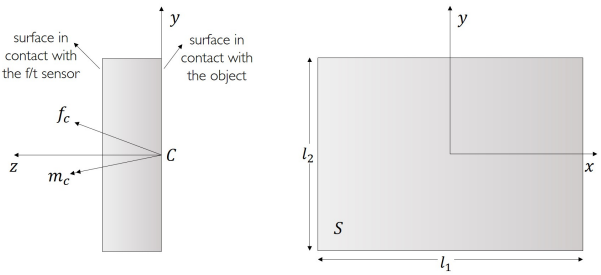

Fig. 4.2 Side and front view of the flat, rectangular plate attached to the force/torque sensor at the robot end-effector.

4.2 Contact models

After some general definitions, here we briefly review the main contact models adopted in grasp analysis, and then introduce a model that considers a finite non-negligible contact area between robot end-effector and grasped object.

4.2.1 Definitions

Let us consider a plate whose surface goes in contact with the grasped object and is attached to a force/torque sensor at the robot end-effector, as in Fig. 4.1. For the sake of clarity, we assume that the contact area is flat and rectangular (Fig. 4.2). Let us define a contact reference frame whose origin C is in the centroid of the contact area, in which the $z-$axis is normal to the contact surface pointing to the plate, and x and y are aligned with plate's edges. When the plate is in contact with an object, it applies an equivalent contact wrench λ_c at the center of the contact patch C. λ_c collects the contact forces $\mathbf{f}_c$ and moments $\mathbf{m}_c$ in C: $\lambda_c = [\mathbf{f}_c^T, \mathbf{m}_c^T]^T$, and it is balanced by the resultant of the tangential stresses and normal pressures applied to the plate. In each infinitesimal

area dS of the contact patch there are a normal pressure $p(x,y)$ and two tangential stress components τ_x and τ_y. The resultant force and moment related to p, τ_x and τ_y, that have to balance λ_c, are:

$$f_{cx} = -\int_S \tau_x dS, \quad f_{cy} = -\int_S \tau_y dS, \quad f_{cz} = -\int_S p dS, \tag{4.1}$$

$$m_{cx} = -\int_S py dS, \quad m_{cy} = \int_S px dS, \quad m_{cz} = -\int_S (-\tau_x y + \tau_y x) dS. \tag{4.2}$$

In the following, we summarize how these components are related in case the plate is approximated with a point (see Section 4.2.2) or in case all geometrical properties of the actual contacting area are explicitly taken into account (Section 4.2.3).

4.2.2 Background

4.2.2.1 Single point with friction (or Hard Finger)

This is one of the simplest contact models, often adopted in grasp analysis literature, and it can be applied when the contact area is relatively small and the materials of the contact surfaces are sufficiently hard. In this situation, the contact can be approximated as a point and the action that is exchanged can be approximated with a force applied at the contact point, i.e., $\lambda_c = [\mathbf{f}_c^T, \mathbf{0}^T]^T$. This force can be represented as the sum of a normal $f_n = f_{cz}$ and a tangential $f_t = \sqrt{f_{cx}^2 + f_{cy}^2}$ component, that are related by the Coulomb's friction constraint, i.e., $f_t \leq \mu_s f_n$, where μ_s is the static friction coefficient. In other words, Coulomb's

law of friction imposes that $\mathbf{f}_c \in FC$, where FC is the *friction cone*:

$$FC = \left\{ \mathbf{f}_c \in \Re^3 : f_n \geq 0, f_t \leq \mu_s f_n \right\}. \tag{4.3}$$

4.2.2.2 Soft finger

As in the previous model, the theoretical contact patch is assumed to be a point, but in this case we consider the local deformation of the contact surface. The action exchanged at the contact surface is the resultant of the distributions of normal pressure and tangential stress. Beside the tangential force f_t, the tangential stress can also generate a moment component m_{cz}. Since tangential stress and normal pressure have to locally satisfy Coulomb's friction law, that is $\tau_t = \sqrt{\tau_x^2 + \tau_y^2} \leq \mu_s p$, there is also a constraint between m_{cz} and f_n, i.e., $m_{cz} \leq \mu_t f_n$ [123].

4.2.3 Extended Patch (EP) model

Both the models described above are based on the hypothesis that, neglecting local deformations, the contact can be approximated with a point. In other words, both the models deal with non-conformal contacts [130]. In many implementations, however, this hypothesis cannot be applied. Here, for instance, we are considering a human and a robot that have to lift and move an object together: it is obviously better to assume that the robot is touching the object with an extended contact patch, through which it can apply forces and torques in all directions, rather than supporting the grasp in a single point. In this way, intuitively, the grasp is more reliable, and the human can fully control the object pose, while a part of the object weight is supported by the robot.

To better explain the contact model that we are proposing, we do two hypotheses simplifying computations: a) the contact is flat, and b) the contacting surfaces are made of linear elastic materials. If one or both these hypotheses are not satisfied, the main steps of the procedure that will be presented can be applied as well by properly specifying contact materials' constitutive relationships and by evaluating the integrals in Eq. (4.1) and Eq. (4.2) over the non-flat surface.

From our hypotheses, it follows that the pressure distribution must be linear in x and y:

$$p = p_0 + ax + by. \tag{4.4}$$

otherwise the contact between the surfaces would be lost after the deformation. In the linear elastic material, indeed, the Hook law holds point-by-point: $\mathbf{f} = -k\hat{\mathbf{z}}$, where k is the elastic constant. This means that $\mathbf{f}$ generates point-by-point a linear displacement of the contact surface. Hence, locally, the pressure is given by $p = -k'z$. To preserve the fact that $\mathbf{f}$ generates a linear displacement of any point of the contact surface, the most general expression of the pressure distribution on that surface has to be linear in x, y (Eq. (4.4)), whose coefficients p_0, a and b depend on the contact wrench λ_c and the plate surface S through:

$$f_{cz} = -\int_S (p_0 + ax + by)\, dS, \tag{4.5}$$

$$m_{cx} = -\int_S (p_0 + ax + by)\, y\, dS, \tag{4.6}$$

$$m_{cy} = \int_S (p_0 + ax + by)\, x\, dS. \tag{4.7}$$

We can express p_0, a and b as functions of f_{cz}, m_{cx}, and m_{cy} by solving the above equations. If we assume that the surface of the plate

is rectangular, with sides l_1 and l_2, and we substitute the obtained p_0, a and b in (4.4), we get:

$$p = \frac{f_{cz}}{l_1 l_2} + \frac{3m_{cy}}{l_1^3 l_2} x + \frac{3m_{cx}}{l_1 l_2^3} y. \tag{4.8}$$

Eq. (4.8) shows that the pressure is the sum of three terms: the first one is the mean pressure, due to the application of a normal force on a surface, while the others are the contributions provided by the applied torques in x and y directions. These components vary according to the Cartesian position of a given point on the surface. So, for instance, if just a counterclockwise rotation about x-axis is considered, the higher is the y-coordinates of a point, the higher is the pressure in that point. If an additional counter-clockwise rotation about y-axis is considered, the highest value of the pressure is in the right upper corner of the plate, while the minimum is in the bottom left corner. This is coherent with what is expected by intuition about forces and torques applied to a rectangular plate surface.

In order for the flat contact to hold, the following constraints must be satisfied for any point on the plate:

$$p(x,y) > 0. \tag{4.9}$$

It should be noticed that if $m_{cx} \neq 0$ and / or $m_{cy} \neq 0$, the pressure distribution over the contact area will not be constant and will have a minimum p_{min} and maximum p_{max} value. Since the pressure distribution is linear and the plate is rectangular, the boundary values p_{min} and p_{max} will result in one of the corners or, in some limit cases (when $m_{cx} = 0$ or $m_{cy} = 0$) on one of the edges. To verify that the contact is present, it

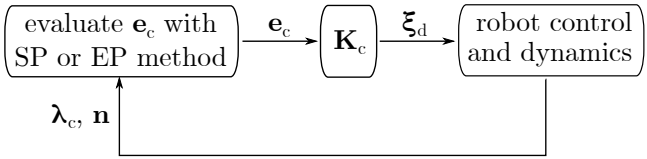

Fig. 4.3 Diagram of the force control with inner velocity loop.

is therefore sufficient to verify that Eq. (4.9) is satisfied for all the plate corners.

4.3 Robot control

The contact models introduced above are the basis of two force control algorithms that were implemented on a robotic arm to perform human-robot hybrid cooperative grasping. In both algorithms, the contact wrench $\boldsymbol{\lambda}_c$ and the normal direction $\mathbf{n}$ are inputs for the evaluation of force and torque correction terms denoted with $\mathbf{e}_f$ and $\mathbf{e}_m$, respectively. Indicating with $\mathbf{e}_c = [\mathbf{e}_f^T,\ \mathbf{e}_m^T]^T$ the complete correction vector, the reference robot speed value is then evaluated as $\boldsymbol{\xi}_d = \mathbf{K}_c\mathbf{e}_c$, where $\boldsymbol{\xi}_d = [\mathbf{v}_d^T,\ \boldsymbol{\omega}_d^T]^T$. $\mathbf{v}_d^T$ and $\boldsymbol{\omega}_d^T$ are the reference linear and angular velocities of the end-effector, respectively, and the subscript $_d$ indicates reference values. $\mathbf{K}_c = \text{diag}[\mathbf{K}_f,\ \mathbf{K}_m]$ is a 6-dimensional diagonal matrix of the contact values transforming force and moment correction terms into translation and angular speed references, respectively. In other terms, in both the control algorithms, a force control scheme with an inner velocity loop is implemented, as shown in Fig. 4.3.

4.3.1 Single Point (SP) method

This control algorithm is based on the single point with friction contact model (Section 4.2.2.1). The robot is controlled so that: a) the normal component of the contact force f_n is bounded between two limits f_{min} and f_{max}; b) the contact force $\mathbf{f}_c$ is inside the friction cone FC (Eq. (4.3)). SP contact model does not take into account moment components, however, since in our experimental implementation a flat end-effector was used, we had also to consider a moment correction term. Concerning this aspect, the control acted so to maintain the moment components as small as possible.

To accomplish these requirements, $\mathbf{e}_f$ and $\mathbf{e}_m$ are evaluated as detailed in Alg. 1 and graphically represented in Fig. 4.4. The inputs of the algorithm are the current contact wrench λ_c, the contact normal $\mathbf{n}$, f_{min} (chosen to assure that $f_n > 0$ with a sufficient reliability), f_{max} (taking into account the maximum force that the robot can apply and/or that can be applied to the object to avoid damages), and the friction coefficient μ_s[2].

The force compensation term is given by the sum of two terms: $\mathbf{e}_f = \mathbf{e}_n + \mathbf{e}_t$, where $\mathbf{e}_n$ is evaluated to ensure that $f_{min} < f_n < f_{max}$, and $\mathbf{e}_t$ keeps f_t within Coulomb's friction limits. The contact moment component, $\mathbf{e}_m$, is an action opposite to $\mathbf{m}_c$ and is applied to keep its value as low as possible, i.e., $\mathbf{e}_m = -\mathbf{m}_c$.

[2] To account for a possibly inaccurate estimate of μ_s, we define $\mu_s = c_s\mu_s'$, where μ_s' is the estimated value and $c_s \in (0,1]$ plays the role of *safety coefficient*. The same applies to μ_t.

Algorithm 1 Evaluation of $\mathbf{e}_c$, **SP** method

Input: $\mathbf{f}_c$, $\mathbf{m}_c$, $\mathbf{n}$, f_{min}, f_{max}, μ_s
Output: $\mathbf{e}_c$

loop
  $f_n \leftarrow \mathbf{f}_c \cdot \mathbf{n}$
  $\mathbf{t} \leftarrow \dfrac{(\mathbf{n} \times \mathbf{f}_c) \times \mathbf{n}}{|\mathbf{n} \times \mathbf{f}_c|}$
  $f_t \leftarrow \mathbf{f}_c \cdot \mathbf{t}$
  if $(f_n \leq f_{min})$ **then**
    $\mathbf{e}_n \leftarrow (f_{min} - f_n)\mathbf{n}$
  else if $(f_n \geq f_{max})$ **then**
    $\mathbf{e}_n \leftarrow (f_{max} - f_n)\mathbf{n}$
  else
    $\mathbf{e}_n \leftarrow \mathbf{0}$
  end if
  if $f_t \leq \mu_s f_n$ **then**
    $\mathbf{e}_t \leftarrow \mathbf{0}$
  else
    $\mathbf{e}_t \leftarrow f_t \left(1 - \frac{\mu_s f_n}{f_t}\right) \mathbf{t}$
  end if
  $\mathbf{e}_f \leftarrow \mathbf{e}_n + \mathbf{e}_t$
  $\mathbf{e}_m \leftarrow -\mathbf{m}_c$
  $\mathbf{e}_c \leftarrow [\mathbf{e}_f^T,\ \mathbf{e}_m^T]^T$
  return $\mathbf{e}_c$
end loop

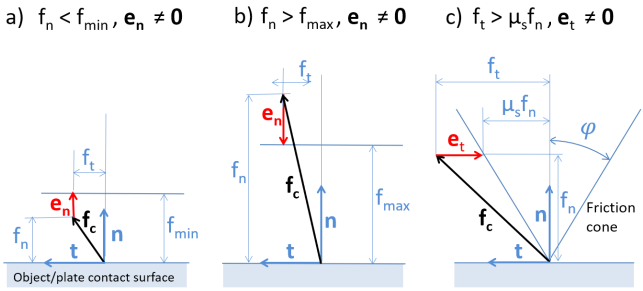

Fig. 4.4 Single Point method, evaluation of $\mathbf{e}_n$ and $\mathbf{e}_t$ for the following cases: a) $f_n < f_{min}$, b) $f_n > f_{max}$, c) $f_t > \mu_s f_n$.

4.3.2 Extended Patch (EP) method

The Extended Patch contact model (Section 4.2.3) is the core of the second control algorithm we discuss. In this case, $\mathbf{e}_f$ is evaluated again as in Alg. 1. The main difference with respect to the SP control resides in the evaluation of the $\mathbf{e}_m = [e_{mx}, e_{my}, e_{mz}]$ term, that here explicitly takes into account the previously introduced contact properties and limits. The e_{mz} action is applied if the normal component of contact moment exceeds torsional friction limits, i.e., if $m_{cz} > \mu_t f_{cz}$, while e_{mx} and e_{my} actions are applied if the pressure distribution $p(x,y) < 0$ in some parts of the contact patch. The p_i values are evaluated by means of Eq. (4.8) in the four plate corners P_i. Let p_{min} be their minimum value. If $p_{min} < 0$, a corrective term $\mathbf{e}_{mb} = [e_{mx}, e_{my}, 0]$ is evaluated as $\mathbf{e}_{mb} = -k_{mb}|p_{min}|\mathbf{b}$. Its magnitude is proportional to $|p_{min}|$, and its direction is opposite to the tangential component of the contact moment, whose direction is defined by the unit vector $\mathbf{b}$. The constant coefficient k_{mb} depends on plate geometry and is necessary to transform

the pressure in a torque reference. The evaluation of the $\mathbf{e}_c$ components, and in particular of $\mathbf{e}_m$, is detailed in Alg. 2.

Algorithm 2 Evaluation of $\mathbf{e}_c$, **EP** method

Input: $\mathbf{f}_c$, $\mathbf{m}_c$, $\mathbf{n}$, f_{min}, f_{max}, μ_s, μ_t, k_{mb}
Output: $\mathbf{e}_c$

loop
  $\mathbf{e}_f \leftarrow$ Alg. 1
  $\mathbf{b} \leftarrow \dfrac{(\mathbf{n} \times \mathbf{m}_c) \times \mathbf{n}}{|\mathbf{n} \times \mathbf{m}_c|}$
  $p_i \leftarrow$ eval Eq. (4.8) at corners P_i, $i = 1 \cdots 4$
  $p_{min} \leftarrow \min[p_1,\ p_2,\ p_3,\ p_4]$
  if $(p_{min} > 0)$ **then**
    $\mathbf{e}_{mb} \leftarrow 0$
  else
    $\mathbf{e}_{mb} \leftarrow -k_{mb}|p_{min}|\mathbf{b}$
  end if
  if $(m_{cz} < \mu_t f_n)$ **then**
    $\mathbf{e}_{mz} \leftarrow 0$
  else
    $\mathbf{e}_{mz} \leftarrow m_{cz}\left(1 - \frac{\mu_t f_n}{m_{cz}}\right)\mathbf{n}$
  end if
  $\mathbf{e}_m \leftarrow \mathbf{e}_{mb} + \mathbf{e}_{mz}$
  $\mathbf{e}_c \leftarrow [\mathbf{e}_f^T,\ \mathbf{e}_m^T]^T$
  return $\mathbf{e}_c$
end loop

4.4 Experiments

To validate the Extended Patch contact model, experiments with a 7 DoF collaborative robotic arm were performed. Skilled and non-skilled participants were involved. A *skilled* experimenter is a person familiar with collaborative robotics, and in particular with the cooperative manipulation setup used in the experiments. *Non-skilled* participants had never collaboratively grasped an object with a robot before.

Two groups of experiments were carried out: *Characterization* (performed by a skilled operator) and *Pick-and-Place* (performed by 10 non-skilled operators). In both cases, the Extended Patch method (EP) was compared to the Single Point approach (SP). Experimenters were not informed about which method they were testing.

Characterization experiments were mainly aimed at evaluating the precision and overall functioning of the proposed control strategies in the most favourable conditions (i.e., user with consolidated experience with collaborative robots and with the specific experimental setup), and this is why they were performed by an expert operator.

Pick-and-Place experiments, instead, were aimed at analysing user behaviour during a representative task that could be useful in industrial and domestic settings, and thus were performed by operators with different levels of experience.

In the experiments, we selected the $\mathbf{K}_c$ gains as follows. The two methods used the same $\mathbf{K}_f$ ($\mathbf{K}_{f,SP} = \mathbf{K}_{f,EP} = diag(k_f, k_f, k_f)$), while two different $\mathbf{K}_m$ matrices ($K_{m,SP}$ and $K_{m,EP}$) were adopted: $\mathbf{K}_{m,SP} = diag(k_{m,SP}, k_{m,SP}, k_{m,SP})$ and $\mathbf{K}_{m,EP} = diag(k_{m,EP}, k_{m,EP}, k_{m,EP})$. The translational correction term, indeed, resides on the same computation for both methods, while the rotational correction operates onto

different quantities (torques for the SP method, pressures for the EP method). The gains k_f, $k_{m,SP}$, and $k_{m,EP}$ were empirically chosen to ensure safe robot reactions (too high gains would result into too high velocities) and acceptable performance in all motion directions.

To have a soft elastic contact between the robot and the object, during experiments the object side closer to the robot was covered by a rubber layer (equivalently, the elastic patch can be embedded directly on the end-effector). A Sawyer robotic arm (by Rethink Robotics) equipped with an ATI Gamma force/torque sensor and a squared contacting plate at the end-effector were used. Communication between the devices was implemented within the Robot Operating System (ROS).

4.4.1 Characterization experiments

In these experiments, the operator was asked to move a box in cooperation with the robot, performing a simple trajectory for each trial, namely: *i*) a lateral translation of 50 cm along the x-axis (Fig. 4.1), *ii*) a vertical ascending translation of 50 cm along the y-axis, and *iii*) a translation of 50 cm towards the operator along the z-axis.

The given task must be accomplished keeping as constant as possible Cartesian coordinates that are not explicitly involved in the task execution (e.g., in task *ii*) x and z must be perturbed as little as possible). However, since in collaborative robotics a special attention is dedicated to the human operator's comfort, the operator is asked to achieve a trade-off between comfort and assigned task. Each task was repeated 5 times with a $33 \times 25 \times 15$ cm box weighting 0.5 kg.

Figs. 4.5 and 4.6 show the results obtained in terms of trajectories in task *ii*) using the the Single Point method and the Extended Patch

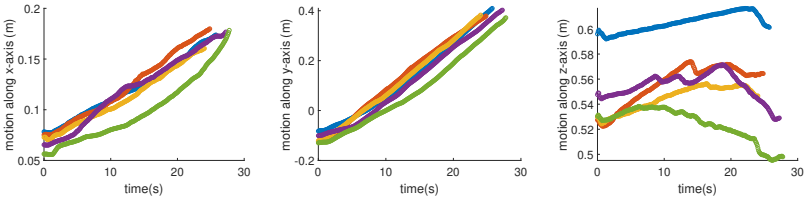

Fig. 4.5 Single Point method, Characterization experiments: results of 5 trials of task *ii*), i.e., object vertical motion. The motion in the *y*-axis is almost linear, similarly to Fig. 4.6. However, in this case, controlling the motion along *x* results to be more difficult than when using the Extended Patch method (see Table in Fig. 4.7).

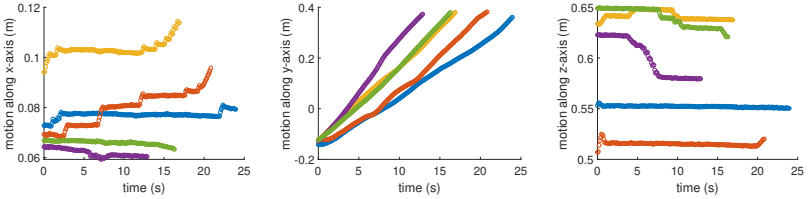

Fig. 4.6 Extended Patch method, Characterization experiments: results of 5 trials of task *ii*), i.e., object vertical motion. The motion in the *y*-axis is almost linear, and the other two directions are kept constant, or piecewise constant.

method, respectively. For the other two tasks we obtained analogous results: *a*) for both methods the motion along the main task direction is almost linear, and *b*) the other two directions show a small variation between initial and final values when considering the EP method, whereas at least one of them varies considerably with the SP method. This is confirmed by the data reported in the right part of the Table in Fig. 4.7. To have insights on how much the Cartesian coordinates are perturbed during the task execution, for each trial of each task, the difference between the initial and the final positions was recorded. The second

to last column of the Table in Fig. 4.7 reports this position difference (*diff*) averaged over the 5 trials. Besides, for each trial of each task, the standard deviations along each motion direction were computed. The last column of the Table in Fig. 4.7 contains the worst case standard deviation (*maxstd*), i.e., the maximum computed value for the standard deviation achieved along each direction.

When considering the secondary coordinates (i.e., the coordinates not explicitly involved in the task), the quantity *diff* is always smaller for the EP method with respect to what was obtained with the SP approach. More precisely, for each task, for at least one coordinate, the ratio between the values obtained for the two methods is about one order of magnitude (see for example the x values for task ii)). While the Extended Patch method allows to well control all coordinates (with a maximum *diff* of about 2 cm), with the Single Point approach the human performance is less satisfactory. Similar conclusions can be drawn by looking at the values of $maxstd$.

In the Table shown in Fig. 4.7, also averaged kinematic quantities and their standard deviations are reported, including the task execution time (t), and the norms of force (f), torque (m) and velocity (linear (v) and angular (ω)) vectors.

TABLE I: Characterization experiments. For each task, we report the average execution time (t), the average norm of force (f) and torque (m), the average norm of the linear (v) and angular (ω) velocities, the average difference ($diff$) between initial and final position of the 5 trials in the three directions, and the maximum recorded standard deviation between the points of the trajectories in the directions different from the main one ($maxstd$).

Test		t (s)	f (N)	m (Nm)	v (m/s)	ω (rad/s)	$diff$ (m)	$maxstd$ (m)
i) x-axis	**SP**	16.34 (±1.74)	8.66 (±0.43)	0.22 (±0.03)	0.033 (±0.003)	0.0016 (±0.0006)	[0.503, 0.067, 0.095]	[-, 0.037, 0.029]
	EP	18.77 (±1.80)	7.83 (±0.31)	0.21 (±0.03)	0.027 (±0.002)	0.0041 (±0.0017)	[0.504, 0.005, 0.021]	[-, 0.004, 0.015]
ii) y-axis	**SP**	25.93 (±1.57)	7.68 (±0.53)	0.26 (±0.02)	0.021 (±0.001)	0.0018 (±0.0003)	[0.104, 0.501, 0.022]	[0.034, -, 0.015]
	EP	18.16 (±4.28)	7.84 (±1.02)	0.25 (±0.02)	0.030 (±0.007)	0.0078 (±0.0039)	[0.012, 0.503, 0.018]	[0.007, -, 0.019]
iii) z-axis	**SP**	18.30 (±1.89)	2.29 (±0.27)	0.07 (±0.01)	0.028 (±0.003)	0.0003 (±0.0002)	[0.039, 0.072, 0.502]	[0.022, 0.029, -]
	EP	19.05 (±2.64)	2.48 (±0.34)	0.07 (±0.01)	0.027 (±0.003)	0.0027 (±0.0010)	[0.005, 0.010, 0.501]	[0.005, 0.007, -]

Fig. 4.7 Results on Characterization experiments.

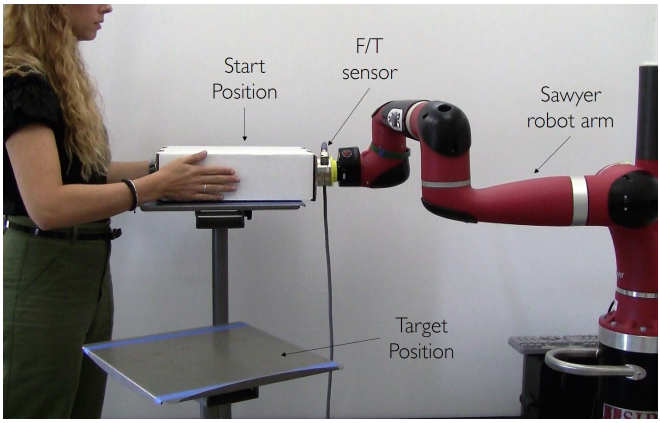

Fig. 4.8 Setup for the Pick-and-Place experiments.

4.4.2 Pick-and-Place experiments

In these experiments, the operator was asked to move a box from a given start position to a given target position, placed 27 cm under it, 47 cm to the right (with respect to the human), and rotated of 35° about the vertical axis. The experimental setup is shown in Fig. 4.8. A box with size $36.5 \times 34 \times 11$ cm and weight 0.4 kg was used.

A total of 10 volunteers, 3 females and 7 males, aged between 26 and 54, participated to this experiment. None of them had previous experience of collaborative robotics and had ever tried the system. To acquire task-specific motor skills involving human-robot collaborative aspects, experimenters first had to accomplish a *training phase* and then a *test phase*. The training was composed of 2 trials with Extended Patch method and 2 trials with Single Point method, alternately proposed to the experimenter. After the training phase, one trial per method was

performed for the test phase. Half of the participants first did the task with the EP method, while the others experimented first the SP method.

It should be remarked that the experimenters were not informed about which method was running, and they were not even aware of the fact that their experiments were finalized to the comparison of two different approaches. None of the other participants was present while one of them was performing the experiment. Experimenters were told to move the box from the start to the target position with the aid of the robot and without loosing the contact with the robot. They were asked to accomplish the task as precisely (staying within the blue lines in Fig. 4.8) and as fast as possible.

Both phases of the experiments (training and test) were analysed and the results are presented in the following.

4.4.2.1 Average quantities

Data collected during the test phase have been processed so to obtain the average completion time and the average norms of the linear velocity and force. Results are reported in Table 4.1, which shows that while forces and velocities are similar for both methods, the average completion time decreases by $\sim 16\%$ for the EP.

	SP	**EP**
t (s)	47.41	39.78
v (m/s)	0.018	0.02
f (N)	6.45	6.41

Table 4.1 Pick-and-Place experiments. Average completion time, average norms of the linear velocity and force during the test phase.

Three of the subjects, corresponding also to those that obtained the best performance in terms of completion time in the test phase, showed an interesting trend between the training and the test phase. The completion time of their experiments, indeed, gradually decreased between the subsequent trials with the EP method and not with SP approach, as shown in Table 4.2. This qualitative consideration suggest that the EP method fosters the familiarization with the task, even when participants are not yet skilled.

Test		1st trial [s]	2nd trial [s]	3rd trial [s]
Subject 1	SP	54.6	57.1	49.6
	EP	42.7	36.9	34.2
Subject 2	SP	41.7	33.8	41.1
	EP	47.2	34.9	26.8
Subject 3	SP	53.3	58.05	38.8
	EP	48.9	48.02	30.9

Table 4.2 Pick-and-Place experiments. Task completion time for the three of the subjects that obtained the best performance. A gradual reduction of the completion time can be observed when using the Extended Patch method. The 1st and 2nd trials belong to the training phase, the 3rd one belongs to the test phase.

Another remark can be done when focusing on the data related to the 5 subjects that performed the first experiment of the training phase with the EP method and the second one with the SP approach. Although the trial with the EP method corresponded to their very first time doing a cooperative robotics experiment, all of them achieved a shorter completion time than what was obtained with the SP method. The average difference was about 7.6 s.

Moving on with this reasoning and taking into account the first two trials of all the subjects, one done with EP and the other done with SP

method no matter the order in which the two methods were presented, 8 out of 10 experimenters achieved a shorter completion time with the EP method, with an average duration difference of 8.75 s. The same comparison applied to data collected in the test phase shows that the EP method allows a shorter completion time for 7 out of 10 subjects, with an average time difference between EP and SP of 11.6 s.

4.4.2.2 Task Precision and Contact Permanence

The proposed Pick-and-Place experiments involved more complex motions if compared to the motions required by the Characterization experiments. In Pick-and-Place experiments, indeed, subjects were asked to perform a composition of translations and rotations.

Concerning *task precision*, participants were asked to precisely place the object in the target, clearly delimited, location. During the experimental trials, no relevant deviations were found with respect to the assigned location (average displacement ~ 0.4 cm, average angular deviation $\sim 6^\circ$).

Regarding *contact permanence*, the subjects were asked not to lose the contact between the box and the robot, and specifically to remain in contact with at least one corner of the contacting plate. During the test phase, with the SP method, an average angle between the end-effector surface and the box side of 30.1° about the plate $y-axis$ was observed. The same angle was just about 4.3° for the EP approach, that, however, also generated an average angle of 11.4° about the plate x-axis between the box and the plate.

4.4.2.3 Movement smoothness

To have a comparative measurement of the movement smoothness achieved with the proposed methods, the SPARC (SPectral ARC length) index [131] has been computed for each experiment performed by the non-skilled subjects, and the average value was then retrieved. Calculations are based on the code available on GitHub[3].

Smoothness indices for movement tasks (i.e., task involving specific motions) rely on the idea of analysing the derivatives of the position profile to highlight jerks. As suggested in [131], the data processing for the SPARC index related to a movement task with position measurements is related to velocities, since velocity "highlights intermittencies, and does not amplify noise as much as the other higher order derivatives".

We computed an average SPARC index for each direction of motion (x, y, z). The ratios between the corresponding SPARC indexes for the EP and for the SP methods are 0.85, 0.99, and 1.02 for the three axes, respectively. These values do not highlight a relevant difference between the proposed approaches, since they are very close to 1. However, the same ratios computed for the subjects that obtained the best completion time (Table 4.2) show a remarkable higher smoothness of the EP with respect to the SP along the x and z axes (1.23, 1.07, 2.08).

4.5 Discussion

Experiments reported in Section 4.4 aimed at characterizing the performance achievable with the proposed Extended Patch method, and

[3] https://github.com/siva82kb/SPARC

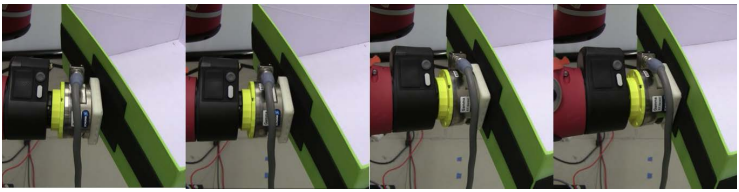

Fig. 4.9 Compensation of object rotation with the EP method.

to provide a comparison with a simplest control strategy based on the Hard Finger contact model, i.e. the Single Point method.

Characterization experiments relied on performing pure translational motions, and were carried out by a skilled operator. What came out is that the average force, moment, linear velocity and task completion time were similar in the two methods (see Fig. 4.7), showing that, as requested, the operator was naturally and comfortably performing the experiments making a similar effort. However, the Extended Patch method allowed to better control the object trajectory along the main direction of motion, keeping both the other directions almost constant or piecewise constant (see *diff* and *maxstd* in the Table shown in Fig. 4.7, and Figs. 4.5, 4.6). Thus, the task was accomplished with more precision. Given that the operator's effort was similar in both the approaches, decreasing the undesired displacement occurring in the secondary coordinates when using the SP method would have required to make more effort.

The Pick-and-Place experiments involved a composition of translations and rotations, and were carried out by non-skilled volunteers. All of them were able to precisely accomplish the task. The most relevant result obtained during these experiments is related to the contact permanence between the plate and the grasped object. For the Single

Point method, at the end of the experiments, an average angle of 30.1° about the plate y-axis appeared between the box and the plate. A much smaller detachment was measured with the Extended Patch method (4.3° about the y-axis, 11.4° about the x-axis). This implies that in the Single Point method, the operator has to choose whether to reduce the detachment actively, thus finishing the task with the box in a final wrong position, or to accomplish the task precisely, risking to lose the object. This would be particularly disadvantageous if the aid of the robot is necessary not only to stabilize the grasp but also to hold part of the object weight. A way to avoid this problem could be to finely tune the $\mathbf{K}_{m,SP}$ values (see Alg. 1), which would require an inconvenient trial-and-error, task-dependent selection procedure.

The small angular displacements observed with the Extended Patch method are due to the fact that the robot does not have enough time to finish its rotational motion, as the experimenters are asked to complete the task as quickly as possible. However, the detachment could be avoided if subjects did slower motions. Subsequent frames of such situation are shown in Fig. 4.9, where the robot follows the object rotation thanks the Extended Patch method.

4.6 Final remarks

This Chapter focused on a soft interaction involving human-robot cooperation for moving large objects. A compliant, extended contact has been assumed to occur between the object and the robotic end-effector. Compliance and geometric properties of the actual contact region allowed to devise a proper contact model named Extended Patch. This contact model and the generalized forces exerted by the human are the

basis of a robot control strategy named the Extended Patch method, that puts the human at the center of the task execution.

The Extended Patch approach has been compared with a control strategy based on a contact model that is more similar to the most commonly used in literature (i.e. the Hard Finger model), and does not consider the actual properties of the contact area.

Experiments revealed that the control strategy relying on modelling the compliant interaction gave better results in terms of trajectory tracking and completion time. Moreover, preliminary, promising, results suggest also that the Extended Patch method allows to reduce users' learning time and increases movement smoothness, but these aspects will be better investigated in future work.

5 Handwriting on touchscreens

In this Chapter we will consider a soft interaction involving a human that interacts with themself. The focus is on a grasping task: writing on a touchscreen device. In the envisaged writing task, the hand will grasps itself, by realizing a hand posture that merges gesture and tool into a single operative organ. This hand posture, named *FingerPen*, is such that the forces that are usually exerted on a tool are here exerted directly on the same hand that exerts such forces. Hence, the same forces that are in charge of generating task-related movements constitute non-mediated kinaesthetic feedback affecting the performance of the writing task, allowing fast motor learning.

The envisioned applications focus on children and elders. In the former case, the aim is to develop pre-writing skills, and in the latter to contrast the decline of neural circuits due to the old age. Both the cases rely on neurophysiological studies showing the outstanding role played by manipulation capabilities on the status of synaptic connections[1].

[1] The content of this Chapter has been published in [132]. Source: Scientific Reports, Nature. Licensed under CC 4.0.

5.1 Introduction

Handwriting requires the sense of self and of what is other than the self, proprioception and exteroception, implies a strong hand-eye coordination, and relies on a fine control of the forces exchanged with the writing tool. However, nowadays the possibility of fast typing on keyboards and touchscreens is making this activity more and more rare, leading to a de-materialization of the writing process. What is clearly missing is the spatial perception of the physical medium, the perception of the tool and also the fine tool management. However, as the embodied cognition model enlightens, handwriting is one of the skills that mainly fostered the human cognitive development: Specific brain synaptic connections and areas specialization were set in a complex interrelation, leading to the simultaneous development of physical and mental capabilities, as remarked by several neuroscientists and educationalists [133–135]. This strong connection between mind and body is becoming thinner and thinner, as the growing concerns about dysgraphia highlight [136]. However, the advantages brought in everyday life by mobile devices cannot be ignored and children are nowadays exposed very early to the use of technology [137, 138].

According to McLuhan, any technology leads simultaneously to an amputation and a sensorial extension [139]. De Kerckhove investigated also the effects on the human mind, and defined a psychotechnology as "any technology that emulates, extends, or amplifies sensory-motor, psychological or cognitive functions of the mind" [140]. Inspired by these concepts, we propose the FingerPen: a posture of the hand thought to exploit smartphones and tablets to keep people used to practise the "language by hand" [141]. In the FingerPen posture, the index finger is

Fig. 5.1 The FingerPen, a hand posture suitable for writing on touchscreens.

constrained by the hand in such a way that it becomes a writing tool (Fig. 5.1) characterized by the fact that "tool and gesture merge into a single organ", similarly to what the anthropologist Leroi-Gourhan observed in animals [142], leading to an intrinsic embodiment of the tool [143, 144].

Notwithstanding that the fine sensorimotor skills required by the classic handwriting cannot be acquired in other ways except by means of pen and paper, the FingerPen can be exploited in parallel to make children familiarize with the writing task and develop reading-writing prerequisite skills. Berninger said that "We use our hands to access our thoughts", and showed that children tend to write more quickly, with more words and more ideas while writing by hand than by keyboard [145]. Since tablets are quite spread in all the age groups, some applications of the FingerPen can be proposed for elders, to keep practicing hand-eye coordination and contrast visual-spatial deficit and memory loss, which are amplified by the lack of exercise [146]. Ex-

ercises similar to those proposed in the SAGE test [147], the Clock Drawing test [148], or the Benton Visual Retention Test [149] can be performed. Recent studies show that memory benefits from the act of drawing, both in younger and in older adults [150, 151].

Related works

The handwriting task involves advanced cognitive processes, and is a paradigmatic action that clearly shows human dexterous manipulation capabilities. It would not be possible without the complex structure of the human hand and its underlying sensorimotor control paradigms [152–155]. The study of the human hand biomechanics [152] has led to the definition of different kinematic models of the human hand, typically characterized by realistic measures of the phalanges and of their relative positioning [156–158]. Usually, the hand is represented as a set of open kinematic chains made of rigid links connected by revolute joints. Each joint represents a degree of freedom (DoF) of the structure. A common choice is to model index, middle, ring and little fingers with four DoFs (three for flexion/extension, and one at the basis for adduction/abduction) [159, 157], whereas the most used representations of the thumb either include four [159, 157] or five DoFs [160]. When it comes to modeling the handwriting posture, not only the kinematic model of the human hand has to be considered, but also the fact that the writing task starts with a prehensile action [161], i.e., the achievement of a stable grasp over the writing tool (e.g., a pen). The adopted grasp configuration can affect the handwriting ability, and four main grip styles have been identified based on how fingers are placed around the writing tool [162, 163].

With the advent of touchscreens, researchers have also focused on studying the *digital* handwriting, i.e., the action of writing over a touchscreen either using an ad-hoc tool or just the index finger. With respect to writing on paper, the surface of touchscreens has a lower friction and this might influence the graphomotor execution [164] and the contribution of different types of sensory feedback (proprioceptive, visual) [165] during handwriting. Several works investigate digital handwriting in children and older adults by comparing it to other writing methods [166, 167], or focus on similar tasks, like tactile exploration through sliding [168], but only a few propose a model of the digital handwriting task [169]. In [169], authors found that using a writing tool allows a more accurate control of the writing action, showing also that the free finger motion is more suitable for tasks requiring a large workspace and short completion time. In this paper, we introduce the FingerPen posture.

5.2 Hand model

To analyze the FingerPen posture from a kinematic point of view, we considered a mechanical model of the human hand in which each finger is an open kinematic chain composed of rigid links connected through revolute joints. In this way, a characterization of the hand operational space can be provided, and the hand in FingerPen posture can be described as a manipulator grasping the distal phalanx of the index finger. The key elements that are needed to model a handwriting posture are: *i)* the links and joints composing the hand, and *ii)* the contact points of the hand with itself and with the environment.

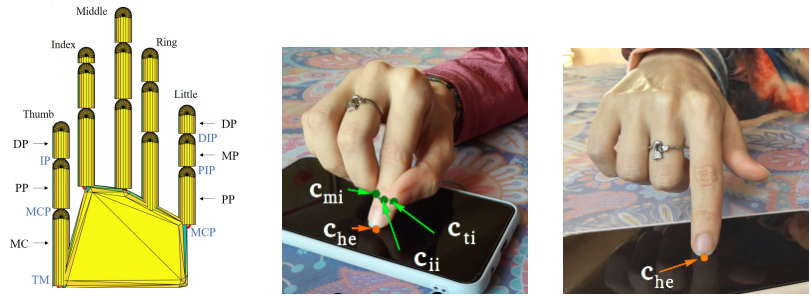

(a) (b) (c)

Fig. 5.2 (a) Model of the human hand adopted in this work, (b) FingerPen contact points. Green arrows indicate the contact points of the hand with itself (i.e., $\mathbf{c}_{hh} = [\mathbf{c}_{ti}, \mathbf{c}_{ii}, \mathbf{c}_{mi}]'$), while the orange arrow indicates the contact point between the hand and the environment (i.e., $\mathbf{c}_{he}$). (c) In the FreeFinger posture only the contact point with the environment must be considered.

We adopted a 20 DoFs model of the human hand (Fig. 5.2a) like the one used in [159, 22, 169]. Index, middle, ring and little fingers are composed of three links, corresponding to proximal (PP), medium (MP) and distal phalanxes (DP), and three joints, corresponding to metacarpophalangeal (MCP), proximal interphalangeal (PIP), and distal interphalangeal (DIP) joints. The thumb has the metacarpal bone (MC), which is connected to the palm through the trapeziometacarpal (TM) joint and to the proximal phalanx (PP) through the metacarpophalangeal (MCP) joint. The proximal and distal phalanges of the thumb are connected through the interphalangeal (IP) joint. The MCP joints of the fingers and the TM joint of the thumb have two degrees of freedom (adduction/abduction and flexion/extension), whereas the other joints only allow flexion/extension movements.

Concerning the contact points, we can indicate with the vector $\mathbf{c}_{hh}$ the position of the contacts between the fingers themselves, and with

$\mathbf{c}_{he}$ the position of the contacts between the hand and the environment. In the FingerPen posture (Fig. 5.2b), the hand has three contact points with itself, whose position is described by the vector $\mathbf{c}_{hh} = [\mathbf{c}_{ti}, \mathbf{c}_{ii}, \mathbf{c}_{mi}]'$, where $\mathbf{c}_{ti}$ is the contact point between thumb and index fingers, $\mathbf{c}_{mi}$ is the contact point between index and middle fingers, and $\mathbf{c}_{ii}$ is the contact point between the last phalanx of the index finger and the remaining part of that finger. To properly model the fact that the index tip and the remaining part of that finger are just consecutive parts of the same finger, the last phalanx of the index finger can be constrained (through the adoption of a suitable contact model, see Section 5.2.2) to be completely attached to the index finger itself. Then, the FingerPen establishes a contact point with the environment located on the tip of the index finger ($\mathbf{c}_{he}$).

To better assess the kinematic properties of the FingerPen, in the following we will compare the FingerPen with the FreeFinger posture, i.e., the posture that we typically use to interact with touchscreens, in which the index finger is considered "free", since it is not constrained by the other fingers ($\mathbf{c}_{hh} = \mathbf{0}$). In this case, the only vector to consider is $\mathbf{c}_{he}$, as the FreeFinger is contacting just the environment (see Fig. 5.2c). In Section 5.2.1 and Section 5.2.2, we will provide details on the hand posture for FingerPen and FreeFinger, respectively. By following the analogy with a manipulator, in both cases the index fingertip will be treated as the manipulator end-effector.

In this work, the mathematical vectors representing position and velocity of the contact points of the hand with itself will be denoted with $\mathbf{c}_{hh}$ and $\dot{\mathbf{c}}_{hh}$, respectively, while $\mathbf{c}_{he}$ and $\dot{\mathbf{c}}_{he}$ will denote position and velocity of the contact point between fingertip of the index and the environment. The vectors including the manipulator joint angles

and angular velocities will be indicated by $\mathbf{q}$ and $\dot{\mathbf{q}}$, respectively. In the next subsections, we will provide the mathematical relations mapping the hand joint velocities onto the velocity of the index fingertip that interacts with the environment.

5.2.1 The FingerPen Posture

In the FingerPen (FP) posture, the position of the index fingertip is generated by the superposition of the effects caused by the kinematic chains of thumb, index, and middle fingers, while ring and little fingers do not play a role and can be neglected. Since each acting finger is a 4-DoF manipulator, $\mathbf{q}, \dot{\mathbf{q}} \in \mathbb{R}^{12\times 1}$. By interpreting the FingerPen posture in the light of the grasping theory [170], we can say that the final part of the index finger is grasped by a manipulator composed by *i)* the kinematic chain of the thumb, *ii)* the kinematic chain of the middle and *iii)* the kinematic chain of the index finger without its final part. As previously mentioned, it is like as if the final part of the index finger has been cut (becoming a separate object) and then grasped by the fingers in specific locations (see Fig. 5.2b). Moreover, since the fingertip is assumed to remain in contact with the environment and the arrangement of the fingers is such that all the fingers are very close to each other, the angular displacement and velocity potentially provided by the interaction with the thumb and middle fingers can be neglected. Hence, the contact points between these fingers and the index fingertip are represented according to the Hard Finger (HF) contact model [170]. To properly render the fact that the index fingertip is actually attached to the rest of the index finger, the (virtual) contact point of the index

with itself is represented according to the Complete Constraint (CC) model [170].

In the theory of grasping, the contact between the hand and the object occurs when specific locations on the hand and on the object coincide. More specifically, it occurs when the velocity of these locations on the hand and on the object are the same (according to the given contact model). This argument is the basis of the theory on quasi-static grasps [170], that we applied in the following.

The velocity of the contact points on the hand is related to the hand joints by $\dot{\mathbf{c}}_{hh} = \mathbf{J}\dot{\mathbf{q}}$, where $\mathbf{J} \in \mathbb{R}^{12\times 12}$ is the Jacobian matrix of the thumb, index and middle fingers. During the grasp, the velocity of the contact points on the hand is related to the velocity of the grasped object (i.e. the index fingertip) by $\dot{\mathbf{c}}_{hh} = \mathbf{G}^T\dot{\mathbf{c}}_{he}$, where $\mathbf{G} \in \mathbb{R}^{3\times 12}$ is the Grasp matrix. Hence, $\mathbf{J}\dot{\mathbf{q}} = \mathbf{G}^T\dot{\mathbf{c}}_{he}$ that leads to $\dot{\mathbf{c}}_{he} = (\mathbf{G}^T)^{\#}\mathbf{J}\dot{\mathbf{q}}$, where $(\mathbf{G}^T)^{\#}$ denotes the pseudoinverse of $\mathbf{G}^T$, and it can be proved that $(\mathbf{G}^T)^{\#} = (\mathbf{G}\mathbf{G}^T)^{-1}\mathbf{G}$. For notation simplicity, we can write

$$\dot{\mathbf{c}}_{he} = \mathbf{J}_{eq}\dot{\mathbf{q}}, \quad \mathbf{J}_{eq} = (\mathbf{G}\mathbf{G}^T)^{-1}\mathbf{G}\mathbf{J}. \tag{5.1}$$

In our simulation, the HF contact point on the thumb is located at 3/4 of the length of the distal phalanx, while the HF contact point on the middle and the CC contact point are located at 1/2 of the length of their respective distal phalanges. The basic FingerPen posture (described here and shown in Fig. 5.1) has been chosen after some preliminary investigations aimed at identifying an arrangement of the fingers easy to be adopted and kept during time without effort. As a matter of fact, if, for instance, the middle finger was not located next to the index finger, but *on* the index finger - as some people tend to do - it would result in a

posture causing physical fatigue, due to the weight of the middle finger that would load the index finger.

5.2.2 The FreeFinger Posture

In the FreeFinger (FF) posture, the position of the fingertip of the index is uniquely determined by the kinematic chain representing the index finger, which is a 4-DoF manipulator. Hence, the joint variables of the other fingers can be neglected, leading to $\mathbf{q}, \dot{\mathbf{q}} \in \mathbb{R}^{4\times 1}$. Thus, the fingertip velocity is described by

$$\dot{\mathbf{c}}_{he} = \mathbf{J}_i \dot{\mathbf{q}}, \tag{5.2}$$

where $\mathbf{J}_i \in \mathbb{R}^{3x4}$ is the Jacobian of the index finger, mapping the actual velocity of the manipulator's joints in the velocity of the end-effector (index fingertip).

5.3 Manipulability analysis

Manipulability analysis [171] gives insights on the role played by the configuration of the manipulator in the map describing the relation between joints and end-effector velocities. More specifically, it allows to identify the directions along which the configuration of the manipulator amplifies the joint velocities and which are the motion directions along which the end-effector velocity is slowed down due to that manipulator configuration. The equation

$$\dot{\mathbf{q}}^T \dot{\mathbf{q}} = 1 \tag{5.3}$$

describes a sphere in the joint velocity space. That set of joint velocities is mapped onto the end-effector operational space by accounting for the actual relation between joint velocities and end-effector velocities, that depends on the manipulator configuration. In Section 5.3.1 and Section 5.3.2, we will provide the manipulability analysis for the FingerPen and FreeFinger configurations, respectively. The analysis was conducted using the SynGrasp MATLAB Toolbox [172].

5.3.1 FingerPen manipulability

In the FingerPen configuration, Eq. (5.3) and Eq. (5.1) yield

$$\dot{\mathbf{c}}_{he}^{T}(\mathbf{J}_{eq}^{\#})^{T}\mathbf{J}_{eq}^{\#}\dot{\mathbf{c}}_{he} = 1.$$

However, it can be shown that $(\mathbf{J}_{eq}^{\#})^{T}\mathbf{J}_{eq}^{\#} = (\mathbf{J}_{eq}\mathbf{J}_{eq}^{T})^{-1}$, leading to

$$\dot{\mathbf{c}}_{he}^{T}(\mathbf{J}_{eq}\mathbf{J}_{eq}^{T})^{-1}\dot{\mathbf{c}}_{he} = 1 \tag{5.4}$$

that describes how the set of points in Eq. (5.3) are mapped in an ellipsoid, whose semi-axes directions and dimensions are given by the eigenvectors and eigenvalues of the matrix $\mathbf{J}_{eq}\mathbf{J}_{eq}^{T}$, respectively. Eigenvectors characterize the orientation of the ellipsoid, while eigenvalues define the ellipsoid shape, encapsulating the information on the directions along which the end-effector is capable of higher and lower velocities. Results are visually shown in Fig. 5.3a.

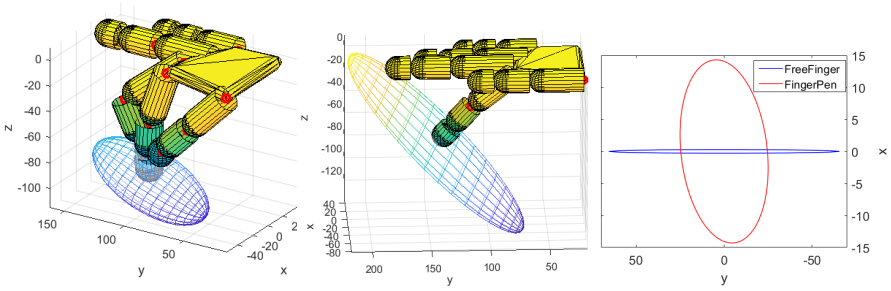

Fig. 5.3 Manipulability analysis: Velocity ellipsoids describing the (a) FingerPen and (b) FreeFinger configurations. (c) Projection of the ellipsoids on the writing plane.

5.3.2 FreeFinger manipulability

In the FreeFinger configuration, Eq. (5.3) and Eq. (5.2) yield

$$\dot{\mathbf{c}}_{he}^T (\mathbf{J}_i^{\#})^T \mathbf{J}_i^{\#} \dot{\mathbf{c}}_{he} = 1$$

that, thanks to the fact that $\mathbf{J}_i \mathbf{J}_i^T$ is a full-rank matrix, can be rewritten as

$$\dot{\mathbf{c}}_{he}^T (\mathbf{J}_i \mathbf{J}_i^T)^{-1} \dot{\mathbf{c}}_{he} = 1. \tag{5.5}$$

Hence, ellipsoid semi-axes directions and lengths are given by the eigenvectors and eigenvalues of the matrix $\mathbf{J}_i \mathbf{J}_i^T$, respectively. Results are visually shown in Fig. 5.3b.

5.3.3 Comparison on the Writing Plane

At first glance, Fig. 5.3a and Fig. 5.3b seem to suggest that the index fingertip is capable of faster motions along the transverse direction, both in the FP and in the FF configurations. However, what is worth

to investigate is the actual motion capability of the fingertip on the writing plane. To this aim, the Cartesian, closed-form equation of the ellipsoids has been retrieved and intersected with the writing plane equation, leading to the equations of the ellipses resulting from the projection of the ellipsoids on the writing plane. For an easy visual comparison, such ellipses are drawn superimposed in Fig. 5.3c.

Despite an apparent similarity between the velocity ellipsoids of the FP and FF configurations, the actual motion capabilities of the index finger are remarkably different on the writing plane. As shown in Fig. 5.3c, indeed, the FingerPen configuration allows a larger velocity along the longitudinal direction, while in the FreeFinger configuration the finger can move faster in the transversal direction (the longer the ray vector, the higher is the allowed velocity along that direction). This argument allows a further consideration. During manipulation tasks, indeed, a trade-off between precision and velocity occurs, meaning that precise motions usually require low velocity, and high speed movements generate an imprecise control of the motion. This is due to the fact that in humans precise movements are the result of hand-eye coordination with continuous visual servoing providing proper feedback on the performed trajectory. The higher is the velocity, the less effective is the visual feedback to change the trajectory, due to a longer distance covered during a given time interval. To reflect this argument on Fig. 5.3c, we can say that the FingerPen allows a more precise motion along the transversal direction and a less precise motion in the longitudinal one. On the contrary, FreeFinger allows a precise motion along the longitudinal direction and a remarkably less precise motion along the transversal direction.

5.4 Experiments

To have quantitative and qualitative evaluations on the actual use of the FingerPen for writing on touchscreens, we carried out an experimental campaign with 25 participants aged between 18 and 46. Two experiments were designed to retrieve quantitative data and, after the experiments, a questionnaire was submitted to the participants to distil insights on the user experience. As in Section 5.3, we carried out a comparative analysis between FingerPen and FreeFinger. Experiments investigated the relation between precision and workspace extension (see Section 5.3), and concerned the fact that the possibility of moving fast along certain directions usually leads to *i)* long traits and *ii)* imprecise movements. Hence, Experiment 1 focused on the extension of the occupied workspace when writing with a given hand posture (FP or FF), whereas Experiment 2 regarded the precision that can be achieved when using the FP and FF postures.

Participants were informed that they would perform experiments with two possible postures for writing on touchscreen devices, but no additional information on the idea behind the FingerPen was provided. The correct way to arrange the hand according to the FingerPen and FreeFinger configurations was shown to the participants by an expert, and they were let familiarize with the FingerPen configuration by performing free movements in the air for a couple of minutes. Informed consent was obtained from all subjects, no sensitive data were acquired and the other data were anonymized (GDPR 2016/679). All methods were carried out in accordance with relevant guidelines and regulations: Participants were free to leave the experiments whenever they wanted,

and the experimental protocols conformed with the principles inspiring the Declaration of Helsinki.

All the experiments required just a smartphone with touchscreen. Data generated by the user touch were acquired through a dedicated webapp implemented in HTML/PHP (see user interface in Fig. 5.4 and 5.6), and sent to a server where they were stored before data processing. Points from the performed finger trajectory were acquired at approximately 50 Hz.

In general, in handwriting tasks, size, speed and precision are highly subject-specific. Hence, we focused on the distribution of the individual differences to have insights on the effect of the FP and FF writing postures. Therefore, quantitative data gathered from all the participants underwent a statistical analysis in SPSS Statistics (Statistical Package for Social Science [173], v.26) to check whether data acquired with FingerPen and FreeFinger differ in a statistically significant manner. If the individual differences were normally distributed (Shapiro-Wilk's test, $p > 0.05$) and without extreme outliers (boxplot inspection), a paired samples T-test was conducted (statical significance for $p < 0.05$). When normality had been violated, a non-parametric test was conducted. To account also for effect size estimate, we considered the Cohen's d coefficient, whose absolute value provides a measure of the signal-to-noise ratio (0.2: small, 0.5: medium, 0.8: large effect [174]).

5.4.1 Experiment 1 - Investigation on the Workspace

In this experiment, participants were asked to write the word "CIAO" (Italian word for "Hello") in capital letters, within a rectangular box, two times: once using the FingerPen, and once using the FreeFinger. In

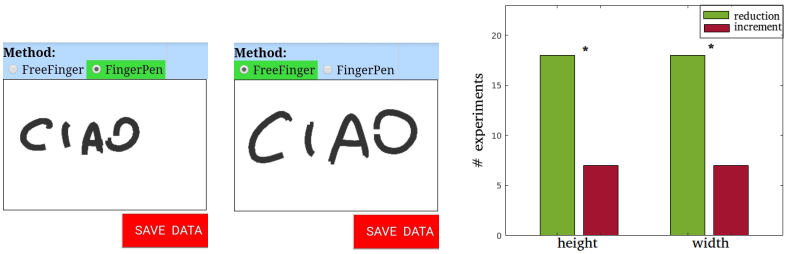

Fig. 5.4 Experiment 1. On the left: example of the performed experiment aimed to investigate the space occupied when writing a simple word using (a) FingerPen and (b) FreeFinger. On the right (c), number of performed experiments leading to occupied workspace reduction/increment, respectively, when using the FingerPen. The "*" symbol stands for "statistically significant difference with $p < 0.05$".

Fig. 5.4a and Fig. 5.4b we show an example of this experiment: The area allowed for writing was defined by the solid, thin, black line.

Bearing in mind the considerations of the sociologists cited in Section 5.1, we deliberately asked people to write in Italian and not in English, because we believe that asking people to write in a language different from the native one (and not used in everyday life) may introduce some artefacts [175, 176].

Data acquired from the webapp were processed in MATLAB (v. 2019) [177]. Width and height of the text bounding box were retrieved for each participant and each hand configuration. A paired-samples T-test has been conducted to compare results for the FingerPen and FreeFinger configurations, revealing that data differ in a statistically significant manner ($p < 0.05$) concerning both text width and height. Concerning height ($p = 0.026$, $t = -2.38$), the FingerPen allows a reduction of the maximum text height of about 10.3 ± 21.6 px, with medium effect

size $d = -0.5$. Regarding text width ($p = 0.01$, $t = -2.77$), the FingerPen allows a decrement of 17.1 ± 30.8 px, with effect size $d = -0.6$. As shown in Fig. 5.4c, the 72% of the experimenters experienced a reduction of the occupied workspace while using the FingerPen.

5.4.2 Experiment 2 - Investigation on Precision

In this experiment, we investigated the precision that can be achieved by exploiting the FingerPen and FreeFinger postures. Participants were asked to trace the outline of different figures using the FP e FF. Four geometrical figures have been chosen on the basis of their shape (Fig. 5.5a): triangle (straight lines and sharp angles), quadrangle (straight lines, sharp and obtuse angles), ellipse (curved line with symmetry axes rotated with respect to the axes of the workspace), puzzle piece (straight and curved lines). To avoid local self-occlusions of the traced contour, we designed a displaced copying task (Fig. 5.6). Participants were provided with a canvas containing a geometrical figure in the upper part and a large blank area in the lower part. On the geometrical figure, there was a small circle coloured in blue: This point was matched with the corresponding, hollow, small circle located in the lower part of the canvas. Starting from this hollow circle, participants had to retrace the figure: Although the user touches the screen in points that are different from the location in which the geometrical figure is located, their trait appears in the region of the geometrical figure. In some sense, it is like to have an extension of the index finger, as it happens in some calligraphic tasks exploiting the oblique pen nib holder. In this way, users have a precise visual feedback on the precision related to their motion.

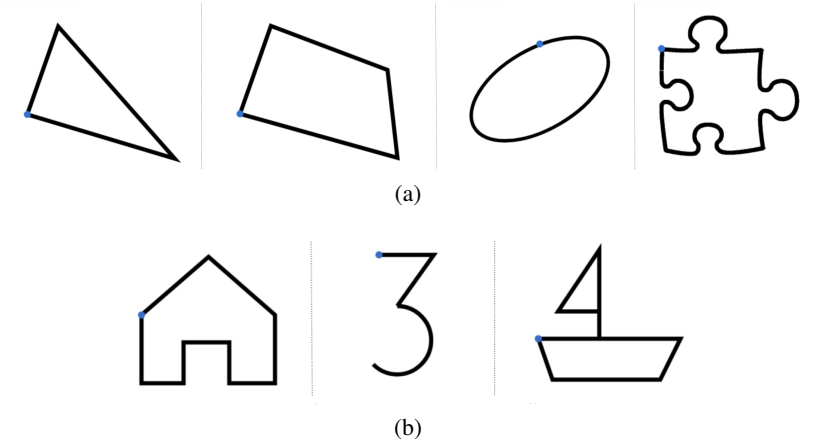

Fig. 5.5 Experiment 2. a) Figures for evaluation: triangle, quadrangle, ellipse, puzzle piece. b) Figures for training: house, three, boat. The blue circle indicates the starting point.

Since the FingerPen posture is somehow unusual for people, we wanted to investigate the effect of a small training on precision. To this aim, we designed three figures (house, number three, boat) that were thought to resemble the pre-writing exercises that people usually perform during childhood. We thought that engaging experimenters by stimulating memories capable of freeing the mind from the current performance would allow users to familiarize better with the FingerPen, leading also to a performance improvement. Figures used for training are shown in Fig. 5.5b.

Each experimenter carried out a session articulated in three steps: *i)* pre-training, *ii)* training; *iii)* post-training. During pre-training, the participant is asked to draw the triangle and the ellipse exploiting FingerPen and FreeFinger, alternately. Training was dedicated, instead, only to the FingerPen, and stopped when the participant felt at ease

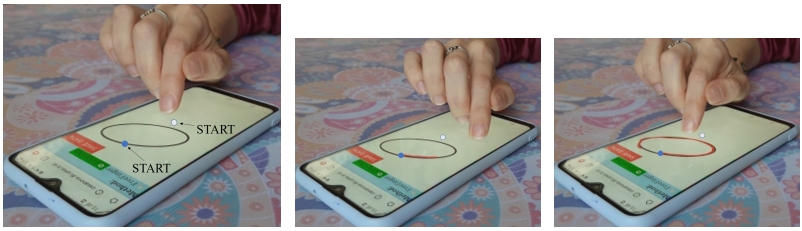

Fig. 5.6 Experiment 2: intermediate steps. The blue circle indicates the starting point of the desired contour, whereas the white circle indicates the starting point of the tracing motion.

with the FingerPen posture; tracing at least three times per figure was recommended. During post-training, participants were asked to trace the quadrangle and the puzzle piece; such figures are slightly more complex than the ones used during pre-training. At the end of the session, three instances of each figure were drawn for each hand posture.

For each trial, the user's trace and the time required to draw it were recorded. The former was saved as a sequence of N points $\mathbf{p}_i$, $i = 1,\ldots,N$; the latter was computed as the interval between the first instant in which the user touched the screen and the instant in which the user lifted the finger from it.

For each gathered user's contour, the mean error has been computed as the average of the distances between each user's point ($\mathbf{p}_i$) and the corresponding nearest neighbour point ($\mathbf{nn}_i$) belonging to the original contour ($e_i = ||\mathbf{p}_i - \mathbf{nn}_i||$). In addition, we computed the maximum error ($e_{max} = \max(\{e_i\}_{i=1,\ldots,N})$). These metrics were intended to be a first indicator of precision. For each contour, also the standard deviation of the error has been computed ($std = \text{std}\{[e_i]_{i=1,\ldots,N}\}$) and considered as an indicator of regularity in the tracing task (i.e., the less is the standard deviation, the more regular is the task execution).

For each participant, all the data related to the same figure and acquired with the same hand posture were averaged to retrieve only one measure per person, figure and method. Such data underwent an analysis in SPSS for statistical significance of possible differences. A paired-samples T-test was conducted to investigate the distribution of the individual differences for all the figures and metrics except for the time in the triangle (a violation of normality occurred, and a Wilcoxon Sign test was performed). In Fig. 5.7, we show a representation of the results. Symbols '*', '**', '***' stand for "statistically significant difference with $p \leq 0.05$, $p \leq 0.01$, $p \leq 0.001$", respectively. d denotes the effect size according to the Cohen's definition.

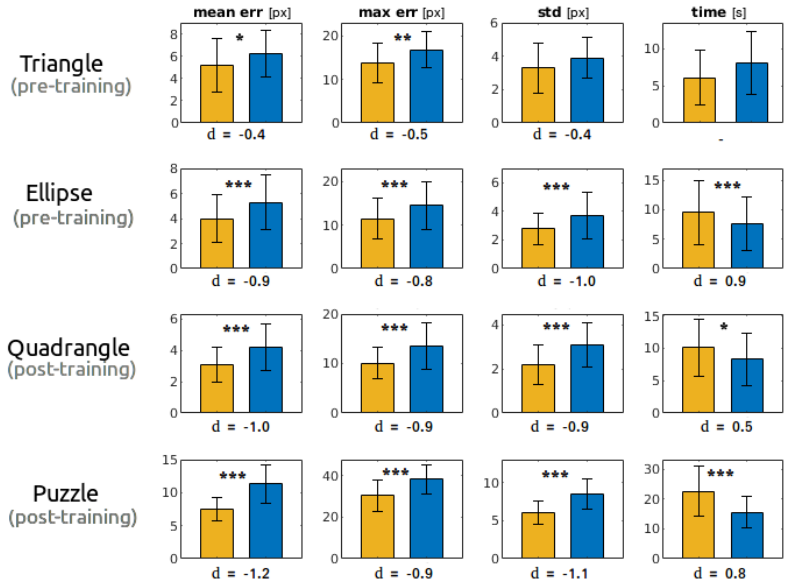

Fig. 5.7 Experiment 2. Barplots of the descriptive statistics related to the metrics mean and max errors, std and time for each investigated figure. Yellow and blue colors are related to FingerPen and FreeFinger, respectively.

5.4.3 Questionnaire

To have insights on the user experience, after the experiments the users filled out a questionnaire concerning aspects specifically related to the FingerPen configuration, and aspects related to the comparison between FingerPen and FreeFinger.

On the FingerPen configuration, the following questions were asked, and results are reported in parentheses:

- FP1: I felt difficult to keep the FP configuration: at the beginning (48%), during all the experiments (4%), no (48%).
- FP2: The difficulty I felt was especially: mental, physical (36%), both mental and physical, not relevant (64%).
- FP3: The training for FingerPen was: very useful (28%), quite useful (56%), a little useful (16%).
- FP4: Keeping the hand in the FingerPen configuration was: natural (56%), artificial (36%), neutral (8%).

The questions on the comparison between FP and FF are reported in the following and results are shown in Fig. 5.8:

- C1: I believe that I was more precise while using...
- C2: I believe I had a greater control of the hand motions while using...
- C3: I found more pleasing the experience with...
- C4: I believe that the configuration inducing the most errors while tracing was...

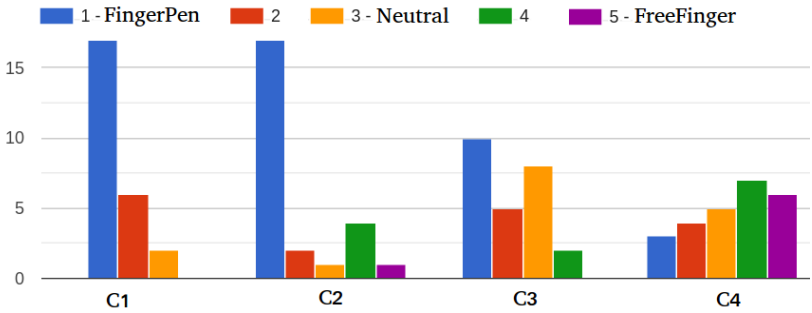

Fig. 5.8 Answers to the questions on the user experience about the comparison of FingerPen and FreeFinger. Values 2 and 4 represent intermediate scores.

5.5 Discussion

Comparison between FingerPen and FreeFinger postures

In Section 5.3, we retrieved a model-based characterization of the hand operational space while using FingerPen and FreeFinger. Experiment 1 (in Section 5.4.1) showed that in the 72% of the trials the FingerPen allowed a reduction of the overall workspace occupied by the written text, and that the reduction was statistically significant both in height and width. Moreover, qualitatively speaking, the text usually appears more similar to what we are used to observe in adults (see also Fig. 5.4).

The hypothesis we made on the basis of the manipulability analysis, i.e. that the FreeFinger would lead to a larger text, has been experimentally confirmed. However, the manipulability analysis provides information on the allowed velocity of the finger; but the actual length of traits depend on how much the manipulator configuration constrains the manipulator movements. Hence, in the FP case the occurring tripod

grasp causes an overall reduction of the reachable planar workspace. Moreover, an additional explanation can be the fact that the extension of the space needed while writing is related to the effectiveness in the hand control while drawing letters. Hence, the better control provided by the FP contributes in reducing the overall size of the text.

Concerning precision (Experiment 2, Section 5.4.2, Fig. 5.7), a first consideration can be done on the difference between pre- and post-training. On average, the effect size in post-training is higher than in pre-training for all the metrics (as expected), suggesting that FP training leads to data distributions that differ more from the FF (see also the p - values). In the case of figures with effect size of similar magnitude (i.e., ellipse, quadrangle and puzzle, disregarding pre- and post-training), it can be noticed that the numerical difference between the values of the FP/FF metrics is larger as the figure is more complex (puzzle piece); however, the relative improvement is quite constant for each metric, independently on the figure complexity.

In general, long straight traits lower the average error, and the main difficulty is near the angles or in the curved parts (see also results on *max err*). Data related to the *std* metric show that in general the FP allows a more regular trait, with less dispersion. As expected, the higher are precision and regularity, the longer is the time required to accomplish the task (see the *time* column).

Concerning the questionnaire (Section 5.4.3, Fig. 5.8), the vast majority of experimenters reported that if a difficulty was present during the experiments, it was related to the need of physically shaping the hand according to the FingerPen posture (FP2), and it was overcome while going on with experiments (FP1). This suggests that the difficulty was due to the need of getting used to another hand configuration, and

is further supported by the fact that more than the 80% of the experimenters found the training step very or quite useful (FP3). Interestingly, the fact that the FingerPen configuration is somehow unusual for people (FP4) and requires some adaptation capabilities, does not impact negatively on the user experience: The vast majority of the experimenters had the perception of having greater control on the hand movements while using the FingerPen rather than the FreeFinger (C2). Moreover, they report that they felt more precise while exploiting FingerPen rather than FreeFinger (C1). Only two experimenters found the experience with the FreeFinger more pleasing (C3), and one half of the experimenters believe that the FreeFinger induces more in errors than the FingerPen, while the 20% of the experimenters found a tie on this aspect (C4). Hence, the analysis of the questionnaires strongly suggests that, from a user perspective, the advantages of adopting the FingerPen configuration for handwriting on touchscreen devices are remarkably more relevant than the disadvantages.

Additional investigation:
Comparison between FingerPen and Pen postures

The focus of this work is on investigating hand postures for writing on touchscreens without using specific tools. Motivations are illustrated in Section 5.1. However, people are used to write with a stylus. Hence, for the sake of completeness, here we provide an experimental comparison of the performance achievable with FingerPen and Pen postures. The Pen posture corresponds to the hand configuration that is typically used to hold a stylus while writing [163] (see, e.g., Fig. 5.9a).

We asked 15 additional participants to perform the experiments on workspace and precision described in Section 5.4 using a capacitive stylus. Figures for training (Fig. 5.5b) were used to let experimenters familiarize with the use of the pen in the proposed tasks before starting the experiments. Then, three instances of each figure shown in Fig. 5.5a were proposed alternately to each user. Data were collected and processed as previously described in Section 5.4, and a statistical analysis was carried out by performing independent T-tests.

Concerning the workspace occupancy (Experiment 1), the Pen allows a statistically significant reduction of the text width (37.6 ± 11.4, $p = 0.003$, $t = 3.3$), see Fig. 5.9b. Also the text height and the completion time are reduced, although without statistical significance.

Concerning the experiments on precision (Experiment 2), in Fig. 5.10 we show the results on the quadrangle and puzzle figures. In general, the task completion time is slightly higher for the Pen, whereas the metrics related to the errors are slightly lower for the Pen than for the FingerPen. The difference is even more negligible for the most complex figure (puzzle). Results on the comparison performed on triangle and ellipse show the same trend as the quadrangle.

In the following lines, we provide a possible interpretation of the obtained results, taking into account that the performance with the stylus is affected by the users' familiarity with the tool. Results on the occupancy of the workspace are consistent with what was expected: the Pen allows tighter and faster writing, although only the width reduction is statistically significant, and with remarkable effect size. In the experiments on precision, we expected a shorter completion time for the Pen, differently from what was obtained in the experiments. However, this can be due two main factors. First, there are two displacements

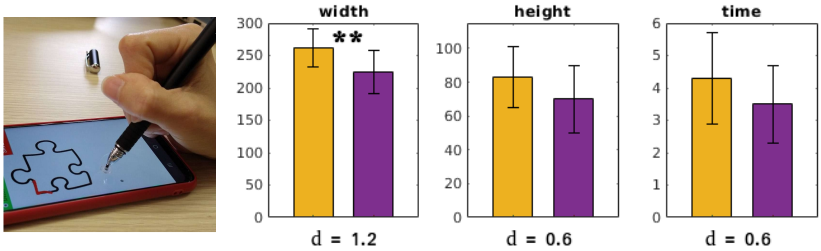

(a) (b)

Fig. 5.9 (a) Pen posture. (b) Comparison between FingerPen (yellow) and Pen (purple): Investigation on workspace occupancy.

to be considered: $D_{p,t}$, i.e., the distance between the pen tip and the point where the trait actually appears (see Fig. 5.6, displaced copy task), and $D_{p,f}$, i.e., the distance between the pen tip and the points where the pen is grasped by the fingers. These two distances make the task with the stylus more demanding than using the FingerPen, because not only $D_{p,t}$, but also $D_{p,f}$ impact the user's tracking of the figures. As a consequence, the visual servoing that the user performs to track a certain profile becomes more challenging, requiring a careful control of the forces and torques applied to the writing tool. Second, not everyone is equally familiar with the adoption of a stylus to interact with touch-screens (and smartphones in particular), whereas all of us are used to interact with screens through our fingers. Hence, it can be reasonably argued that the above mentioned factors partially reduce user's familiarity and ability with styluses, resulting in a task performance with a slightly higher precision at the cost of a higher task completion time.

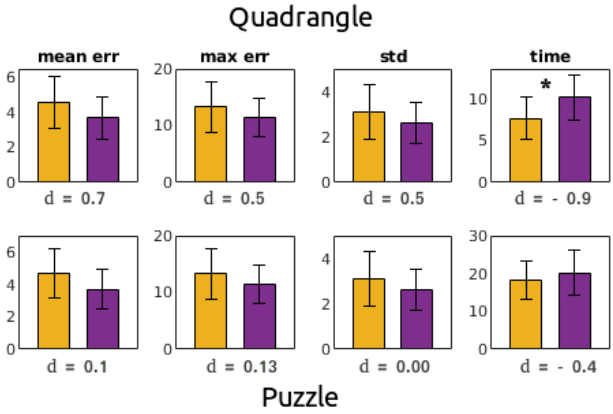

Fig. 5.10 Comparison between FingerPen (yellow) and Pen (purple): Investigation on precision.

5.6 Final remarks

In this Chapter, we considered a soft interaction involving the human hand. More specifically, we presented the FingerPen, a novel hand posture that can be adopted for writing on touchscreens without the use of specific input devices (e.g., a stylus). By exploiting modeling tools from biomechanics and the theory of grasping, a characterization of the workspace of this posture as been provided. A comparison with the hand posture that people typically adopt for interacting with touchscreens, i.e., the free index finger (FreeFinger), showed that FingerPen allows a greater control of the hand and more precise motions. The conducted experimental campaign with 25 participants confirmed the model-based results, and a questionnaire on the user experience reported a strongly positive opinion on the FingerPen adoption.

Conclusions

The Research work contained in this Thesis was aimed at finding modelling and control tools capable of capturing meaningful elements for effective manipulation of objects. We identified the core of such tools in what we called *soft interactions*, i.e. interactions exploiting material compliance of robotic and human hands, or compliance of objects.

Although the softness of end-effectors allows delicate and robust manipulation, it makes the control of such devices difficult (see *Part A*). To face this drawback, we introduced modelling and design techniques. On one side, indeed, we proposed to abstract from the kinematic and morphological structure of such devices, by devising functional models capturing the way in which the hand actually works (Chapter 1). Consequently, we computed and extensively validated the Closure Signature for diverse types of closing motions of robotic hands with different actuation, showing that the Closure Signature allows high success rate in grasping task accomplishment. However, as discussed in Chapter 1, what makes the Closure Signature powerful is also its main limitation: treating a soft hand as a parallel-jaw gripper leads to a lack of complexity in the description of the hand capabilities. A richer representation would require a different kind of modeling, with increased complexity. However, despite its apparent simplicity, experiments show that the Closure Signature allows a compact and effective representation.

Future work will focus on applications in real-world scenarios, as well as on the investigation of the possibility of explicitly considering the interaction with the environment within that framework. Moreover, the Closure Signature could also play an important role in the open quest for standards and benchmarks in robotic manipulation.

On the other side, concerning design techniques for controlling soft interactions, we proposed a physics-based framework to exploit magnetic elements properly located in the hand to compensate for uncertainties on fingers' trajectories, affordance exploitation and augmentation of the hand's Degrees of Actuation (Chapter 2). The main limitation of this work is that the analytical computation of the acting forces requires the knowledge of the internal structure of the chosen magnetic elements (i.e., geometric shape, magnetic permeability, number of turns, etc). However, in off-the-shelves components such information is usually protected by industrial design rights, and the identification of their features by reverse-engineering is not easy to achieve. The most straightforward way is to design ad-hoc devices and outsource the manufacture of such devices, that then would be ready for the desired use-cases. Future work will focus on the development of a 3D-printed prototype of a compliant hand specifically designed to exploit magnetic actuation jointly with more classic actuation sources (e.g., pneumatic or tendon-driven), realizing a synergistic approach capable of enhancing the hand manipulation capabilities.

Concerning interactions with soft objects present in the environment, we focused on autonomous garment manipulation (Chapter 3), due to the challenge posed to the Research community by the extreme intrinsic deformability of the fabric. To achieve effective and repeatable grasp execution, we proposed to exploit an attractive force between the

desired grasping points and the robotic gripper. To this aim, we developed Mag-Gripper, an end-effector capable of successful interactions with garments equipped with small ferromagnetic parts (ornamental or brand elements, like buttons and labels). Mag-Gripper has two main limitations: the first one concerns the dexterity allowed by the proposed gripper, the second one regards the need of ferromagnetic plates in the garments. Concerning the former issue, the gripper allows by design only a one-dimensional approach to the garment and a jaw-like closing motion. However, in future work we will design multifingered robotic hands with more dexterity. Concerning the second issue, it should be remarked that the ferromagnetic plates add some structure in the difficult-to-manage environment constituted by deformable fabrics, and that this structure allows to address the challenge of grasp repeatability. However, as discussed in Chapter 3, the ferromagnetic parts can be easily removed during final steps of garment production, before delivery to sealers or customers. Future work will focus also on testing our approach in setups for bimanual autonomous garment manipulation.

Concerning human-robot interactions, we introduced the Extended Patch method (Chapter 4), which is a technique exploiting forces and torques exerted during a cooperative grasping task to devise force and pressure constraints that generate robot velocity commands for effective task execution. Such constraints were retrieved by modelling an extended linear-elastic contact with known geometry. It can be noticed that the identification of such contact area could be non-trivial when the involved surfaces are not flat. However, a matrix of force sensors can be exploited to localize the occurred contacts, and retrieve as a consequence an estimate of the geometry involved in the contact. Then, pressure constraints could be easily adapted to the case. Future work

will concern the application of the proposed method to cooperative manipulation between teams composed of multiple humans and multiple robots, and to trimanual tasks during which the human guides the motion of the object with one hand and performs operations with the other. Moreover, we will investigate how providing the human with haptic feedback carrying information on the task execution reflects on motor learning and performance.

Mechanical forces exerted during a grasping task are also the core of the FingerPen (Chapter 5), a posture of the hand for writing on touchscreens and based on a biomechanical model of the hand that merges gesture and tools in a single operative organ. The main limitations in the adoption of the FingerPen are related to possible individual physiological constraints: people with large hands or with arthritis can have some difficulties in arranging the hand in such a posture. Moreover, people used to squeeze the pen while writing tend to squeeze also their index finger, and this results in a sense of fatigue at the wrist. Although there is no a recipe valid for everybody, experiments show that people usually tend to feel more at ease after some familiarization, which allows also to slightly modify the posture according to individual needs. Future work will focus on the analysis of the FingerPen performance when adopted by experimenters of different age groups, with particular attention to children and elders.

Beyond deepening the presented Research activities, we aim at testing and refining the proposed approaches in real-world scenarios, with the strong motivation of bringing Robotics Research out of labs and in touch with people.

References

[1] J. Bohg, A. Morales, T. Asfour, and D. Kragic, "Data-driven grasp synthesis – a survey," *IEEE Transactions on Robotics*, vol. 30, pp. 289–309, April 2014.

[2] A. M. Dollar and R. D. Howe, "The highly adaptive sdm hand: Design and performance evaluation," *The international journal of robotics research*, vol. 29, no. 5, pp. 585–597, 2010.

[3] S. Hirose and Y. Umetani, "The development of soft gripper for the versatile robot hand," *Mechanism and machine theory*, vol. 13, no. 3, pp. 351–359, 1978.

[4] L. Birglen, T. Lalibertè, and C. Gosselin, *Underactuated Robotic Hands*, vol. 40 of *Springer Tracts in Advanced Robotics*. Springer, 2008.

[5] J. Hughes, U. Culha, F. Giardina, F. Guenther, A. Rosendo, and F. Iida, "Soft manipulators and grippers: A review," *Frontiers in Robotics and AI*, vol. 3, p. 69, 2016.

[6] A. T. Miller, S. Knoop, H. I. Christensen, and P. K. Allen, "Automatic grasp planning using shape primitives," in *Robotics and Automation, 2003. Proceedings. ICRA'03. IEEE International Conference on*, vol. 2, pp. 1824–1829, IEEE, 2003.

[7] M. Bonilla, D. Resasco, M. Gabiccini, and A. Bicchi, "Grasp planning with soft hands using bounding box object decomposition," in *Proceedings IEEE/RSJ International Conference on Intelligent Robots and Systems, IROS*, pp. 518–523, Sept 2015.

[8] J.-H. Bae, S.-W. Park, J.-H. Park, M.-H. Baeg, D. Kim, and S.-R. Oh, "Development of a low cost anthropomorphic robot hand with high capability," in *2012 IEEE/RSJ International Conference on Intelligent Robots and Systems*, pp. 4776–4782, IEEE, 2012.

[9] M. Grebenstein, *Approaching human performance*. PhD thesis, Springer, 2012.

[10] M. G. Catalano, G. Grioli, E. Farnioli, A. Serio, C. Piazza, and A. Bicchi, "Adaptive synergies for the design and control of the pisa/iit softhand," *The*

International Journal of Robotics Research, vol. 33, no. 5, pp. 768–782, 2014.

[11] M. Santello, M. Flanders, and J. F. Soechting, "Postural hand synergies for tool use," *The Journal of Neuroscience*, vol. 18, pp. 10105–10115, December 1998.

[12] A. Bicchi and V. Kumar, "Robotic grasping and contact: a review," in *Proceedings 2000 ICRA. Millennium Conference. IEEE International Conference on Robotics and Automation. Symposia Proceedings (Cat. No.00CH37065)*, vol. 1, pp. 348–353 vol.1, 2000.

[13] O. Brock, J. Park, and M. Toussaint, "Mobility and manipulation," in *Springer handbook of robotics* (B. Siciliano and O. Khatib, eds.), pp. 1007–1030, Springer Science & Business Media, 2016.

[14] R. Deimel and O. Brock, "A novel type of compliant and underactuated robotic hand for dexterous grasping," *International Journal of Robotics Research*, 2015.

[15] C. Della Santina, C. Piazza, G. Grioli, M. G. Catalano, and A. Bicchi, "Toward dexterous manipulation with augmented adaptive synergies: The pisa/iit softhand 2," *IEEE Transactions on Robotics*, vol. 34, no. 5, pp. 1141–1156, 2018.

[16] J. Bimbo, E. Turco, M. Ghazaei Ardakani, M. Pozzi, G. Salvietti, V. Bo, M. Malvezzi, and D. Prattichizzo, "Exploiting robot hand compliance and environmental constraints for edge grasps," *Frontiers in Robotics and AI*, vol. 6, p. 135, 2019.

[17] D. Prattichizzo, M. Malvezzi, M. Gabiccini, and A. Bicchi, "On motion and force controllability of precision grasps with hands actuated by soft synergies," *IEEE transactions on robotics*, vol. 29, no. 6, pp. 1440–1456, 2013.

[18] A. Bhatt, A. Sieler, S. Puhlmann, and O. Brock, "Surprisingly robust in-hand manipulation: An empirical study," *Robotics: Science and Systems XVII*, 2021.

[19] J. Mahler, J. Liang, S. Niyaz, M. Laskey, R. Doan, X. Liu, J. A. Ojea, and K. Goldberg, "Dex-net 2.0: Deep learning to plan robust grasps with synthetic point clouds and analytic grasp metrics," 2017.

[20] M. Pozzi, S. Marullo, G. Salvietti, J. Bimbo, M. Malvezzi, and D. Prattichizzo, "Hand closure model for planning top grasps with soft robotic hands," *The International Journal of Robotics Research*, vol. 39, no. 14, pp. 1706–1723, 2020.

[21] M. Pozzi, G. Salvietti, J. Bimbo, M. Malvezzi, and D. Prattichizzo, "The closure signature: A functional approach to model underactuated compliant robotic

hands," *IEEE Robotics and Automation Letters*, vol. 3, pp. 2206–2213, July 2018.

[22] G. Gioioso, G. Salvietti, M. Malvezzi, and D. Prattichizzo, "Mapping synergies from human to robotic hands with dissimilar kinematics: an approach in the object domain," *IEEE Trans. on Robotics*, 2013.

[23] B. Siciliano, L. Sciavicco, L. Villani, and G. Oriolo, *Robotics: Modeling, Planning and Control*. Springer, 2009.

[24] R. Goldman, *Recovering the Data from the Transformation Matrix*, vol. VII-2 of *GEMS*. Academic Press, 1991.

[25] D. Prattichizzo, M. Malvezzi, M. Gabiccini, and A. Bicchi, "On motion and force controllability of precision grasps with hands actuated by soft synergies," *IEEE Transactions on Robotics*, vol. 29, no. 6, pp. 1440–1456, 2013.

[26] A. Bicchi, "On the closure properties of robotic grasping," *The Int. J. of Robotics Research*, vol. 14, no. 4, pp. 319–334, 1995.

[27] N. J. Higham and R. S. Schreiber, "Fast polar decomposition of an arbitrary matrix," *SIAM Journal on Scientific and Statistical Computing*, vol. 11, no. 4, pp. 648–655, 1990.

[28] G. Salvietti, "Replicating human hand synergies onto robotic hands: a review on software and hardware strategies," *Frontiers in Neurorobotics*, vol. 12, pp. 27–31, 2018.

[29] M. R. Cutkosky and I. Kao, "Computing and controlling compliance of a robotic hand," *IEEE Transactions on Robotics and Automation*, vol. 5, no. 2, pp. 151–165, 1989.

[30] M. R. Cutkosky, "On grasping choice, grasp models, and the design of hands for manufacturing tasks," *IEEE Transactions on Robotics and Automation*, vol. 5, pp. 269–279, June 1989.

[31] J. Mahler, F. T. Pokorny, B. Hou, M. Roderick, M. Laskey, M. Aubry, K. Kohlhoff, T. Kröger, J. Kuffner, and K. Goldberg, "Dex-net 1.0: A cloud-based network of 3d objects for robust grasp planning using a multi-armed bandit model with correlated rewards," in *IEEE International Conference on Robotics and Automation (ICRA)*, pp. 1957–1964, IEEE, 2016.

[32] M. Quigley, K. Conley, B. P. Gerkey, J. Faust, T. Foote, J. Leibs, R. Wheeler, and A. Y. Ng, "Ros: an open-source robot operating system," in *ICRA Workshop on Open Source Software*, 2009.

[33] B. Calli, A. Walsman, A. Singh, S. Srinivasa, P. Abbeel, and A. M. Dollar, "Benchmarking in manipulation research: Using the yale-cmu-berkeley object and model set," *IEEE Robotics Automation Magazine*, vol. 22, pp. 36–52, Sept 2015.

[34] C. Eppner, S. Höfer, R. Jonschkowski, R. Martín-Martín, A. Sieverling, V. Wall, and O. Brock, "Four aspects of building robotic systems: lessons from the amazon picking challenge 2015," *Autonomous Robots*, vol. 42, pp. 1459–1475, Oct 2018.

[35] N. Bira, P. Dhagat, and J. R. Davidson, "A review of magnetic elastomers and their role in soft robotics," *Frontiers in Robotics and AI*, vol. 7, p. 146, 2020.

[36] F. Qiu and B. J. Nelson, "Magnetic helical micro-and nanorobots: Toward their biomedical applications," *Engineering*, vol. 1, no. 1, pp. 021–026, 2015.

[37] J. Hwang, J.-y. Kim, and H. Choi, "A review of magnetic actuation systems and magnetically actuated guidewire-and catheter-based microrobots for vascular interventions," *Intelligent Service Robotics*, vol. 13, no. 1, pp. 1–14, 2020.

[38] C. Di Natali, M. Beccani, and P. Valdastri, "Real-time pose detection for magnetic medical devices," *IEEE Transactions on Magnetics*, vol. 49, no. 7, pp. 3524–3527, 2013.

[39] N. Ebrahimi, C. Bi, D. J. Cappelleri, G. Ciuti, A. T. Conn, D. Faivre, N. Habibi, A. Hosovsky, V. Iacovacci, I. S. Khalil, *et al.*, "Magnetic actuation methods in bio/soft robotics," *Advanced Functional Materials*, vol. 31, no. 11, p. 2005137, 2021.

[40] R. Pelrine, A. Wong-Foy, A. Hsu, and B. McCoy, "Self-assembly of milli-scale robotic manipulators: A path to highly adaptive, robust automation systems," in *2016 International Conference on Manipulation, Automation and Robotics at Small Scales (MARSS)*, pp. 1–6, IEEE, 2016.

[41] S. Miyashita, S. Guitron, M. Ludersdorfer, C. R. Sung, and D. Rus, "An untethered miniature origami robot that self-folds, walks, swims, and degrades," in *2015 IEEE International Conference on Robotics and Automation (ICRA)*, pp. 1490–1496, IEEE, 2015.

[42] M. E. Alshafeei, A. Hosney, A. Klingner, S. Misra, and I. S. Khalil, "Magnetic-based motion control of a helical robot using two synchronized rotating dipole fields," in *5th IEEE RAS/EMBS International Conference on Biomedical Robotics and Biomechatronics*, pp. 151–156, IEEE, 2014.

[43] C. Li, G. C. Lau, H. Yuan, A. Aggarwal, V. L. Dominguez, S. Liu, H. Sai, L. C. Palmer, N. A. Sather, T. J. Pearson, *et al.*, "Fast and programmable locomotion of hydrogel-metal hybrids under light and magnetic fields," *Science Robotics*, vol. 5, no. 49, p. eabb9822, 2020.

[44] V. K. Venkiteswaran, D. K. Tan, and S. Misra, "Tandem actuation of legged locomotion and grasping manipulation in soft robots using magnetic fields," *Extreme Mechanics Letters*, vol. 41, p. 101023, 2020.

[45] Y. Alapan, A. C. Karacakol, S. N. Guzelhan, I. Isik, and M. Sitti, "Reprogrammable shape morphing of magnetic soft machines," *Science advances*, vol. 6, no. 38, p. eabc6414, 2020.

[46] Q. Peyron, Q. Boehler, K. Rabenorosoa, B. J. Nelson, P. Renaud, and N. Andreff, "Kinematic analysis of magnetic continuum robots using continuation method and bifurcation analysis," *IEEE Robotics and Automation Letters*, vol. 3, no. 4, pp. 3646–3653, 2018.

[47] M. N. Faddis and B. D. Lindsay, "Magnetic catheter manipulation," *Coronary artery disease*, vol. 14, no. 1, pp. 25–27, 2003.

[48] N. Kim, S. Lee, W. Lee, and G. Jang, "Development of a magnetic catheter with rotating multi-magnets to achieve unclogging motions with enhanced steering capability," *AIP Advances*, vol. 8, no. 5, p. 056708, 2018.

[49] V. N. Le, N. H. Nguyen, K. Alameh, R. Weerasooriya, and P. Pratten, "Accurate modeling and positioning of a magnetically controlled catheter tip," *Medical physics*, vol. 43, no. 2, pp. 650–663, 2016.

[50] C. Hu, M. Q.-H. Meng, and M. Mandal, "A linear algorithm for tracing magnet position and orientation by using three-axis magnetic sensors," *IEEE transactions on magnetics*, vol. 43, no. 12, pp. 4096–4101, 2007.

[51] J. Jose, D. Dinakaran, M. Ramya, and D. Harris, "A survey on magnetic wall-climbing robots for inspection," *Transst. J*, vol. 8, pp. 59–68, 2018.

[52] S. W. Kwok, S. A. Morin, B. Mosadegh, J.-H. So, R. F. Shepherd, R. V. Martinez, B. Smith, F. C. Simeone, A. A. Stokes, and G. M. Whitesides, "Magnetic assembly of soft robots with hard components," *Advanced Functional Materials*, vol. 24, no. 15, pp. 2180–2187, 2014.

[53] B. T. Kirby, B. Aksak, J. D. Campbell, J. F. Hoburg, T. C. Mowry, P. Pillai, and S. C. Goldstein, "A modular robotic system using magnetic force effectors," in *2007 IEEE/RSJ International Conference on Intelligent Robots and Systems*,

pp. 2787–2793, IEEE, 2007.

[54] L. Gerez, G. Gao, and M. Liarokapis, "Employing magnets to improve the force exertion capabilities of adaptive robot hands in precision grasps," in *2019 IEEE/RSJ International Conference on Intelligent Robots and Systems (IROS)*, pp. 7630–7635, IEEE, 2019.

[55] A. Mohammadi, Y. Xu, Y. Tan, P. Choong, and D. Oetomo, "Magnetic-based soft tactile sensors with deformable continuous force transfer medium for resolving contact locations in robotic grasping and manipulation," *Sensors*, vol. 19, no. 22, p. 4925, 2019.

[56] A. H. Memar and E. T. Esfahani, "A robot gripper with variable stiffness actuation for enhancing collision safety," *IEEE Transactions on Industrial Electronics*, vol. 67, no. 8, pp. 6607–6616, 2019.

[57] A. Gafer, D. Heymans, D. Prattichizzo, and G. Salvietti, "The quad-spatula gripper: a novel soft-rigid gripper for food handling," in *2020 3rd IEEE International Conference on Soft Robotics (RoboSoft)*, pp. 39–45, IEEE, 2020.

[58] S. Marullo, S. Bartoccini, G. Salvietti, M. Z. Iqbal, and D. Prattichizzo, "The mag-gripper: A soft-rigid gripper augmented with an electromagnet to precisely handle clothes," *IEEE Robotics and Automation Letters*, vol. 5, no. 4, pp. 6591–6598, 2020.

[59] F. Reitz, J. Milford, and R. Christy, *Foundations of Electromagnetic Teory*. 2003.

[60] J. D. Jackson, "Classical electrodynamics," 1999.

[61] L. D. Landau, *The classical theory of fields*, vol. 2. Elsevier, 2013.

[62] R. Deimel and O. Brock, "Soft hands for reliable grasping strategies," in *Soft Robotics*, pp. 211–221, Springer, 2015.

[63] A. Sieverling, *Robust Motion Generation for Mobile Manipulation: Integrating Control and Planning under Uncertainty*. Technische Universitaet Berlin (Germany), 2019.

[64] M. Mason, "The mechanics of manipulation," in *Proceedings. 1985 IEEE International Conference on Robotics and Automation*, vol. 2, pp. 544–548, IEEE, 1985.

[65] R. Deimel and O. Brock, "A novel type of compliant and underactuated robotic hand for dexterous grasping," *The International Journal of Robotics Research*, vol. 35, no. 1-3, pp. 161–185, 2016.

[66] M. Pozzi, E. Miguel, R. Deimel, M. Malvezzi, B. Bickel, O. Brock, and D. Prattichizzo, "Efficient fem-based simulation of soft robots modeled as kinematic chains," in *2018 IEEE International Conference on Robotics and Automation (ICRA)*, pp. 1–8, IEEE, 2018.

[67] E. P. Furlani, *Permanent magnet and electromechanical devices: materials, analysis, and applications*. Academic press, 2001.

[68] J. Bimbo, E. Turco, M. Ghazaei Ardakani, M. Pozzi, G. Salvietti, V. Bo, M. Malvezzi, and D. Prattichizzo, "Exploiting robot hand compliance and environmental constraints for edge grasps," *Frontiers in Robotics and AI*, vol. 6, p. 135, 2019.

[69] E. P. Furlani, *Permanent magnet and electromechanical devices: materials, analysis, and applications*. Academic press, 2001.

[70] H. H. Woodson and J. R. Melcher, *Electromechanical Dynamics: Fields, forces, and motion*. No. 2, Wiley, 1968.

[71] A. Caciagli, R. J. Baars, A. P. Philipse, and B. W. Kuipers, "Exact expression for the magnetic field of a finite cylinder with arbitrary uniform magnetization," *Journal of Magnetism and Magnetic Materials*, vol. 456, pp. 423–432, 2018.

[72] D. Vokoun, M. Beleggia, L. Heller, and P. Sittner, "Magnetostatic interactions and forces between cylindrical permanent magnets," *Journal of magnetism and Magnetic Materials*, vol. 321, no. 22, pp. 3758–3763, 2009.

[73] I. Hussain, G. Salvietti, G. Spagnoletti, and D. Prattichizzo, "The soft-sixthfinger: a wearable emg controlled robotic extra-finger for grasp compensation in chronic stroke patients," *IEEE Robotics and Automation Letters*, vol. 1, no. 2, pp. 1000–1006, 2016.

[74] D. Triantafyllou, I. Mariolis, A. Kargakos, S. Malassiotis, and N. Aspragathos, "A geometric approach to robotic unfolding of garments," *Robot. Auton. Syst.*, vol. 75, p. 233–243, Jan. 2016.

[75] M. Cusumano-Towner, A. Singh, S. Miller, J. F. O'Brien, and P. Abbeel, "Bringing clothing into desired configurations with limited perception," in *2011 IEEE International Conference on Robotics and Automation*, pp. 3893–3900, 2011.

[76] C. Bersch, B. Pitzer, and S. Kammel, "Bimanual robotic cloth manipulation for laundry folding," in *2011 IEEE/RSJ International Conference on Intelligent Robots and Systems*, pp. 1413–1419, Sep. 2011.

[77] A. Doumanoglou, A. Kargakos, T. Kim, and S. Malassiotis, "Autonomous active recognition and unfolding of clothes using random decision forests and probabilistic planning," in *2014 IEEE International Conference on Robotics and Automation (ICRA)*, pp. 987–993, May 2014.

[78] Y. Li, Danfei Xu, Yonghao Yue, Y. Wang, S. Chang, E. Grinspun, and P. K. Allen, "Regrasping and unfolding of garments using predictive thin shell modeling," in *2015 IEEE International Conference on Robotics and Automation (ICRA)*, pp. 1382–1388, May 2015.

[79] E. Corona, G. Alenyà, A. Gabas, and C. Torras, "Active garment recognition and target grasping point detection using deep learning," *Pattern Recognition*, vol. 74, pp. 629–641, 2018.

[80] M. Bell and D. Balkcom, "Grasping non-stretchable cloth polygons," *The International Journal of Robotics Research*, vol. 29, no. 6, pp. 775–784, 2010.

[81] S. Miller, J. van den Berg, M. Fritz, T. Darrell, K. Goldberg, and P. Abbeel, "A geometric approach to robotic laundry folding," *The International Journal of Robotics Research*, vol. 31, no. 2, pp. 249–267, 2012.

[82] V. Petrík, V. Smutný, P. Krsek, and V. Hlavác, "Robotic garment folding: Precision improvement and workspace enlargement," in *TAROS*, 2015.

[83] P. Yang, K. Sasaki, K. Suzuki, K. Kase, S. Sugano, and T. Ogata, "Repeatable folding task by humanoid robot worker using deep learning," *IEEE Robotics and Automation Letters*, vol. 2, pp. 397–403, April 2017.

[84] Y. Tsurumine, Y. Cui, E. Uchibe, and T. Matsubara, "Deep reinforcement learning with smooth policy update: Application to robotic cloth manipulation," *Robotics and Autonomous Systems*, vol. 112, pp. 72 – 83, 2019.

[85] A. Colomé and C. Torras, "Dimensionality reduction for dynamic movement primitives and application to bimanual manipulation of clothes," *IEEE Transactions on Robotics*, vol. 34, pp. 602–615, 2018.

[86] J. Borràs, G. Alenyà, and C. Torras, "A grasping-centered analysis for cloth manipulation," *IEEE Transactions on Robotics*, vol. 36, no. 3, pp. 924–936, 2020.

[87] A. Ramisa, G. Alenyà, F. Moreno-Noguer, and C. Torras, "Using depth and appearance features for informed robot grasping of highly wrinkled clothes," in *2012 IEEE International Conference on Robotics and Automation*, pp. 1703–1708, May 2012.

[88] L. Twardon and H. Ritter, "Interaction skills for a coat-check robot: Identifying and handling the boundary components of clothes," in *2015 IEEE International Conference on Robotics and Automation (ICRA)*, pp. 3682–3688, 2015.

[89] T.-H.-L. Le, M. Jilich, A. Landini, M. Zoppi, D. Zlatanov, and R. Molfino, "On the development of a specialized flexible gripper for garment handling," 2013.

[90] P. N. Koustoumpardis, K. X. Nastos, and N. A. Aspragathos, "Underactuated 3-finger robotic gripper for grasping fabrics," in *2014 23rd International Conference on Robotics in Alpe-Adria-Danube Region (RAAD)*, pp. 1–8, Sep. 2014.

[91] C. Eppner, R. Deimel, J. Álvarez Ruiz, M. Maertens, and O. Brock, "Exploitation of environmental constraints in human and robotic grasping," *Int. J. Rob. Res.*, vol. 34, p. 1021–1038, June 2015.

[92] D. Roy, "Development of novel magnetic grippers for use in unstructured robotic workspace," *Robotics and Computer-Integrated Manufacturing*, vol. 35, pp. 16 – 41, 2015.

[93] B. Calli, A. Walsman, A. Singh, S. Srinivasa, P. Abbeel, and A. M. Dollar, "Benchmarking in manipulation research: Using the yale-cmu-berkeley object and model set," *IEEE Robotics Automation Magazine*, vol. 22, no. 3, pp. 36–52, 2015.

[94] C. Torras, "Assistive robotics: research challenges and ethics education initiatives," *Dilemata*, vol. 30, pp. 63–77, 2019.

[95] G. Salvietti, Z. Iqbal, M. Malvezzi, T. Eslami, and D. Prattichizzo, "Soft hands with embodied constraints: The soft scoopgripper," in *2019 International Conference on Robotics and Automation (ICRA)*, pp. 2758–2764, 2019.

[96] S. L. Gilman, ""stand up straight": Notes toward a history of posture," *Journal of Medical Humanities*, vol. 35, no. 1, pp. 57–83, 2014.

[97] W. K. Gregory, "The upright posture of man: A review of its origin and evolution," *Proceedings of the American Philosophical Society*, vol. 67, no. 4, pp. 339–377, 1928.

[98] G. C. Westergaard, H. E. Kuhn, and S. J. Suomi, "Bipedal posture and hand preference in humans and other primates.," *Journal of Comparative Psychology*, vol. 112, no. 1, p. 55, 1998.

[99] G. W. Hewes, "Food transport and the origin of hominid bipedalism 1," *American Anthropologist*, vol. 63, no. 4, pp. 687–710, 1961.

[100] E. Burdet, D. W. Franklin, and T. E. Milner, *Human robotics: neuromechanics and motor control*. MIT press, 2013.

[101] T. E. Milner, "Dependence of elbow viscoelastic behavior on speed and loading in voluntary movements," *Experimental Brain Research*, vol. 93, no. 1, pp. 177–180, 1993.

[102] F. A. Mussa-Ivaldi, N. Hogan, and E. Bizzi, "Neural, mechanical, and geometric factors subserving arm posture in humans," *Journal of neuroscience*, vol. 5, no. 10, pp. 2732–2743, 1985.

[103] R. D. Trumbower, M. A. Krutky, B.-S. Yang, and E. J. Perreault, "Use of self-selected postures to regulate multi-joint stiffness during unconstrained tasks," *PloS one*, vol. 4, no. 5, p. e5411, 2009.

[104] R. Shadmehr and F. A. Mussa-Ivaldi, "Adaptive representation of dynamics during learning of a motor task," *Journal of neuroscience*, vol. 14, no. 5, pp. 3208–3224, 1994.

[105] J. I. Laszlo, "Kinaesthetic and exteroceptive information in the performance of motor skills," *Physiology & Behavior*, vol. 2, no. 4, pp. 359–365, 1967.

[106] T. Brashers-Krug, R. Shadmehr, and E. Bizzi, "Consolidation in human motor memory," *Nature*, vol. 382, no. 6588, pp. 252–255, 1996.

[107] S. Marullo, M. Pozzi, D. Prattichizzo, and M. Malvezzi, "Cooperative human-robot grasping with extended contact patches," *IEEE Robotics and Automation Letters*, vol. 5, no. 2, pp. 3121–3128, 2020.

[108] S. Haddadin and E. Croft, "Physical human–robot interaction," in *Springer Handbook of Robotics* (B. Siciliano and O. Khatib, eds.), pp. 1835–1874, Springer, 2016.

[109] A. Mörtl, M. Lawitzky, A. Kucukyilmaz, M. Sezgin, C. Basdogan, and S. Hirche, "The role of roles: Physical cooperation between humans and robots," *The International Journal of Robotics Research*, vol. 31, no. 13, pp. 1656–1674, 2012.

[110] Y. Hayashibara, T. Takubo, Y. Sonoda, H. Arai, and K. Tanie, "Assist system for carrying a long object with a human-analysis of a human cooperative behavior in the vertical direction," in *Proceedings 1999 IEEE/RSJ International Conference on Intelligent Robots and Systems. Human and Environment Friendly Robots with High Intelligence and Emotional Quotients (Cat. No. 99CH36289)*, vol. 2, pp. 695–700, IEEE, 1999.

[111] R. Ikeura and H. Inooka, "Variable impedance control of a robot for cooperation with a human," in *Proceedings of 1995 IEEE International Conference on Robotics and Automation*, vol. 3, pp. 3097–3102, IEEE, 1995.

[112] C. A. Parker and E. A. Croft, "Design & personalization of a cooperative carrying robot controller," in *2012 IEEE International Conference on Robotics and Automation*, pp. 3916–3921, IEEE, 2012.

[113] Y. Maeda, T. Hara, and T. Arai, "Human-robot cooperative manipulation with motion estimation," in *Proceedings 2001 IEEE/RSJ International Conference on Intelligent Robots and Systems. Expanding the Societal Role of Robotics in the the Next Millennium (Cat. No. 01CH37180)*, vol. 4, pp. 2240–2245, Ieee, 2001.

[114] M. Lawitzky, A. Mörtl, and S. Hirche, "Load sharing in human-robot cooperative manipulation," in *19th International Symposium in Robot and Human Interactive Communication*, pp. 185–191, IEEE, 2010.

[115] F. Caccavale and M. Uchiyama, "Cooperative manipulation," in *Springer Handbook of Robotics* (B. Siciliano and O. Khatib, eds.), pp. 989–1006, Springer, 2016.

[116] P. Chiacchio, S. Chiaverini, and B. Siciliano, "Direct and inverse kinematics for coordinated motion tasks of a two-manipulator system," *Journal of dynamic systems, measurement, and control*, vol. 118, no. 4, pp. 691–697, 1996.

[117] A. Bicchi, "Hands for dextrous manipulation and robust grasping: a difficult road towards simplicity," *IEEE Trans. on Robotics and Automation*, vol. 16, pp. 652–662, December 2000.

[118] D. Prattichizzo and J. C. Trinkle, "Grasping," in *Springer handbook of robotics* (B. Siciliano and O. Khatib, eds.), pp. 955–988, Springer Science & Business Media, 2016.

[119] M. Malvezzi and D. Prattichizzo, "Evaluation of grasp stiffness in underactuated compliant hands," in *2013 IEEE International Conference on Robotics and Automation*, pp. 2074–2079, IEEE, 2013.

[120] M. A. Roa and R. Suarez, "Grasp quality measures: review and performance," *Autonomous Robots*, vol. 38, no. 1, pp. 65–88, 2015.

[121] M. Erdmann, "An exploration of nonprehensile two-palm manipulation," *The International Journal of Robotics Research*, vol. 17, no. 5, pp. 485–503, 1998.

[122] A. Gupta and W. H. Huang, "A carrying task for nonprehensile mobile manipulators," in *Proceedings 2003 IEEE/RSJ International Conference on Intelligent Robots and Systems (IROS 2003) (Cat. No.03CH37453)*, vol. 3, pp. 2896–2901 vol.3, Oct 2003.

[123] F. Barbagli, A. Frisoli, K. Salisbury, and M. Bergamasco, "Simulating human fingers: a soft finger proxy model and algorithm," in *12th International Symposium on Haptic Interfaces for Virtual Environment and Teleoperator Systems, 2004. HAPTICS'04. Proceedings.*, pp. 9–17, IEEE, 2004.

[124] C. Melchiorri, "Translational and rotational slip detection and control in robotic manipulation," *IFAC Proceedings Volumes*, vol. 32, no. 2, pp. 647 – 652, 1999. 14th IFAC World Congress 1999, Beijing, Chia, 5-9 July.

[125] M. T. Mason, "Mechanics and planning of manipulator pushing operations," *The International Journal of Robotics Research*, vol. 5, no. 3, pp. 53–71, 1986.

[126] S. Goyal, A. Ruina, and J. Papadopoulos, "Planar sliding with dry friction part 1. limit surface and moment function," *Wear*, vol. 143, no. 2, pp. 307 – 330, 1991.

[127] N. Chavan-Dafle, R. Holladay, and A. Rodriguez, "Planar in-hand manipulation via motion cones," *The International Journal of Robotics Research*, vol. 0, no. 0, p. 0278364919880257, 2019.

[128] R. Deimel, C. Eppner, J. Alvarez-Ruiz, M. Maertens, and O. Brock, "Exploitation of environmental constraints in human and robotic grasping," in *International Symposium on Robotic Research*, 2013.

[129] S. Dharbaneshwer, S. J. Subramanian, and K. Kohlhoff, "Robotic grasp analysis using deformable solid mechanics," *Meccanica*, pp. 1–18.

[130] K. L. Johnson and K. L. Johnson, *Contact mechanics*. Cambridge university press, 1987.

[131] S. Balasubramanian, A. Melendez-Calderon, A. Roby-Brami, and E. Burdet, "On the analysis of movement smoothness," *Journal of neuroengineering and rehabilitation*, vol. 12, no. 1, p. 112, 2015.

[132] S. Marullo, M. Pozzi, M. Malvezzi, and D. Prattichizzo, "Analysis of postures for handwriting on touch screens without using tools," *Scientific reports*, vol. 12, no. 1, pp. 1–11, 2022.

[133] K. James and T. Atwood, "The role of sensorimotor learning in the perception of letter-like forms: Tracking the causes of neural specialization for letters," *Cognitive Neuropsychology*, vol. 26, pp. 110 – 91, 2009.

[134] K. James and L. Engelhardt, "The effects of handwriting experience on functional brain development in pre-literate children," *Trends in Neuroscience and Education*, vol. 1, pp. 32–42, 2012.

[135] M. Montessori and C. Claremont, *The Absorbent Mind*. Dell Pub. Co., 1969.

[136] "Children struggle to hold pencils due to too much tech, doctors say." The Guardian. https://www.theguardian.com/society/2018/feb/25/children-struggle-to-hold-pencils-due-to-too-much-tech-doctors-say. Accessed: 2021-06-22.

[137] K. Kostyrka-Allchorne, N. R. Cooper, and A. Simpson, "Touchscreen generation: children's current media use, parental supervision methods and attitudes towards contemporary media," *Acta Paediatrica*, vol. 106, no. 4, pp. 654–662, 2017.

[138] M. Dardanou, T. Unstad, R. Brito, P. Dias, O. Fotakopoulou, Y. Sakata, and J. O?Connor, "Use of touchscreen technology by 0–3-year-old children: Parents? practices and perspectives in norway, portugal and japan," *Journal of Early Childhood Literacy*, vol. 20, no. 3, pp. 551–573, 2020.

[139] M. McLuhan, *Understanding Media: The Extensions of Man*. McGraw-Hill, 1964.

[140] D. De Kerckhove, *Brainframes: Technology, Mind and Business*. Bosch & Keuning, 1991.

[141] V. Berninger, "Development of language by hand and its connections with language by ear, mouth, and eye," *Topics in Language Disorders*, vol. 20, pp. 65–84, 2000.

[142] A. Leroi-Gourhan, *Gesture and Speech*. MIT Press, 1993.

[143] B. A. Kahrs and J. Lockman, "Tool using.," *Child development perspectives*, vol. 8 4, pp. 231–236, 2014.

[144] V. U. Weser and D. Proffitt, "Expertise in tool use promotes tool embodiment.," *Topics in cognitive science*, 2021.

[145] V. W. Berninger, R. D. Abbott, A. Augsburger, and N. Garcia, "Comparison of pen and keyboard transcription modes in children with and without learning disabilities," *Learning Disability Quarterly*, vol. 32, no. 3, pp. 123–141, 2009.

[146] L. Y. Robert S. Wilson, P. Boyle, J. S. L. Barnes, and D. Bennett, "Life-span cognitive activity, neuropathologic burden, and cognitive aging," *Neurology*, vol. 81, pp. 314 – 321, 2013.

[147] The Ohio State University. Wexner Medical Center, "SAGE: A Test to Detect Signs of Alzheimer's and Dementia." Accessed: 2021-06-14.

[148] B. Agrell and O. Dehlin, "The clock-drawing test," *Age and ageing*, vol. 27, no. 3, pp. 399–404, 1998.

[149] D. Arenberg, "Differences and changes with age in the benton visual retention test," *Journal of Gerontology*, vol. 33, no. 4, pp. 534–540, 1978.

[150] M. A. Fernandes, J. D. Wammes, and M. E. Meade, "The surprisingly powerful influence of drawing on memory," *Current Directions in Psychological Science*, vol. 27, no. 5, pp. 302–308, 2018.

[151] M. E. Meade, J. D. Wammes, and M. A. Fernandes, "Drawing as an encoding tool: Memorial benefits in younger and older adults," *Experimental Aging Research*, vol. 44, no. 5, pp. 369–396, 2018.

[152] R. J. Schwarz and C. Taylor, "The anatomy and mechanics of the human hand," *Artificial limbs*, vol. 2, no. 2, pp. 22–35, 1955.

[153] G. Anastasi, E. Gaudio, and C. Tacchetti, *Human Anatomy. Atlas. English version*. Edi. Ermes, 2019.

[154] P. Haggard and J. R. Flanagan, *Hand and brain: the neurophysiology and psychology of hand movements*. Elsevier, 1996.

[155] G. Azeredo, T. Pereira, and M. Marques, "Biomechanics of handwriting," *Computational Vision and Medical Image Processing: VipIMAGE 2009*, p. 201, 2009.

[156] V. J. Santos and F. J. Valero-Cuevas, "Reported anatomical variability naturally leads to multimodal distributions of denavit-hartenberg parameters for the human thumb," *IEEE Transactions on Biomedical Engineering*, vol. 53, no. 2, pp. 155–163, 2006.

[157] P. Cerveri, E. De Momi, N. Lopomo, G. Baud-Bovy, R. Barros, and G. Ferrigno, "Finger kinematic modeling and real-time hand motion estimation," *Annals of biomedical engineering*, vol. 35, no. 11, pp. 1989–2002, 2007.

[158] G. Fischer, D. Jermann, R. List, L. Reissner, and M. Calcagni, "Development and application of a motion analysis protocol for the kinematic evaluation of basic and functional hand and finger movements using motion capture in a clinical setting?a repeatability study," *Applied Sciences*, vol. 10, no. 18, p. 6436, 2020.

[159] G. Baud-Bovy, D. Prattichizzo, and N. Brogi, "Does torque minimization yield a stable human grasp?," in *Multi-point Interaction with Real and Virtual Objects*, pp. 21–40, 2005.

[160] F. J. Valero-Cuevas, M. E. Johanson, and J. D. Towles, "Towards a realistic biomechanical model of the thumb: the choice of kinematic description may be more critical than the solution method or the variability/uncertainty of musculoskeletal parameters," *Journal of biomechanics*, vol. 36, no. 7, pp. 1019–1030, 2003.

[161] L. A. Jones and S. J. Lederman, *Human hand function*. Oxford University Press, 2006.

[162] H. Schwellnus, H. Carnahan, A. Kushki, H. Polatajko, C. Missiuna, and T. Chau, "Effect of pencil grasp on the speed and legibility of handwriting in children," *American Journal of Occupational Therapy*, vol. 66, no. 6, pp. 718–726, 2012.

[163] K. M. Farris, R. E. Fehrenbacher, E. L. Hayes, R. R. McEvoy, A. P. Smith, and R. S. McCulloch, "The relationship between muscle activation and handwriting quality with non-native grip styles," *Journal of Hand Therapy*, 2021.

[164] D. Alamargot and M.-F. Morin, "Does handwriting on a tablet screen affect students? graphomotor execution? a comparison between grades two and nine," *Human Movement Science*, vol. 44, pp. 32–41, 2015.

[165] J. Guilbert, D. Alamargot, and M.-F. Morin, "Handwriting on a tablet screen: Role of visual and proprioceptive feedback in the control of movement by children and adults," *Human Movement Science*, vol. 65, pp. 30–41, 2019. Special issue: Articles on graphonomics.

[166] E. d. C. Valderrama Bahamóndez, T. Kubitza, N. Henze, and A. Schmidt, "Analysis of children's handwriting on touchscreen phones," in *Proc. international conference on Human-computer interaction with mobile devices and services*, pp. 171–174, 2013.

[167] J. Jacquier-Bret, P. Gorce, G. Motti Lilian, and N. Vigouroux, "Biomechanical analysis of upper limb during the use of touch screen: motion strategies identification," *Ergonomics*, vol. 60, no. 3, pp. 358–365, 2017.

[168] D. Babu, M. Konyo, H. Nagano, and S. Tadokoro, "Introducing whole finger effects in surface haptics: An extended stick-slip model incorporating finger stiffness," *IEEE transactions on haptics*, vol. 11, no. 3, pp. 417–430, 2018.

[169] D. Prattichizzo, L. Meli, and M. Malvezzi, "Digital handwriting with a finger or a stylus: a biomechanical comparison," *IEEE Transactions on Haptics*, vol. 8, no. 4, pp. 356–370, 2015.

[170] D. Prattichizzo and J. C. Trinkle, "Grasping," in *Springer handbook of robotics* (B. Siciliano and O. Khatib, eds.), pp. 955–988, Springer Science & Business Media, 2016.

[171] B. Siciliano, L. Sciavicco, L. Villani, and G. Oriolo, *Robotics: modelling, planning and control*. Springer Science & Business Media, 2010.

[172] M. Malvezzi, G. Gioioso, G. Salvietti, and D. Prattichizzo, "Syngrasp: A matlab toolbox for underactuated and compliant hands," *IEEE Robotics and Automation Magazine*, 2015. In press.

[173] "SPSS - Statistical Package for Social Science by IMB." https://www.ibm.com/analytics/spss-statistics-software. Accessed: 2021-06-22.

[174] J. Cohen, *Statistical Power Analysis for the Behavioural Sciences*. LEA, 1988.

[175] A. Proverbio, R. Adorni, and A. Zani, "Inferring native language from early bio-electrical activity," *Biological Psychology*, vol. 80, pp. 52–63, 2009.

[176] J. K. Hartshorne, J. B. Tenenbaum, and S. Pinker, "A critical period for second language acquisition: Evidence from 2/3 million english speakers," *Cognition*, vol. 177, pp. 263–277, 2018.

[177] "MATLAB." Software by MathWorks Inc. https://www.mathworks.com. Accessed: 2021-06-22.